Modelling of Atmospheric Mercury Emission, Transport, Transformation and Deposition in North America

by

Deyong Wen

A thesis
presented to the University of Waterloo
in fulfilment of the
thesis requirement for the degree of
Doctor of Philosophy
in
Chemistry

Waterloo, Ontario, Canada, 2006
© Deyong Wen 2006

I hereby declare that I am the sole author of this thesis. This is a true copy of the thesis, including any required final revisions, as accepted by my examiners.

I understand that my thesis may be made electronically available to the public.

Abstract

A modelling study was conducted to explore the emission, transport, transformation and deposition behaviour of atmospheric Hg. A detailed natural Hg emission model was developed to estimate the natural Hg emissions from soil, water and vegetation. U.S. Environmental Protection Agency (EPA) Community Multiscale Air Quality (CMAQ) Hg model system was improved by incorporating the detailed treatment of natural Hg emissions, adopting boundary conditions from a global Hg model (Seigneur et al., 2004) and including the calculation of the dry deposition velocity of elemental Hg. The natural Hg emission model and the improved CMAQ-Hg model were validated with some measurements and then applied to North America for a whole year (2002).

A detailed natural Hg emission model was developed in this study. This model made use of detailed soil Hg concentration measurements, meteorological data and soil conditions to estimate Hg emissions from soil, water and vegetation. The influence of snow cover and low temperature was also considered in the model. This model was then applied to simulate one-year natural Hg emissions in North America in 2002. The modelled results, compared to some reported natural Hg emission measurements, demonstrated a strong simulation ability. The spatial and temporal variations of emission fluxes were examined through numerical simulations. A pronounced diurnal cycle and a seasonal cycle were found in the emissions from most land uses. Compared with summer, natural Hg emission was significantly limited in winter. Simulation results showed that about 229 metric tons of total natural Hg

emission, 1.8 times anthropogenic Hg emission, was emitted from the simulation domain in 2002.

U.S. EPA CMAQ Hg model system was improved and then applied to simulate the emission, transport, transformation and deposition of atmospheric Hg in North America for the year 2002. The simulated results were compared with measured hourly Total Gaseous Hg (TGM) for 3 sites. The good agreement between them demonstrated the good performance of this improved model in modelling the behaviour of emission, transport, transformation and deposition of atmospheric Hg. Hg budget and net evasion of Hg in North America were also investigated.

A sensitivity analysis was conducted to assess the effects of emissions, including Hg and non-Hg emissions, on the air concentration and deposition of atmospheric Hg. The results indicated that ambient concentration of TGM was much more sensitive to Hg emissions than non-Hg emissions. Natural Hg emission was more significant than anthropogenic emission to affect ambient concentration of TGM, illustrating natural Hg emission is a key factor influencing TGM ambient concentration. Unlike TGM concentration, Hg dry deposition was not only sensitive to Hg emissions but also to non-Hg emissions such as VOCs and NO_x. Anthropogenic Hg emission, natural Hg emission and NO_x emission had almost the same effect on total dry deposition of Hg. The results also illustrated that Hg wet deposition was only sensitive to non-Hg emissions such as NO_x and VOCs, especially of VOCs emission. Because of the inverse effect of VOCs on Hg wet deposition, reducing NO_x emission should be an ideal solution to mitigate Hg wet deposition. A possible

pathway through which atmospheric Hg was greatly affected by emissions changes was identified: emissions of pollutants, especially VOCs and NO_x, greatly affect the level of OH in the atmosphere; OH influences the concentration and deposition of Hg by significantly affecting the gas phase reaction between Hg(0) and OH.

Acknowledgments

I would like to thank my advisor, Dr. James J. Sloan, for his scientific, financial and moral support through the completion of this thesis. Without his advice, motivation and dedication, this thesis simply would not have been possible.

Special thanks to Dr. Philip K. Gbor for his guidance on my thesis and his collaboration on parts of my thesis work. Dr. Philp K. Gbor and I worked together to develop the natural Hg emission model (Sections 3.2, 3.3, 3.5.1 of my thesis) and to modify the CMAQ-Hg Modelling system (Sections 2.3, 4.2.4, 4.2.5). The remaining work of the thesis was done by myself.

I would like to express my sincerest gratitude to the members of my thesis committee: Dr. Jacek Lipkowski, Dr. Tadeusz Gorecki and Dr. Rob Bloxam. Thanks for their guidance and invaluable comments on this thesis.

Thank Russ Bullock and Marc Houyoux of US EPA for providing their CMAQ-Hg model and Hg speciation profiles.

I wish to thank everyone in our research group for their great help and friendship. I also thank all people in the department of Chemistry who have provided me help and friendship over years.

Funding for this research was provided by Ontario Power Generation, Ontario Ministry of the Environment and the Ontario Research and Development Challenge Fund.

Finally, I would like to thank my family and friends for of all their support. I couldn't have done this without all of you.

Contents

1 Introduction **1**

1.1 Atmospheric mercury 1

1.1.1 Physical and chemical properties of Hg 1

1.1.2 Species of atmospheric Hg 4

1.1.3 Sources and emissions 6

1.1.4 Transport and transformation 13

1.1.5 Deposition 20

1.1.6 Environmental concerns 23

1.2 Modelling of Atmospheric Mercury 24

1.2.1 Modelling of transport and deposition of atmospheric Hg . . 25

1.2.2 Modelling of natural Hg emissions 43

1.3 Research Objectives 45

2 EPA CMAQ-Hg model system **48**

2.1 The standard CMAQ model system 48

2.2 Hg version of CMAQ model system (CMAQ-Hg) 54

2.3 Additions to CMAQ-Hg model system 57

2.3.1 Calculation of dry deposition of Hg(0) and Hg(II) 57

2.3.2 Natural mercury emissions 58

3 Development of a natural mercury emission model 60

3.1 Introduction 60

3.2 Theoretical consideration 62

3.3 Generation of natural mercury emission 76

3.4 Simulation procedure 77

3.4.1 Domain of simulation 77

3.4.2 Land use data 77

3.4.3 Meteorology conditions 79

3.4.4 Snow cover 80

3.4.5 Hg(0) concentrations 81

3.5 Results and discussions 82

3.5.1 Validation 82

3.5.2 Characteristics in modelled natural Hg emission 82

3.6 Summary and conclusions 97

4 Simulation of atmospheric Hg transport, transformation and deposition in North America 100

4.1 Introduction 100

4.2 Simulation procedures 102

4.2.1 Model description 102

4.2.2 Domain definition 102

4.2.3 Meteorological conditions 102

4.2.4 Initial and boundary conditions 103

4.2.5 Emissions 104

4.3 Simulation Results 107

4.3.1 Hg Emissions 107

4.3.2 Natural and anthropogenic emissions in different regions . . 107

4.3.3 Ambient mercury concentration 109

4.3.4 Dry deposition 114

4.3.5 Wet deposition 115
4.3.6 Total deposition 118
4.3.7 Net Evasion 121
4.3.8 Regional Hg budget 122
4.4 Summary and conclusions 122

5 A sensitivity analysis **126**
5.1 Introduction 126
5.2 Model description 127
5.3 Sensitivity simulations 128
5.4 Results of sensitivity analysis 130
5.4.1 Sensitivity of TGM 130
5.4.2 Sensitivity of Hg dry deposition 133
5.4.3 Sensitivity of Hg wet deposition 138
5.4.4 Discussion 146
5.5 Conclusions 147

6 Conclusions and recommendations **149**
6.1 Conclusions 150
6.2 Recommendations for future research 153

Bibliography **155**

List of Tables

1.1 Properties of Hg and selected mercury compounds (Schroeder and Munthe, 1998) . . . 3

1.2 Gas-phase reactions of mercury in the atmosphere . . . 16

1.3 Aqueous phase reactions of mercury in the atmosphere (Bullock and Brehme, 2002) . . . 18

2.1 Reactions and rate constants used by the latest CMAQ-Hg model (Bullock et al., 2002) . . . 55

3.1 Vegetation types and parameter values in the model . . . 69

3.2 Land uses and the fraction of each land use in the simulation domain 79

3.3 Physical options and configurations in MM5 simulation . . . 80

3.4 Some measured natural mercury emission fluxes . . . 83

3.5 Correlation between monthly total natural Hg emission and other factors . . . 89

3.6 Correlation coefficients (r) between natural Hg emissions from several land uses and other factors . . . 91

3.7 Total Hg emissions and average emission fluxes from different land covers in modelling domain for 2002 . . . 94

3.8 Monthly average and total natural Hg emissions in January and July for different land uses . . . 98

4.1 Reported anthropogenic and natural (including re-emission) mercury emissions (metric ton) . . . 110

4.2 Summary statistics for modelled and measured hourly TGM concentrations for different sites. . . . 113

4.3 Hg budget modelled within entire domain over the simulation period 123

5.1 The design of the sensitivity study 128

List of Figures

1.1 U.S. anthropogenic mercury emissions over past decades (U.S. EPA, 2006) 8

1.2 Anthropogenic mercury emissions: distributed by region in 1990 and 2000 (Cain, 2006) 9

1.3 Global mercury cycle schematic (Bullock, 2000a) 14

1.4 Physical and chemical transformation of mercury in the atmosphere (Bullock, 2003) 15

2.1 The components of the standard CMAQ modelling simulation . . . 49

2.2 The components of improved CMAQ-Hg modelling simulation . . . 56

2.3 The flow chart of the standard CMAQ modelling simulation and the incorporation of Natural Mercury Emission Model into MCIP . . . 59

3.1 Average snow cover fraction in January, 2002 76

3.2 The modelling domain 78

3.3 Land uses in modelling domain 78

3.4 Spatial distribution of soil Hg concentration in the simulation domain 82

3.5 Average natural Hg emission fluxes in the domain for different land covers in July, 2002 83

3.6 Spatial distribution of annual average natural Hg emission flux for 2002 84

3.7 Correlation between soil Hg concentration and annual average flux of natural Hg emission for 2002 85

3.8 Natural Hg emission flux averaged along longitude direction in the simulation domain 86

3.9 Average daily variation of natural Hg emissions for different land uses 87

3.10 coefficients (r) between natural Hg emission fluxes and solar radiation reaching surface 88

3.11 coefficients (r) between natural Hg emission fluxes and surface temperature 88

3.12 Monthly average natural Hg emission flux over the simulation domain in 2002 90

3.13 Monthly average of natural Hg emission fluxes from different land uses in the simulation domain in 2002 91

3.14 Monthly total natural Hg emissions from different land uses in the simulation domain in 2002 92

3.15 The contribution of each land use to 2002 total natural Hg emission 93

3.16 The contribution of each month to 2002 total natural Hg emission . 95

3.17 Ratio of average emission flux in July to that in January 96

4.1 Natural mercury emission flux averaged over whole simulation period 108

4.2 Anthropogenic Hg emission flux averaged over whole simulation period 108

4.3 Anthropogenic Hg emission distribution 109

4.4 Natural Hg emission flux for regions A and B in Figure 4.3 111

4.5 Modelled and measured hourly TGM for Point Petre for 2002. (a) January to March, (b) April to June, (c) July to September (d) October to December. 112

4.6 Location of sites used to compare model results with measurements. All the sites are wet mercury deposition sites used except the three sites labelled B, E and P which are TGM measurement sites. B is Burnt Island (45°49´42″/ 82°56´53″W, 184 m above sea level), E is Egbert (44°43´57″N / 79°46´53″, 251 m above sea level), and P is Point Petre (43°50´34″N / 77°09´13″W, 78 m above sea level). . . . 114

4.7 Spatial distribution of average TGM ambient concentration 115

4.8 Spatial distribution of annual total dry deposition 116

4.9 Average dry deposition velocity of Hg(0) 116

4.10 Average dry deposition velocity of Hg(II) 117

4.11 Correlation between model and measurements for weekly mercury wet precipitation for all data 118
4.12 Correlation between model and measurements for weekly mercury wet precipitation for data for which model precipitation depth is within a factor of two of measurement 119
4.13 Total wet deposition during the simulation period (2002) 119
4.14 Total precipitation during the simulation period (2002) 120
4.15 Total deposition of Hg during the simulation period 120
4.16 Annual net Hg emission flux over whole simulation period 121

5.1 Percentage changes in domain-averaged surface TGM concentration resulting from (a) -50% emissions changes, and (b) +50% emissions changes. 129
5.2 Percentage changes in average (a) TGM, (b) Hg(0) and (c) Hg(II) concentration resulting from ±50% emissions changes 132
5.3 Spatial distribution of percentage changes in TGM concentration resulting from (a) -50%, and (b) 50% natural Hg emissions changes 133
5.4 Percentage changes in total dry deposition for the whole domain resulting from (a) -50% emissions changes, and (b) +50% emissions changes. 134
5.5 Percentage changes in total (a) TGM, (b) Hg(0), (c) Hg(II) and (d) Hg(p) dry deposition resulting from ±50% emissions changes 135
5.6 Spatial distribution of percentage changes in dry deposition of Hg resulting from (a) -50%, and (b) 50% anthropogenic Hg emissions changes 137
5.7 Spatial distribution of percentage changes in dry deposition of Hg resulting from (a) -50%, and (b) 50% natural Hg emissions changes 137
5.8 Spatial distribution of percentage changes in dry deposition of Hg resulting from (a) -50%, and (b) 50% NO_x emissions changes 137
5.9 Spatial distribution of percentage changes in dry deposition of Hg resulting from (a) -50%, and (b) 50% VOCs emissions changes . . . 138
5.10 Percentage changes in total wet deposition for the whole domain resulting from (a) -50% emissions changes, and (b) +50% emissions changes. 139

5.11 Percentage changes in total (a) TGM, (b) Hg(0), (c) Hg(II) and (d) Hg(p) wet deposition resulting from ±50% emissions changes 141

5.12 Spatial distribution of percentage changes in wet deposition of Hg resulting from (a) -50%, and (b) 50% NO_x emissions changes 142

5.13 Spatial distribution of percentage changes in wet deposition of Hg resulting from (a) -50%, and (b) 50% VOCs emissions changes . . . 142

5.14 Percentage changes in average OH concentration for the whole domain resulting from (a) -50% emissions changes, and (b) +50% emissions changes. 143

5.15 Percentage changes in average O_3 concentration for the whole domain resulting from (a) -50% emissions changes, and (b) +50% emissions changes. 144

5.16 Percentage changes in average H_2O_2 concentration for the whole domain resulting from (a) -50% emissions changes, and (b) +50% emissions changes. 145

List of Symbols and Abbreviations

Symbol or Abbreviation	Description
a,b	Constants
ADOM	**A**cid **D**eposition and **O**xidant **M**odel
AER	**A**tmospheric and **E**nvironmental **R**esearch
AMAP	**A**rctic **M**onitoring and **A**ssessment **P**rogramme
API	**A**pplication **P**rogramming **I**nterface
ASTRAP	**A**dvanced **S**tatistical **T**rajectory **R**egional **A**ir **P**ollution model
BCON	**B**oundary **CON**ditions
BEIS2	Version **2** of the **B**iogenic **E**missions **I**nventory **S**ystem
BEIS3	Version **3** of the **B**iogenic **E**missions **I**nventory **S**ystem
CAM	**C**hemistry of **A**tmospheric **M**ercury
CAMNet	**C**anadian **A**tmospheric **M**ercury Measurement **Net**work
CAMx	**C**omprehensive **A**ir Quality **M**odel with e**x**tensions
CB-IV	**C**arbon **B**ond-**IV** Mechanism
CCTM	**C**MAQ **C**hemistry **T**ransport **M**odel
Cl^*	Chloride atom radical
Cl_2	Chlorine molecule
CMAQ	**C**ommunity **M**ultiscale **A**ir **Q**uality model
CO	Carbon oxide
c_p	Specific heat of the air (MJ°C/kg)
C_s	Hg(0) concentration in the surface soil solution (ng/m^3)

Symbol or Abbreviation	Description
CTM	**C**hemical **T**ransport **M**odel
C_w	Concentration of dissolved gaseous mercury in the water
d	Zero-plane displacement height
D	Diffusivity of Hg(0) in water, cm^2/s
D_0	Vapour pressure deficit of the air
DEHM	**D**anish **E**ulerian **H**emispheric **M**odel
DGM	**D**issolved **G**aseous **M**ercury
DMM	Dimethylmercury
DOM	**D**issolved **O**rganic **M**atter
E_c	Canopy transpiration rate (m/s)
E_{cs}	Canopy transpiration rate without considering rain
EMAP	**E**ulerian **M**odel for **A**ir **P**ollution
EMC	**E**nvironmental **M**odelling **C**enter
EMEP	**E**uropean **M**onitoring and **E**valuation **P**rogram
EPA CMAQ-Hg	US EPA **C**ommunity **M**ultiscale **A**ir **Q**uality Mercury model
EPRI	**E**lectric **P**ower **R**esearch **I**nstitute
EU	**E**uropean **U**nion
F^*	Fluoride atom radical
F_1	Effect of photosynthetically active radiation on canopy resistance
F_2	Effect of soil water stress on the canopy resistance
F_3	Effect of the vapour pressure deficit on canopy resistance
F_4	Effect of air temperature on canopy resistance
F_c	Elemental Hg emission flux from canopy
f_G	Dimensionless number accounting for the heat flux density G into the ground
F_s	Mercury emission flux from soil
F_w	Hg emission flux from water
G	Soil heat flux
GEM	**G**lobal **E**nvironment **M**ultiscale
GKSS TCM	**T**ropospheric **C**hemical **M**odule of German research center **G**esellschaftfur **K**ernenergieverwertung in **S**chiffbau und **S**chiffahrt (GKSS)

Symbol or Abbreviation	Description
GMT	**G**reenwich **M**ean **T**ime
GRAHM	**G**lobal/**R**egional **A**tmospheric **H**eavy **M**etals Model
h_c	Height of canopy
Hg_2Cl_2	Mercurous chloride
H_2O_2	Hydrogen peroxide
Hg(0)	Elemental mercury
Hg(II)	Gaseous divalent mercury
Hg^{2+}	Mercury (II) or mercuric ion
Hg(p)	Particulate mercury
$HgCl_2$	Mercuric chloride
$Hg(NO_3)_2$	Mercuric nitrate
HgO	Mercuric oxide
$Hg(OH)_2$	Mercury(II) hydroxide
$HgOH^+$	Mercury(II) hydroxide ion
HgS	Mercuric sulfide
$[Hg]_s$	Mercury soil concentration
$HgSO_3$	Mercury(II) sulfite
HO^*	Hydroxyl radical
HO_2^*	Hydroperoxyl radical
HO_x	H, HO and HO_2
HPC	**H**igh **P**erformance **C**omputing
HYSPLIT	**H**ybrid **S**ingle **P**article **L**agrangian **I**ntegrated **T**rajectory model
I/O	**I**nput/**O**utput
ICON	**I**nitial **CON**ditions
IDA	**I**nventory **D**ata **A**nalyzer
IVL CAM	**C**hemistry of **A**tmospheric **M**ercury model of the Swedish environmental research institute
JPROC	**J**-values (Photolysis rate) **PROC**essor
k	Rate constant
k_w	Mass transfer coefficient
LAI	Leaf Area Index
MBR	**M**odified **B**owen **R**atio
MCIP	**M**eteorological **C**hemistry **I**nterface **P**rocessor
MCNC	**M**icroelectronics **C**enter of **N**orth **C**arolina
MDN	**M**ercury **D**eposition **N**etwork
MeHg	Methylmercury

Symbol or Abbreviation	Description
MM5	Fifth-Generation NCAR/Penn State **M**esoscale **M**odel
MOGUNTIA-Hg	Mercury version of the **M**odel **O**f the **G**lobal **U**niversal **T**racer Transport **I**n the **A**tmosphere
MSC	**M**eteorological **S**ervice of **C**anada
MSCE	**M**eteorological **S**ynthesizing **C**entre-**E**ast
MSC-E HM	**M**eteorological **S**ynthesizing **C**entre "**E**ast" **H**eavy **M**etal model
NADP	**N**ational **A**tmospheric **D**eposition **P**rogram
NEI	**N**ational **E**missions **I**nventory
NH_3	Ammonia
NMEM	**N**atural **M**ercury **E**mission **M**odel
NO_3^*	Nitrogen trioxide radical
NO_x	Nitrogen oxides
NOAA	**N**ational **O**ceanic and **A**tmospheric **A**dministration
O_3	Ozone
$O(^3P)$	Oxygen atom (triplet)
OH^-	Hydroxide ion
OMOE	**O**ntario **M**inistry **O**f **E**nvironment
RELMAP	**R**egional **L**agrangian **M**odel of **A**ir **P**ollution
p	Atmospheric pressure (kP_a)
P	Precipitation
PBL	**P**lanetary **B**oundary **L**ayer
PM	**P**articulate **M**atter
PM2.5	**P**articulate **M**atter less than **2.5** microns in diameter
PM10	**P**articulate **M**atter **10** microns or less in diameter
r_a	Aerodynamic resistance
r_{ac}	Aerodynamic resistance of canopy
RADM	**R**egional **A**cid **D**eposition **M**odel
RADM2	Version **2** of **R**egional **A**cid **D**eposition **M**odel
REMSAD	**R**egional **M**odelling **S**ystem for **A**erosols and **D**eposition
r_c	Bulk canopy resistance
R_G	Flux of visible solar radiation
R_{Gc}	Solar radiation reaching the soil under the canopy

Symbol or Abbreviation	Description
R_{GL}	Visible solar radiation flux for which F_1 is about double its minimum value
$R_L \downarrow$	Long-wave downward irradiance
R_n	Net radiation above the canopy
$R_s \downarrow$	Short-wave downward irradiance
R_{smax}	Cuticular resistance of the leaves
R_{smin}	Minimum stomatal resistance
SAQM	**S**armap **A**ir **Q**uality **M**odel
SCAM	**S**implified **C**anopy-**A**tmosphere **M**odel
Sc_w	Schmidt numbers
SMOKE	**S**parse **M**atrix **O**perator **K**ernel **E**mission
SO_2	Sulfur dioxide
SO_4^{2-}	Sulfuric acid ion
SST	**S**ea **S**urface **T**emperature
T_1	Air temperature at z_1
TEAM	**T**race **E**lement **A**nalysis **M**odel
TGM	**T**otal **G**aseous **M**ercury
T_h	Air temperature at height of h (℃)
T_s	Soil temperature
U_{10}	Wind speed at 10m
u_a	Wind speed at reference Height z
UAM	**U**rban **A**irshed **M**odel
UNEP	**U**nited **N**ations **E**nvironment **P**rogramme
U.S. ATSDR	**U.S. A**gency for **T**oxic **S**ubstances and **D**isease **R**egistry
U.S. EPA	**U.S. E**nvironmental **P**rotection **A**gency
USGS	**U.S. G**eological **S**urvey
VOCs	Volatile organic compounds
W_{fr}	Power function of the moisture content of the interception reservoir
W_r	Interception of rainfall
W_r^{max}	Water holding capacity (mm)
z_{0h}	Roughness length for heat and water vapour transfer
z_{0m}	Roughness length for momentum
α	Factor affecting transpiration rate due to rain
α_c	Canopy albedo
β	A constant
γ	Psychrometric constant ($kP_a/°C$)
δ	Fraction of vegetation

Symbol or Abbreviation	Description
ϵ_c	Canopy emissivity
η	A constant
θ	Mean volumetric water in the root zone
θ_{cr}	Moisture content below which transpiration is stressed by soil moisture
θ_{sat}	Satured soil moisture
θ_{wilt}	Soil moisture at wilting point
κ	Von-Karman's constant
μ	A constant (0.2)
$\triangle$	First-order derivative of saturation vapour pressure with temperature ($kP_a/°C$)
ρ	Mean air density at constant pressure
σ	Stefan-Boltzman constant
ν	Kinetic viscosity of water, cm^2/s

Chapter 1

Introduction

1.1 Atmospheric mercury

1.1.1 Physical and chemical properties of Hg

Mercury has been recognized for decades as a persistent and bio-accumulative toxic substance in the environment. The investigation of mercury behaviour in the environment is a field of particular concern due to its wide distribution in the different environmental compartments (Fitzgerald and Clarkson, 1991).

Elemental mercury is known as the only common metal existing as liquid at ordinary temperature and pressure. It has low vapour pressure (0.25 Pa at 25 °C) (Hsi et al., 1998), low melting point (Table 1.1) and the highest solubility in water (Table 1.1) of any metal, therefore, it is very mobile and persistent in the environment, readily released from soil, water and plant canopies, transported in the air

and deposited back to the earth's surface. Other properties of mercury such as relatively poor thermal conductivity, good electric conductivity, the ability to expand and contract evenly with temperature changes, the ability to easily form alloys with other metals, and high surface tension make it widely used in the manufacture of industrial chemicals and electric and electrical applications, some of which have been identified as the important sources of anthropogenic mercury emission into the environment.

Inorganic mercury compounds include mercuric sulfide (HgS), mercurous chloride (Hg_2Cl_2), mercuric chloride ($HgCl_2$), mercuric nitrate ($Hg(NO_3)_2$) and mercuric oxide HgO. Mercuric chloride is the major part of inorganic mercury compounds (U.S. EPA, 1999). Most inorganic mercury compounds are white powders or crystals, and are unstable when exposed to heat and light and readily decompose to elemental mercury. Some mercury salts such as $HgCl_2$ are volatile enough to evaporate into the atmosphere at room temperature and pressure. However, their high water solubility and chemical reactivity make them deposit from the atmosphere more rapidly than elemental mercury.

Organic mercury compounds, sometimes called organomercurials, are those containing covalent bonds between carbon and mercury. Examples are methylmercury, dimethylmercury and methylmercury chloride (methylmercuric chloride). Organic mercury compounds include a large number of compounds, however, methylmercury is by far the most toxic and prevalent form of organic mercury compound in the environment (Storelli et al., 1998).

Elemental mercury has been found to have many diverse and unique properties.

	Hg^0	$HgCl_2$	HgS	HgO	$(CH_3)_2Hg$
Melting point (°C)	-39	277	584 sublimation	500 decomposition	-
Boiling Point (°C) at 1atm	356 at 1atm	303	-	-	96 at 1atm
Water Solubility (g/l)	49.4×10^{-6} (20°C)	66 (20°C)	2×10^{-24} (25°C)	5.3×10^{-2} (25°C)	2.95 (24°C)
Vapour pressure(Pa)	0.180 (20°C)	8.99×10^{-3} (20°C)	-	9.2×10^{-12} (25°C)	8.3×10^3 (25°C)

Table 1.1: Properties of Hg and selected mercury compounds (Schroeder and Munthe, 1998)

It has been widely used for the manufacture of industrial chemicals or for electrical and electronic applications such as thermometers, barometers, diffusion pumps, coulometers, some gaseous electron tubes, fluorescent lamps, mercury switches, pesticides, dental amalgams, anti-fouling paint, electrodes and batteries.

Mercuric chloride (corrosive sublimate, $HgCl_2$) is used as an insecticide, in rat poison, and as a disinfectant. Mercuric oxide is used in skin ointments. It is also used as a material for anodes for mercury batteries. Mercuric sulfate is used as a catalyst in organic chemistry. Vermilion, a red pigment, is mercuric sulfide. Although most agricultural and pharmaceutical uses of inorganic mercury have been discontinued in the United States, mercuric chloride is still used as a catalyst or reagent in various reactions, and to a lesser extent as a disinfectant or pesticide (U.S. EPA, 1994; U.S. ATSDR, 1999). Methyl-mercury has no industrial uses; it is formed in the environment from the methylation of the inorganic mercurial ion (U.S. ATSDR, 1999). Ethylmercury compounds are often used as fungicides.

1.1.2 Species of atmospheric Hg

There are three main species of mercury occurring in the atmosphere: elemental mercury, gaseous divalent mercury and particulate mercury.

Elemental mercury (Hg(0))

Hg(0) has been found to be the predominant form of the gaseous phase mercury, accounting for 90% in the atmosphere (Schroeder et al., 1991). It is present globally in ambient air at concentrations on the order of 1.5-2.0 ng/m^3. The least water-

reactivity of Hg(0) among the atmospheric species of mercury allows it to persist in the atmosphere with a lifetime of 1-2 years (Lindqvist and Rodhe, 1985; Slemr et al., 1985) and transport globally, making it a true global pollutant. Evidence indicates that the concentration of Hg(0) in the atmosphere has been increasing over the past century as a result of anthropogenic activities, and 50-75 percent of this increase originates from anthropogenic sources (Expert Panel on Mercury Atmospheric Processes, 1994). Removal occurs by dry or wet deposition after oxidation of Hg(0) to Hg(II) in cloud droplets. Hg(0) is transported back to the earth's surface mainly through dry deposition.

Gaseous divalent mercury (Hg(II))

Hg(II) constitutes about 1-3% of total gaseous mercury in the atmosphere (Lindberg and Stratton, 1998). It is believed that the most part of Hg(II) consists of mercury dichloride ($HgCl_2$), but other divalent Hg species are also possible (Munthe et al., 2003). Hg(II) is likely to be rapidly scavenged via dry and wet deposition processes within roughly 100 to 1000 kilometers as a result of its high water-solubility and chemical reactivity, therefore, it has a much shorter life (from a few days to a few weeks) than elemental gaseous mercury. Air concentrations of Hg(II) are likely to be highly variable spatially and temporally and related to local sources, meteorological conditions and some other pollutants (Poissant et al., 2005). To date, only few attempts have been made for atmospheric mercury speciation measurements (Johnson and Braman, 1974; Lindberg and Stratton, 1998; Malcolm and Keeler, 2002; Poissant et al., 2004).

Particulate Mercury (Hg(p))

Hg(p) occurs in both gaseous and aqueous phases. It can be formed by physical adsorption of Hg(II) to atmospheric particulate matter in aqueous phase as the secondary particulate mercury. It can also be emitted directly into the atmosphere from anthropogenic and natural sources. However, it is largely of anthropogenic origin (Xiao et al., 1991). Background concentrations of Hg(p) indicated that Hg(p) was a minor constituent (0.39% of total gaseous mercury (Slemr et al., 1985)) except in industrialized regions (up to 40% of total gaseous mercury (Lamborg et al., 1994)). Hg(p) tends to be dry deposited at significant rates when and where measurable concentrations of these mercury species exist. The deposition velocity of Hg(p) is dependent on atmospheric conditions and particle size. Hg(p) is also assumed to be subject to wet deposition due to scavenging by cloud and subsequent precipitation.

1.1.3 Sources and emissions

Mercury is released into the environment from a variety of sources. In this thesis, I refer to the sources of mercury as natural, anthropogenic and re-emission. Natural mercury emission is defined as the mobilization or release of geologically bound mercury by natural processes, with mass transfer of mercury to the atmosphere; Anthropogenic mercury emission is the mobilization or release of the mercury by human activities, with mass transfer of mercury to the atmosphere; Re-emitted mercury is the mass transfer of mercury to the atmosphere by the processes drawing on mercury that was deposited to the earth's surface after initial mobilization by

either anthropogenic or natural activities (U.S. EPA, 1997). In the following chapters of this thesis, the term "natural Hg emission" refers to all non-anthropogenic Hg emissions, including natural and re-emitted, as defined in the above.

Anthropogenic sources

A large portion of the mercury present in the atmosphere today is the result of many years of releases due to anthropogenic activities. The natural component of the total atmospheric burden is difficult to estimate, although anthropogenic releases of mercury to the atmosphere were estimated to cause a three-fold increase in its concentration in air and marine surface waters since the pre-industrial era (Allan, 1996).

Chlor-alkali plants were thought to be the single largest source category of anthropogenic Hg emissions to the environment in many industrialized countries until the 1970s (Schroeder and Munthe, 1998). After that, its ranking among the remaining source categories has been substantially changed due to antipollution measures. Coal combustion, waste incineration, metal smelting, refining and manufacturing are currently major source categories in the industrialized world (Schroeder and Munthe, 1998).

Canadian anthropogenic mercury emissions were reduced from approximately 32 to 8 Metric tons from 1990 to 2000. The largest source of mercury prior to 1995 was base metal mining industry. From 1995 to 2000, electricity generation and metal smelting were equally the largest sources of mercury into the atmosphere, each accounting for 25% of Canadian emissions (Environment Canada, 2006).

U.S. Emissions of mercury to the air from anthropogenic sources have fallen by more than 45% since passage of the 1990 Clean Air Act Amendments (Figure 1.1). These amendments provided new authority to EPA to reduce emissions of mercury and other toxic pollutants to the air (U.S. EPA, 2006).

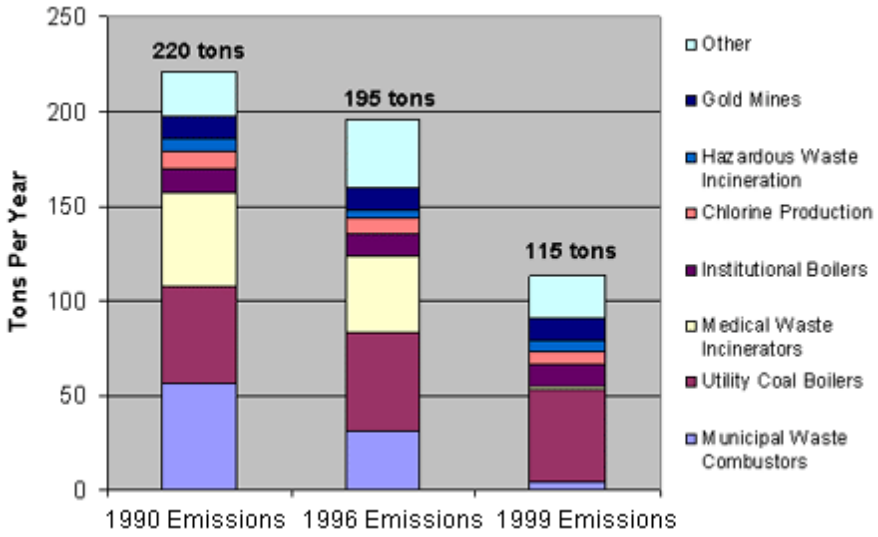

Figure 1.1: U.S. anthropogenic mercury emissions over past decades (U.S. EPA, 2006)

Anthropogenic emissions from a number of major sources have been estimated to be decreasing in North America and Europe due to reduction efforts during the last decade, while the anthropogenic emissions from some developing countries have been increasing dramatically over past ten years (Figure 1.2). Asia was the biggest anthropogenic mercury emission region, accounting for about 46% of the global anthropogenic budget in recent years.

Anthropogenic sources of mercury to the atmosphere can be quantified with relative ease. To date, a large number of studies have investigated and quantified

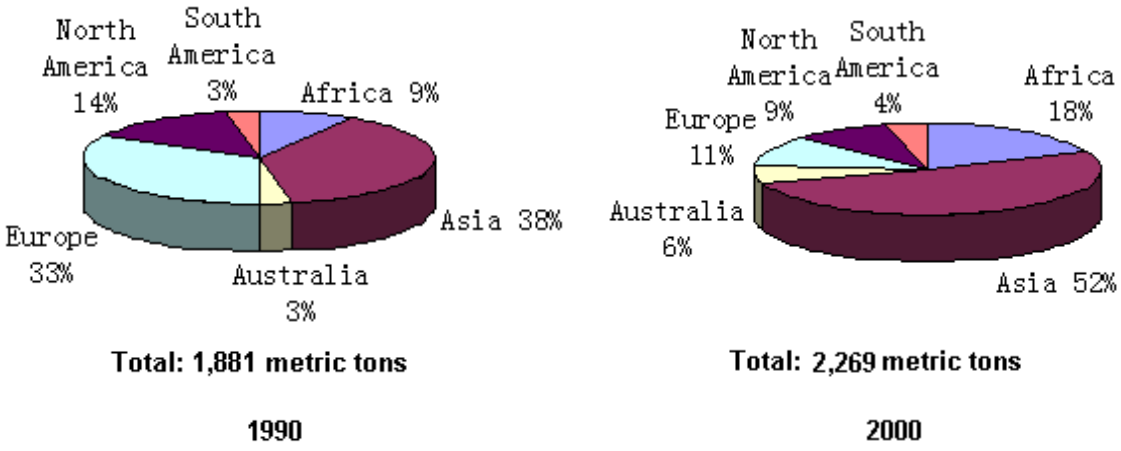

Figure 1.2: Anthropogenic mercury emissions: distributed by region in 1990 and 2000 (Cain, 2006)

anthropogenic mercury emissions. However, there are considerable uncertainties still existing in the estimation of anthropogenic mercury emission. For example, an emission factor-based approach, used during the investigation of most anthropogenic source categories, was thought to produce some inexact emission estimates. Uncertainties were produced when estimating emission factors, control efficiencies and the activity level measures. Further uncertainty in the emission estimates may be added by the sources of information used on source activity levels, which vary in reliability (U.S. EPA, 1997).

Natural sources

Mercury is a naturally occurring element in earth's crust with an average abundance of 0.5 ppm (μg/g) (Schroeder and Munthe, 1998). Low levels of mercury can be found everywhere in the environment - in rocks, plants, animals, water and the

air. High temperature in the Earth mantle results in high mercury mobility and mercury continuously diffuses to the surface. Elemental and some forms of oxidized mercury come to the atmosphere due to their volatility. Some natural processes (volcanic activity, deposition of Hg) can result in higher concentrations of mercury in certain compartments within the natural environment (Pollution Probe, 2006).

Mercury can also be emitted into the air through natural weathering and erosion or through the transpiration of plant canopy. Natural mercury emission sources include volcano eruption, re-emission of deposited mercury, degassing of the earth's mantle/crustal material, evasion from soil, water, vegetation surfaces, wild fires, and geothermal sources.

Active volcanoes release prodigious quantities of volatile materials into the atmosphere in the form of gases and aerosol. Pyle and Mather (2003) estimated that the time-averaged volcanic Hg emission is about 700 Mg/yr, or 20-40% of total natural emissions. Continuous degassing accounts for only 10% of this flux, while 75% of volcanic Hg is released during smaller sporadic eruptions (<10-102 Mg/event). Rare, large (>103 Mg) explosive eruptions overwhelm the total atmospheric burden several times per century, and account for about 15% of total volcanic Hg emissions. However, the extent of the volcanic contribution to global Hg budgets remains highly uncertain. Due to this uncertainty, current atmospheric mercury modelling studies ignored the volcanic contribution of mercury.

Emission from surficial soil, water and vegetation surfaces is another important pathway. Several estimates of natural mercury emission have been made (Mason et al., 1994; Seigneur et al., 2001), but the estimates differ significantly. Earth

surfaces might act as dynamic exchange interfaces which can be sources or sinks of atmospheric mercury depending on ambient Hg concentration, Hg deposition velocities, micro-meteorological conditions and Hg concentration in the transpiration stream (Hanson et al., 1995), water or soil. Lindberg and Stratton (1998) reported that a background deciduous forest in the southeastern United States exhibited bidirectional Hg(0) fluxes, and that the recorded emission fluxes exceeded those of deposition. The author suggested that atmospheric exchange of Hg(0) was the dominant flux in the forest. Mercury flux measurements over vegetation have indicated that foliar emission of Hg is more significant than emission from soil or water. Mercury emission flux from water was found to be strongly correlated to the intensity of solar radiation and water temperature which were factors that induce the conversion of divalent mercury into elemental mercury in water (Feng et al., 2004). Air-soil exchange might be highly dependent on soil temperature and the mercury concentration gradient between the TGM in the soil and the ambient TGM above the soil surface (Gillis and Miller, 2000). Wet soil decreases soil absorption, thus maintains higher rates of soil TGM emission. Emissions increased with increasing soil water, peaked at approximately field water capacity, and then decreased slightly until saturation. Other studies showed that solar radiation and soil temperature were the important factors influencing air-soil exchange flux (Carpi and Lindberg, 1998).

Mercury can be taken up by the roots of trees and later released to the environment when that wood is burned in a stove or a forest fire. Emission of mercury due to biomass burning is currently being studied. Veiga et al. (1994) reported on mercury release in biomass burning in Brazil and noted that fuel containing 40 ng/g

mercury resulted in unburned material containing 32 ng/g mercury, indicating at least partial release of mercury. Artaxo et al. (2000) measured TGM and Hg(p) in ambient air over the Amazon basin. Brunke et al. (20001) measured mercury in the plume of a wildland fire in South Africa and estimated the global contribution to the atmospheric budget to be as high as 1×10^6 kg/yr.

Other pathways of evasion of mercury include emission from the bottom of the oceans, from geothermal or tectonically active areas and anthropogenic activities. To date, considerable uncertainties still remain in the estimations of the quantitative significance of evasion. Too little has been known about the amounts of mercury evading from soil, water and vegetation, and about the factors associated with this process.

The sources of natural mercury emission can be identified, and a number of attempts have been made to estimate the regional and global natural emissions of mercury (Fitzgerald et al., 1986; Lindqvist et al., 1991; Mason et al., 1994; Nriagu and Pacyna, 1988; Pacyna and Pacyna, 1996; Pirrone et al., 2001). However, estimates of the emission vary widely. Lindqvist et al. (1991) estimated that global emission of mercury from natural sources was between 2000 and 9000 Mg/yr, while Nriagu (1989) estimated that natural emissions to the atmosphere contribute as much as 2.5 million kilograms per year.

Current emissions of mercury from soil, water and vegetation not only include emission of mercury which naturally exists in the substrates but also include re-emission of previously deposited mercury from anthropogenic sources (UNEP chemicals, 2002). This makes it very difficult to discriminate actual natural emissions

from re-emission.

There has been considerable debate on the relative contributions of mercury from natural sources versus releases from human activity. The challenge with this debate is the lack of accurate information on mercury emissions, past and present. Estimates of mercury emissions to the global atmosphere indicated that the contribution from industrial sources ranged from 1660 Mg/yr (1990 estimate by Pacyna and Pacyna (1996)) to 2200 Mg/yr (1992 estimate by Pirrone et al. (1996)), whereas emissions from natural sources might represent the major (up to 60% of the total) contribution to the global atmospheric mercury budget.

1.1.4 Transport and transformation

Atmospheric emissions are a major concern with respect to the mercury entering the environment. Hg released to the atmosphere is transported, transformed, and deposited back to the earth's surface (Figure 1.3). The distance of Hg transport depends upon the chemical form of the emitted Hg, the height of the emissions, the chemical and physical processes, and the atmospheric conditions (e.g., wind speeds, precipitation, composition of oxidizing and reducing species).

Atmospheric transport is likely the primary mechanism by which Hg(0) is distributed throughout the environment. Elemental Hg emitted high above the ground can persist in the atmosphere up to a year or more and be transported around the world due to its low chemical reactivity and low water solubility. However, the reactive form of Hg can be deposited to land or water surfaces much closer to the sources due to its high chemical reactivities and high water solubility. Airborne

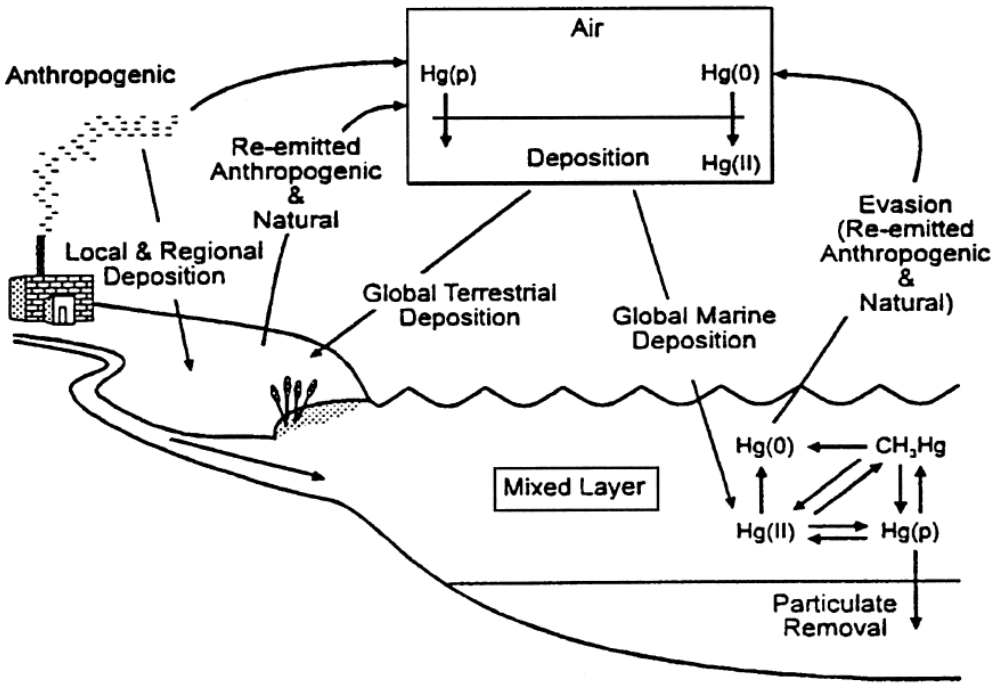

Figure 1.3: Global mercury cycle schematic (Bullock, 2000a)

mercury can also undergo chemical reactions which may significantly affect the life time of atmospheric mercury. Hg(p) is likely to be transported and deposited at an intermediate distances depending on aerosol diameter or mass.

Before Hg is deposited back to the earth's surfaces, a series of complex physical and chemical transformations of Hg can take place in the atmosphere. The transformations include the equilibria of Hg species among gaseous, aqueous and solid phases, the aqueous phase chemistry of Hg, and the gaseous phase chemistry of Hg (Figure 1.4).

Gas-liquid equilibria The gas-liquid equilibria of Hg species are governed by Henry's law. Although Hg(0) is the dominant constitute of atmospheric Hg, since

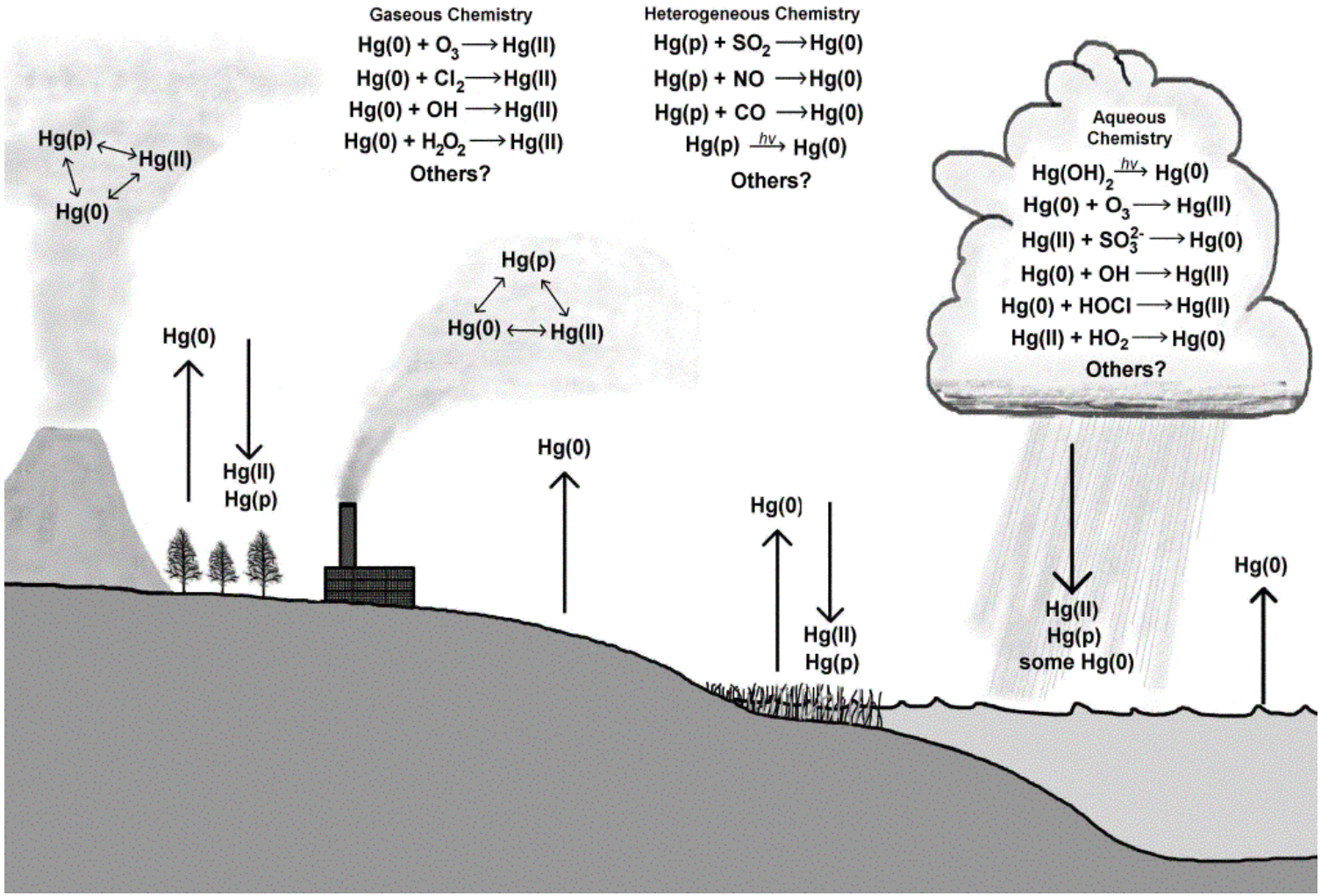

Figure 1.4: Physical and chemical transformation of mercury in the atmosphere (Bullock, 2003)

the Henry's law constant for Hg(0) is quite small, the cloud-water concentration of Hg(0) in Henry's equilibrium with gaseous Hg(0) range only from 1.3 to 5.3 $\times 10^{-14}$ M (Lin and Pehkonen, 1999), which is relatively low compared to the total dissolved and absorbed Hg(II). In contrast, the Henry's law constants for $Hg(OH)_2$ and $HgCl_2$ are 4 and 6 orders of magnitude bigger than that for Hg(0). Solid Hg species are not likely present in atmospheric water given the low atmospheric concentration of mercury (Lin and Pehkonen, 1999). The quantitative description of gas-solid equilibria is rather limited due to uncertain nature of atmospheric particles.

Gas phase reactions

Table 1.2 summarizes the important reactions identified to be relevant to the gas-phase chemistry of mercury.

Reaction	Rate $(cm^{-3}molec^{-1}s^{-1})$	Reference
$Hg^0_{(g)} + O_{3(g)} \rightarrow HgO_{(g,s)}$	$(3.0 \pm 2) \times 10^{-19}$	Hall, 1995
$Hg^0_{(g)} + H_2O_{2(g)} \rightarrow HgOH_{2(g,s)}$	8.5×10^{-19}	Tokos et al., 1998
$Hg^0_{(g)} + Cl_{2(g)} \rightarrow HgCl_{2(g,s)}$	4.8×10^{-18}	Calhoun and Prestbo, 2001
$Hg^0_{(g)} + HO^*_{(g)} \rightarrow Hg^{2+}_{(g,s)}$	8.7×10^{-14}	Sommar et al.,2001
$Hg^0_{(g)} + HCl_{(g)} \rightarrow$ products	1.0×10^{-19}	Hall et al., 1993
$Hg^0_{(g)} + NO^*_{3(g)} \rightarrow$ products	4.0×10^{-15}	Sommar et al., 1997
$Br_{(g)} + Hg^0_{(g)} \rightarrow$ products	4.0×10^{-15}	Sommar et al., 1997
$Br_{2(g)} + Hg^0_{(g)} \rightarrow$ products	4.0×10^{-15}	Sommar et al., 1997
$BrO_{(g)} + Hg^0_{(g)} \rightarrow$ products	4.0×10^{-15}	Sommar et al., 1997

Table 1.2: Gas-phase reactions of mercury in the atmosphere

The only important gaseous reaction globally identified so far is that between Hg(0) and O_3 with an expected lifetime of 1.4 years at an ozone concentration of 30

ppb (Sommar et al., 2001). This is in the range of current estimates of the residence time of Hg(0) in the atmosphere, classifying mercury as a global pollutant (Bergan et al., 1999; Lindqvist and Rodhe, 1985; Mason et al., 1994; Shia et al., 1999; Slemr et al., 1995). Schroeder et al. (1991) suggested that O_3 and Cl_2 may be important oxidants of Hg(0), while SO_2 and CO may be important reductants of Hg(II). Both oxidation of Hg(0) and reduction of Hg(II) by H_2O_2 are thermodynamically favourable, although H_2O_2 has been reported to be incapable of oxidizing Hg(0) directly (Wigfield and Perkins, 1985). The gaseous phase reactions of Hg with HO^*, HO_2^*, and Cl deserve additional experimental investigation, since these species have been shown to readily react with various mercury species in aqueous phase (Lin and Pehkonen, 1999). Recent work in the Arctic involving springtime depletion of atmospheric Hg(0) may involve reactive chlorine or bromine species and may aid in determining the relative importance of these gas-phase oxidation reactions (Schroeder and Munthe, 1998). In general, gas-phase reactions of Hg appear to be of minor importance to its oxidation state as compared to its aqueous-phase reactions (Bullock and Brehme, 2002).

Aqueous phase reactions

Aqueous phase reactions of mercury or mercury compounds occur in rainwater, cloud-water or fog-water in the atmosphere. Table 1.3 summarizes the important reactions identified to be relevant to aqueous phase chemistry of mercury.

Oxidations of dissolved Hg(0) in cloud droplets by O_3, hydroxyl radical (HO^*) and chlorine ($HOCl/OCl^-$) lead to the formation of Hg(II) in rain or cloud water, which may then be removed from the atmosphere on shorter time scales. Elemental

Reaction	Rate	Reference
$Hg^0_{(aq)} + O_{3(aq)} \rightarrow Hg^{2+}_{(aq)} + \text{products}$	$4.7 \times 10^7 M^{-1}s^{-1}$	Munthe(1991)
$HgSO_{3(aq)} \rightarrow Hg^0_{(aq)} + \text{products}$	$Texp((31.971T) - 12595T)Ts^{-1}$	Van Loon et al.,(2000)
$Hg(OH)_{2(aq)} + h\nu \rightarrow Hg^0_{(aq)} + \text{products}$	$6.0 \times 10^{-7}s^{-1}(maximum)^a$	adapted from Xiao et al.,(1994)
$Hg^0_{(aq)} + OH_{(aq)} \rightarrow Hg^{2+}_{(aq)} + \text{products}$	$2.0 \times 10^9 M^{-1}s^{-1}$	Lin and Pehkonen(1997)
$Hg^{2+}_{(aq)} + HO_{2(aq)} \rightarrow Hg^0_{(aq)} + \text{products}$	$4.7 \times 10^7 M^{-1}s^{-1}$	Pehkonen and Lin(1998)
$Hg^0_{(aq)} + HOCl_{(aq)} \rightarrow Hg^{2+}_{(aq)} + \text{products}$	$2.09 \times 10^6 M^{-1}s^{-1}$	Lin and Pehkonen(1998)
$Hg^0_{(aq)} + OCl^-_{(aq)} \rightarrow Hg^{2+}_{(aq)} + \text{porducts}$	$1.99 \times 10^6 M^{-1}s^{-1}$	Lin and Pehkonen(1998)
$Hg^0_{(aq)} + H_2O_{2(aq)} \rightarrow HgO_{(s)} + Hg^{2+}_{(aq)} + \text{products}$	$6.0 M^{-1}s^{-1}$	Smith and Martell(1976)
$Hg^{2+} + SO^{2-}_3 \rightleftharpoons HgSO_3$	$2.0 \times 10^{-13} M$	Smith and Martell(1976)
$HgSO_3 + SO^{2-}_3 \rightleftharpoons Hg(SO_3)^{2-}_2$	$4.0 \times 10^{-12} M$	Smith and Martell(1976)
$Hg^{2+} + 2Cl^- \rightleftharpoons HgCl_2$	$1.0 \times 10^{-14} M^2$	Lin and Pehkonen(1999)
$Hg^{2+} + OH^- \rightleftharpoons HgOH^+$	$2.51 \times 10^{-11} M$	Smith and Martell(1976)
$HgOH^+ + OH^- \rightleftharpoons Hg(OH)_2$	$6.31 \times 10^{-12} M$	Smith and Martell(1976)
$HgOH^+ + Cl^- \rightleftharpoons HgOHCl$	$3.72 \times 10^{-8} M$	Smith and Martell(1976)
$Hg(OH)_{2(s)} \rightleftharpoons Hg(OH)_{2(aq)}$	$3.5 \times 10^{-4} M$	
$HgCl_{2(s)} \rightleftharpoons HgCl_{2(aq)}$	$0.27 M$	

Table 1.3: Aqueous phase reactions of mercury in the atmosphere (Bullock and Brehme, 2002)

mercury in cloud droplets is oxidized mainly by O_3, forming $HgO_{(aq)}$, which reacts further to divalent mercury, Hg(II) or $Hg^{2+}_{(aq)}$. Another oxidant of potential significance is $OH_{(aq)}$, which is capable of oxidizing elemental mercury in cloud droplets to divalent mercury. A modelling study involving known atmospheric reactions of mercury (Lin and Pehkonen, 1999) concluded that aqueous phase reactions involving OH and chlorine were the most important Hg(0) oxidation reactions during the daytime and nighttime respectively.

Atmospheric reduction reactions involving the chemical conversion of Hg(II) to Hg(0) take place in the aqueous phase. The proposed mechanism of the reduction of Hg(II) by sulfite in the aqueous solution involves the formation of an intermediate, $HgSO_3$, which decomposes to produce Hg(II) which in turn is rapidly reduced to Hg(0). The overall rate of the reaction is inversely dependent on the concentration of sulfite. This reaction may influence the concentration of Hg in cloud and rain water by reducing water soluble Hg(II) to volatile Hg(0) (Munthe et al., 1991). $Hg^{2+}_{(aq)}$ and the hydroxide ion, OH^-, form $HgOH^+$ and $Hg(OH)_2$, and the divalent mercury bound as $Hg(OH)_2$ can be reduced back to $Hg^0_{(aq)}$ by photolysis (Pleijel and Munthe, 1995). Aqueous phase reductions involving hydroperoxy radical (HO^*_2) and conversion of Hg^{2+} to Hg(0) may also play a role in counterbalancing oxidation reactions in cloud waters and fogs (Lin and Pehkonen, 1999).

The relevance of competing atmospheric mercury oxidation and reduction reactions remains unclear at present, although it is evident that pollutants such as SO_2 and O_3 may play a role in the atmospheric fate and transport of mercury. Gas-phase reactions are unlikely to affect local-scale depositional phenomena but

aqueous reactions could have this effect. The rate kinetics for these reactions is an important area of uncertainty and accurate characterization will be critical for making meaningful predictions using atmospheric models.

The gas phase oxidation of Hg(0) by halogen atoms (Cl, Br) and molecular halogens (Cl_2, Br_2) has recently been investigated by Ariya et al. (2002). The homogeneous Hg+Cl_2 reaction was found to be too slow to be important under atmospheric conditions (k = $(2.6\pm0.2)\times10^{-18}$ cm^3/s). The measured rates for the fast Hg + Cl and Hg + Br are very high and these reactions may be of relevance, at least under certain conditions (e.g. Br in polar spring) (Ryaboshapko et al., 2002).

Dimethylmercury (DMM) was found to react with HO^*, Cl^*, O_3, $O(^3P)$ and NO_3^* and F^* (Niki et al., 1983a,b; Sommar et al., 1996; Thomsen and Egsgaard, 1986) and has a lifetime of just several hours. The reactions with OH and Cl lead to the formation of MeHg. Current knowledge of the atmospheric chemistry of MeHg and DMM is limited to the results of investigations of DMM reactions with different radical species.

1.1.5 Deposition

All three major forms of mercury can be dry deposited and the rates of deposition vary depending upon surface characteristics and meteorological conditions. The dry deposition velocity of a gaseous pollutant is governed by three factors: turbulent diffusive transport in the atmosphere, molecular diffusive transport through the quasi-laminar sublayer at the ground surface and uptake by the surface or vegetation. Hg(0) is relatively inert, therefore it is likely that Hg(0) deposits with a small

dry deposition velocity. Due to high background concentration of Hg(0), the total dry deposition of Hg is sensitive to dry deposition velocity of Hg(0). Both particulate and gaseous divalent mercury are thought to dry deposit at significant rates when and where measurable concentrations of these mercury species exist. The deposition velocity of particulate mercury is dependent on atmospheric conditions and particle size.

Wet deposition is often parameterized through the precipitation rate and the washout ratio, which is the ratio of the Hg concentration in rainwater divided by the Hg concentration in air. Scavenging of mercury by precipitation varies considerably. It is generally accepted that Hg(0) is not susceptible to any major process of direct wet deposition. The gaseous divalent mercury is expected to be scavenged readily by precipitation. Particulate mercury is also subject to wet deposition due to scavenging by cloud microphysics and precipitation. Roughly half of Hg(p) may be scavenged by atmospheric water (e.g., Seigneur et al. (2003)).

The wet deposition of Hg can be determined with the concentration measured in wet deposition samples and the precipitation amount measured independently for each collection period. A few methods such as the dry deposition inferential measurement method (Hicks et al., 1987), the flux chamber method (Carpi, 1997; Xiao et al., 1991), and the modified Bowen Ratio (MBR) have been used to estimate dry deposition of Hg. However, many uncertainties exist in the methods used to quantify dry deposition, including direct measurements and modelled estimates. Quantification of dry deposition is difficult due to large spatial and temporal variations of meteorological conditions and surface characteristics. The dry deposition is

primarily estimated from the multiplication of the atmospheric concentration and the dry deposition velocity of each Hg species. Recently, an attempt to measure dry deposition of Hg using a water surface sampler has been made (Sakata and Marumoto, 2004).

Reported proportion of dry deposition or wet deposition varies greatly. A monitoring study of wet and dry deposition fluxes of Hg at 10 sites in Japan covering from December 2002 to November 2003 indicated that wet deposition plays a dominant role in mercury deposition in Japan, contributing fluxes ranging from 0.99 to 2.2 times (1.6 times on average at nine sites) bigger than those of the dry deposition fluxes (Sakata and Marumoto, 2005). Seasonal variation of dry deposition fluxes were very small compared to those of wet deposition. Some modelling and observational studies have demonstrated that dry deposition processes may contribute amounts of mercury to the landscape equal to or greater than wet deposition (Cohen et al., 2004; Grigal et al., 2000). Although too much uncertainty still exists, several studies indicate that the relative contribution of mercury loadings to land and water from atmospheric deposition can be substantial.

There have been several attempts to measure or estimate the mercury deposition. The National Atmospheric Deposition Program - Mercury Deposition Network (NADP - MDN) has been used to collect weekly wet deposition data for the past 10 years. Currently, nearly 85 sites are in operation in the United States and Canada.

1.1.6 Environmental concerns

Environmental contamination from mercury has been recognized as a growing problem to humans and wildlife. Increasing attention has been drawing to the hazards of mercury since 1956, when many residents of Minamata, Japan, became seriously ill, or died, after eating the mercury-contaminated fish and shellfish in Minamata Bay. Later in the mid 1960's a similar episode of mercury poisoning happened in Niigata, Japan. During the winter of 1971-1972, mercury poisoning occurred in rural areas of Iraq. In the Iraq poisoning, of an estimated 50,000 people were exposed to the contaminated bread due to methylmercury-treated wheat seeds; 459 died, and 6,530 were hospitalized (Bakir et al., 1973). Mercury released from a variety of sources exhibits a complicated chemistry, and proceeds via several different pathways to humans and wildlife.

All forms of mercury have been found to be toxic, and each form exhibits different health effects. The main route of exposure to elemental mercury is breathing. Elemental mercury is fat soluble, so it is able to cross the blood-brain barrier and the placenta (Baldwin and Marshall, 1999). Human exposure to elemental mercury vapour can cause serious injury or death. Recovery can take place after a short term and low level of exposure since the body is able to excrete mercury slowly. High levels of exposure may cause birth defects, permanent brain or kidney damage, and death.

Inorganic mercury can be absorbed through the gastro-intestinal tract but also through the skin. Inorganic mercury mainly causes poisoning by ingestion. Acute exposure to inorganic mercury by the oral route may result in effects such as nausea,

vomiting, and severe abdominal pain. The major effect from chronic exposure to inorganic mercury is kidney damage (U.S. ATSDR, 1999).

In the environment, inorganic mercury can be methylated by microorganisms to methylmercury and accumulated in the tissues of organisms. It is the ingestion of methylmercury via fish consumption that poses the greatest risk of exposure to the general public and, therefore, has the greatest potential for adverse environmental and human health effects. Methylmercury can enter blood and organs, especially the brain. Once it enters the body it crosses the blood-brain barrier and the placenta and appears in breast milk. It also concentrates in the kidneys. Mercury can damage the brain and nervous system, and is therefore referred to as a neurotoxicant.

Although all forms of mercury have been found to be toxic, most exposures to mercury are from breathing metallic mercury vapours and consuming methyl mercury.

1.2 Modelling of Atmospheric Mercury

The modelling framework of atmospheric mercury always involves complicated nonlinear physical-chemical processes which make it impossible to study quantitatively without the aid of computers. Routine monitoring of mercury is essential for atmospheric mercury investigation; however, it is always impractical to perform a high resolution and long-term monitoring because of high cost or special circumstances. Very high resolution data can be provided by a numerical model and can be

used to interpret the field measurements. Models are able to link emission sources with deposition at receptors and thus be used to identify which sources contribute most in sensitive areas and how deposition rates might vary across the region. New chemical mechanisms might be discovered from discrepancies between model output and measurements. In addition, numerical models are a cost-effective way to carry out sensitivity analysis of processes, factors and pollution control strategies. All of these reasons have been stimulating the rapid development of atmospheric mercury modelling during the last decade. Numerical modelling has become an effective way to investigate the atmospheric emission, transport, transformation and deposition of mercury. A number of atmospheric mercury models are in operation today.

1.2.1 Modelling of transport and deposition of atmospheric Hg

According to the mathematical description of transport, atmospheric Hg models can be classified into two large groups: Eulerain-type models and Lagrangian-type models.

Lagrangian-type models

Lagrangian models calculate the trajectories of masses of particles through space and time. Lagrangian Hg models that have been published are discussed below.

- **The Regional Lagrangian Model of Air Pollution (RELMAP)**

RELMAP was developed by the U.S. Environmental Protection Agency (EPA) in 1985 to simulate concentrations, wet and dry deposition patterns of SO_2, SO_4^{2-}, and fine and coarse particulate matter. In 1995, the RELMAP was extended to simulate three forms of atmospheric mercury and particulate mercury (Bullock et al., 1998). Carbon soot or total carbon aerosol was included as a modelled pollutant, which is important in determining the wet deposition of Hg(0). Wet deposition was simulated for all forms of mercury using the same scavenging ratios used by Petersen et al. (1995). Dry deposition was simulated using deposition velocity calculation which was somewhat different from those used by Petersen et al. (1995). Dry deposition of Hg(0) was assumed to be zero.

RELMAP has been used by Bullock et al. (1998) to simulate the fate and transport of mercury emitted in the continental US. The simulation covered an area from 25°N to 55°N latitude and from 60°W to 130°W longitude with a resolution of 0.33° latitude and 0.5° longitude. A constant background concentration of Hg(0) equal to 1.6 ng/m^3 was used and the effects from this background concentration were calculated separately from those due to modelled anthropogenic sources (Bullock et al., 1998). Air emissions and speciation sensitivity, source-type specific sensitivities and sensitivity of the modelled deposition from all sources were thoroughly tested. There was a general trend towards over-estimating wet deposition. Bullock et al. (1998) believed that emissions speciation was required to improve the model estimates.

- **The Advanced Statistical Trajectory Regional Air Pollution model (ASTRAP)**

ASTRAP was initially developed in 1981 at the Argonne National Laboratory to simulate long-range transport and deposition of SO_x and NO_x over North America. It was extended to simulate Hg concentrations and depositions of three mercury species: Hg(0), Hg(II) and Hg(p) (Shannon and Voldner, 1995). Horizontal dispersion in ASTRAP is estimated by computing the statistical variability of the trajectory centerlines of a series of puffs emitted from each of the series of virtual sources. Wet deposition rate is a function of the half-power of the 6 hour precipitation. Dry deposition, vertical dispersion, and loss to the free troposphere are calculated from the puff's age using time and location dependent parameterizations. The model can generate source-receptor relationship for the grid of virtual sources, which are combined with geographically resolved emissions to calculate the concentration and deposition at specified receptors (Cohen, 1997; Shannon and Voldner, 1995).

Shannon and Voldner (1995) applied ASTRAP to model regional patterns of seasonal and annual average air concentrations and cumulative deposition of mercury to the Great Lakes basin. Primary anthropogenic emission inventories included surface and elevated sources of each of three Hg species for eastern North America. Natural and secondary anthropogenic emissions were estimated by defining an emission term for Hg(0) that varies with latitude and season. The simulation result showed that 78% of the mercury deposited in the Great Lakes was Hg(II).

- **The Chemistry of Atmospheric Mercury model (CAM) of the Swedish environmental research institute (IVL) (IVL CAM)**

IVL CAM is a 1-D Lagrangian trajectory, mesoscale chemical model that in-

cludes a comprehensive chemical scheme to treat gas and aqueous phase processes using 180 reactions among 90 species. It treats the chemistry of VOCs and nitrogen oxides (NO_x) in addition to Hg chemistry since they can play an important role in the chemistry of ozone and HO_x. CAM treats the gas-phase oxidation of Hg(0) by O_3, Cl_2 and OH. The aqueous phase Hg redox system includes the oxidation of Hg(0) by O_3 and OH and the reduction of Hg(II) via two reactions ($HgSO_3$ decomposition and reaction of all Hg(II) species with HO_2). Other processes include gas/droplet equilibria, aqueous-phase equilibria and adsorption to soot particles within the droplets.

CAM has been used by Pleijel and Munthe (1995) to examine the influence of a number of chemical parameters on dissolved divalent mercury, Hg(II), in fog droplets. Representation of chlorine chemistry was found to be important for modelling of mercury species.

- **The Hybrid Single Particle Lagrangian Integrated Trajectory model (HYSPLIT)**

HYSPLIT was developed at the National Oceanic and Atmospheric Administration (NOAA) United States for operational medium and long-range transport modelling of accidental releases of radioactive materials. A special version of the NOAA HYSPLIT 4 model was developed and used to estimate the atmospheric fate and transport of mercury in North American (Cohen et al., 2004). At each model time step for a given mercury-containing puff, a determination was first made as to whether the atmospheric particles were wet or dry; droplets were assumed if the relative humidity was above 80%, while the particles were assumed to be dry for lower

relative humidity. The chemistry scheme used in the model is based on the syntheses of Bullock (2000b) and Seigneur et al. (2000). In the droplet situation, the set of 8 gas-liquid equations plus 11 aqueous phase equilibrium equations were solved. If the particles were dry, then a simple vapour/particle partitioning calculation was done for Hg(0) and Hg(II), and only the gas-phase reactions were considered. Hg(p) was obviously assumed to reside only on particles in the dry-particle case.

Cohen et al. (2004) has used HYSPLIT to estimate the atmospheric fate and transport of mercury in North American and found that incineration and metallurgical sources up to 2000km from the Great Lakes contributed significantly. Coal combustion was found to be the largest contributor to atmospheric mercury deposition to the Great Lakes.

A Lagrangian model has the potential advantage in that it may calculate more accurately the advection and dispersion from various sources and allow more complete characterization of the impact of turbulence on the transport of air pollutants. Lagrangian-type model is suitable for modelling the short time turbulent transport of tracers released from local sources. This is of special importance in the vicinity of the source of an air pollutant, where the pollutant is instantaneously mixed over at least one grid box, which can cause large subsequent transport errors. The Lagrangian algorithm for advection-diffusion totally eliminates the numerical diffusion which impairs the accuracy of solutions of the equations governing the convective transport of a scalar when the grid lines are oblique to the streamlines, and provides an exact solution and low-cost method. Other advantages include: easy to handle emissions from point and line sources, numerically accurate (mainly, no numerical

diffusion due to the advection scheme) and computationally inexpensive.

However, Lagrangian-type models are formulated under assumptions of simplified turbulent diffusion, no convergent or divergent flows and no wind shear. In these approaches only first-order chemical reactions can be treated rigorously. Therefore Lagrangian-type model cannot handle a large number of sources and cannot model a system in which complex nonlinear chemistry occurs. As the scientific understanding of atmospheric mercury processes continued to develop in the late 1990's, it became apparent that Lagrangian-type models would have difficulties simulating the complex chemical and physical interactions of mercury with other pollutants that were being discovered. Thus, the focus for atmospheric mercury model development was moved to Eulerian-type models.

Eulerian-type models

Eulerian-type models calculate the pollutant's fate and transport everywhere in the modelling domain using a fixed coordinate system in which a succession of different air parcels are viewed as being carried by the wind past a stationary observer. The Eulerian model is ideal for complex chemistry interactions from different emissions sources. Eulerian-type Hg models include the following:

- **Tropospheric Chemical Module (TCM) of German research center Gesellschaft für Kernenergieverwertung in Schiffbau und Schiffahrt (GKSS) (GKSS TCM)**

GKSS TCM is a comprehensive mercury model system developed on the base of

the Eulerian reference frame of the Acid Deposition and Oxidant Model (ADOM) (Petersen et al., 2001). The cloud mixing, scavenging, chemistry and wet deposition modules of the ADOM, originally designed for regional-scale acid precipitation and photochemical oxidants studies, have been restructured to accommodate recent developments in atmospheric mercury chemistry. The TCM is able to simulate long-range transport of mercury over the entire depth of the troposphere with a basic time step of one hour. The TCM chemistry scheme was developed by systematic simplification of the detailed Chemistry of Atmospheric Mercury (CAM) process model, which is based on the current knowledge of physico-chemical forms and transformation reactions of atmospheric mercury species. The TCM contains modules to calculate the chemical interactions that move the gas phase mercury into aqueous phase within clouds and calculate the aqueous phase chemical transformations that occur within cloud and precipitation droplets.

The transport and diffusion modules in TCM use a sophisticated cell-centered flux formulation solver for the three-dimensional advection-diffusion equation. Dry deposition is modelled in terms of a deposition velocity for gaseous and particle associated mercury species, which is calculated as the inverse of the sum of the aerodynamic, deposition layer and surface canopy resistance. The mass transfer, chemistry and adsorption components of the model incorporate 14 mercury species and 21 reactions including mass transfer, aqueous phase and gas phase chemical reactions and adsorption processes on particles. The reaction rates are derived from published data and from assumption of the rates of complex formation. The cloud physics module simulates the vertical distribution of mercury species in clouds. Two different modules are incorporated: one describes stratus (layer) clouds and

the other simulates cumulus (convective) type clouds. One or the other or a combination (cumulus deck embedded in a stratus cloud) is used in the calculation depending on the characteristics of the precipitation observed.

The TCM has been applied within the EU to study the regional transport and deposition fluxes of atmospheric mercury species to the Baltic Sea (Petersen et al., 1998). The predictions of mercury concentrations in rainwater were compared with observation at four European sites and test runs have shown that adsorption of mercury species to particulate matter was very important to the atmospheric fate of mercury.

- **Meteorological Synthesizing Centre "East" heavy metal model (MSC-E HM)**

MSC-E HM is a regional-scale model operated within the European Monitoring and Evaluation Program (EMEP) region. This is a three-dimensional Eulerian model including processes of emission, advection, turbulent diffusion, chemical transformations of mercury, wet and dry depositions, and inflow of pollutant into the model domain. The model consists of five non-uniform vertical layers up to about 4km. Horizontal grid of the model is defined using stereographic projection. It is based on the GKSS TCM chemistry but includes the aqueous-phase reactions of Hg species with radicals i.e., OH and HO_2 (Ryaboshapko et al., 2001).

MSC-E HM includes three gas phase Hg species, one particulate species, and six aqueous phase species and also three mercury species adsorbed to soot particles within droplets.

The model considers basic processes governing transport and deposition of mercury: advection, diffusion, dry/wet removal and chemical reactions. Scavenging of mercury encompasses wet removal by precipitation and dry uptake by the underlying surface. Wet removal of Hg(p) and RGM is described using a washout ratio approach. Within clouds Hg(II) and Hg(0) are rained out via dissolution in cloud drops. It is assumed that half the mercury is contained in the composition of insoluble particles within cloud and rainwater droplets. After drop evaporation an aerosol particle is formed containing all earlier dissolved and insoluble mercury compounds. Dry uptake of Hg(p) is differentiated with regard to land-use category of the underlying surface and depends basically on properties of the underlying surface and atmospheric stability. Dry uptake of Hg(0) is calculated depending on the vegetation type. Dry deposition velocity of Hg(0) is assumed to exhibit the diurnal cycle. Dry deposition velocity of RGM is prescribed based on data available in the literature (Ilyin et al., 2002; Ryaboshapko et al., 1999).

In spite of a wide variety of reactions involving mercury species, only several key reactions were introduced into the modelling scheme. They are oxidation of elemental mercury by O_3, dissolution of Hg(0) and RGM in cloud droplets, oxidation of mercury within drops by O_3 with further sorption on insoluble particles within drops and partial reduction by dissolved HO_2 radical because of decomposition of mercury-sulfite complex. All products of gaseous phase oxidation are treated as aerosol particles.

The model was applied for the Northern Hemisphere. The results showed that gaseous mercury was more or less uniformly distributed in the Northern hemisphere;

on the contrary, deposition fluxes vary significantly (up to 2 order of magnitude) from industrialized to remote regions. It is possible to distinguish three most mercury contaminated regions: Southeastern Asia, Europe, and the eastern part of North America (Travnikov and Ryaboshapko, 2002).

- **The Trace Element Analysis Model (TEAM)**

TEAM, a comprehensive grid-based regional/continental atmospheric mercury model, was developed by Atmospheric and Environmental Research (AER) and the Electric Power Research Institute (EPRI). The TEAM is actually a part of a multiscale modelling system that has been used (e.g., Vijayaraghavan et al. (2002)). The TEAM mercury chemistry mechanism includes the gas phase oxidation of Hg(0) to Hg(II), the aqueous phase oxidation of Hg(0) to Hg(II), the aqueous phase reduction of Hg(II) to Hg(0), various aqueous phase equilibria of Hg(II) species and the aqueous phase adsorption of Hg(II) to Hg(p). In the TEAM modelling system, dry deposition is simulated in the conventional fashion using species-specific deposition velocities. A dry deposition velocity of 0.01 cm/s is used for Hg(0) while a value of 0.5 cm/s is used for Hg(II). The scavenging coefficient of Hg(II) is estimated from its similarity with HNO_3. Since Hg(0) has a very low solubility, it is assumed in TEAM to have a negligible wet deposition. In the TEAM applications reported in the literature (e.g., Pai et al. (1997); EPRI (2000)), the concentrations of O_3, SO_2, HCl, Cl_2 and H_2O_2, and cloud water pH were estimated from measurements (i.e., not modelled with a "one-atmosphere" model) and the other gas phase and aqueous phase chemical species set to zero. This approach significantly reduces the computational burden of model such as CMAQ-Hg which include the full set of

gas-phase photochemical and secondary aerosol reactions in order to calculate the concentrations of the various pollutant species that react with atmospheric mercury constituents.

The model was applied to the continental US and estimated deposition for some states was larger than observed. Understanding the chemical reactions of the Hg(0)/Hg(II) system may improve the model results (Pai et al., 1997). Pai et al. (1999) identified that input parameters such as emission speciation, Hg(II) dry deposition velocity, concentration of redox species, Hg(II) boundary conditions and precipitation amounts significantly influenced the model results. The speciation of mercury emissions had a larger influence on the model results near high deposition regions than in low-deposition regions. Chemistry had a larger influence on mercury wet deposition in low-deposition regions than in high-deposition regions. This non-linear response clearly suggested that it was critical to know the speciation of mercury emissions. Furthermore, Pai et al. (1999) pointed out that very little was known about other issues such as the role of dimethylmercury or the influence of size distribution of Hg(p) on observed mercury concentration and deposition.

- **The US EPA Community Multiscale Air Quality Mercury model (EPA CMAQ-Hg)**

The Community Multiscale Air Quality model (CMAQ) of the United States Environmental Protection Agency (EPA) is a comprehensive 3-D chemical transport model that was developed to simulate oxidant concentrations, particulate matter (PM) concentrations and acid deposition (Byun and Ching, 1999). CMAQ-Hg is a revised version of CMAQ which allows the simulation of mercury chemistry in

air and cloud water (Bullock and Brehme, 2002). A more detailed description of CMAQ-Hg can be found in Chapter 2.

- **Global/Regional Atmospheric Heavy Metals Model (GRAHM)**

GRAHM, developed by Meteorological Service of Canada (MSC), is an Eulerian multiscale, comprehensive, on-line, high resolution mercury model and currently it is being used to investigate atmospheric mercury. The GRAHM, coupled with Canada/s operational Global Environment Multiscale (GEM) model at the Canadian Meteorological Center, is based on the gas phase and aqueous phase mercury chemistry mode of Petersen et al. (1998, 2001), which is a simplified form of the Pleijel and Munthe (1995) mercury kinetic mechanism. The model solves dynamic equations for all meteorological processes and physio-chemical processes for mercury species.

Four mercury species (Hg(0), $HgCl_2$, HgO, Hg(p)) are included in the model. The model uses TGM gas and aqueous phase mercury chemistry parameterizations as described by Petersen et al. (1998). It incorporates 14 mercury species and 21 reactions including mass transfer reactions, aqueous phase and gas phase chemical reactions and equilibrium reaction for adsorption on particles. Gas and aqueous phase chemistry, multiple resistance based dry deposition, vertical planetary boundary layer diffusion, cloud chemical interactions using detailed cloud schemes and wet deposition form the set of mercury processes in the model.

The GRAHM model runs in lock-step with the GEM forecast model, providing near-real time forecasts of mercury air quality and deposition estimates. The

model's formulations also reflect recent advances in boundary layer physics, cloud processing, and surface removal. However, reflecting its linkage to the Petersen et al. (1998) and Pleijel and Munthe (1995) mechanism, the GRAHM modelling system does not treat the time and space variation in the various oxidant, SO_2, and particulate species that play key roles in mercury chemistry. These species are simply prescribed based on measurements and on information available with which to assess the impact of these approximations on the reliability of the resulting mercury species predictions.

The model was integrated from June 1995 for 2.5 years with no mercury in the atmosphere at the start and only anthropogenic emissions added to establish the atmospheric burden of mercury. Horizontal resolution for this simulation was globally uniform at $1^{\circ}\times1^{\circ}$ latitude-longitude with 28 vertical levels with top at 10mb. For accurate representation of dry deposition, vertical resolution in the surface planetary boundary layer was kept high. After 1.5 years of mercury spin-up in the atmosphere, the modelling results showed a well-balanced atmosphere (with respect to mercury) in the Northern Hemisphere for the entire year 1997. The results indicated that the global model was able to capture the observed seasonal variability in atmospheric mercury concentrations and equator-to-pole gradient in mercury concentrations was also well simulated (Dastoor and Larocque, 2004).

- **Mercury version of National Environmental Research Institute (Denmark), Danish Eulerian Hemispheric Model (DEHM)**

Mercury version of DEHM, A 3-D mercury model, has been developed within the Danish Arctic Monitoring and Assessment Programme (AMAP). The model is

based on the Danish Eulerian Hemispheric Model (DEHM) which was originally used to study the transport of SO_2, SO_4^{2-} and Pb into the Arctic.

The mercury version of DEHM model is based on a set of coupled full three-dimensional advection diffusion equations. In the present version there are 13 mercury species, 3 in the gas-phase (Hg(0), HgO and $HgCl_2$), 9 species in the aqueous-phase and 1 in the particulate phase. The chemistry is based on the scheme of GKSS model. Some experiments with the formulation of the mercury chemistry during the Polar Sunrise were carried out in order to investigate the observed depletion (Christensen et al., 2004). The dry deposition velocities of the reactive gaseous mercury species are based on the resistance method, where the surface resistance similar to HNO_3 is used. The dry deposition velocity for particulate mercury is similar to SO_4^{2-}, and over land it is given by Walcek et al. (1986), while the dry deposition over open water is based on the work of Slinn and Slinn (1980). The wet deposition of reactive and particulate mercury is parameterized using a simple scavenging ratio formulation for in-cloud and below-cloud scavenging (Christensen, 1997).

The mercury version of the DEHM model has been run for a domain with 96×96 grids that covers most of the Northern Hemisphere with a grid resolution of 150km ×150km at 60°N from October 1998 to December 2000 (Christensen et al., 2004). The model results for the Arctic have been compared with measurements, and there was reasonable agreement between observed and calculated concentrations. The model has been used to make the first quantitative estimate of the importance of the mercury depletion in the Arctic troposphere during the Polar Sunrise for the

mercury deposition in the Arctic (Christensen et al., 2004). The model was able to reproduce the general patterns due to the depletion during the Polar Sunrise.

- **Eulerian Model for Air Pollution (EMAP)**

EMAP, developed by National Institute of Meteorology and Hydrology (Bulgaria), is a 3-D simulation model that allows the description of the dispersion of multiple pollutants. Such processes as horizontal and vertical advection, horizontal and vertical diffusion, dry deposition, wet removal, gravitational settling and specific chemical transformations are accounted for in this model. Within EMAP, the semi-empirical diffusion-advection equations for scalar quantities are treated.

The mercury scheme, developed in MSC-East (Ryaboshapko et al., 2001), was incorporated in the model describing the transformation of 8 Hg species in air and cloud droplets. Elemental mercury, gaseous oxidized mercury (treated as $HgCl_2$) and particulate mercury (treated as $HgCl_2$) are emitted to the atmosphere by anthropogenic sources. Hg(p) was divided into two equal parts, soluble and insoluble ones, that further evolve separately. The first form is entirely absorbed by cloud water, if any. The second one does not take part in wet reactions. It is believed that in air only oxidation by ozone takes place, and the products are treated as $HgCl_2$. Different transformations between species occur in the cloud liquid phase.

The EMAP model was applied for calculating the Bulgarian impact of lead, cadmium, mercury and benzo(a)pyrene in the same region (BC-EMEP, 1994-1998). It was also applied for the intercomparison study of numerical models for long-range atmospheric transport of mercury (EMEP/MSC-E Technical Report, 2005)

- **Revised Sarmap Air Quality Model (SAQM)**

The revised SAQM, a three-dimensional regional scale Eulerian air quality model based on the framework of SAQM (SARMAP Air Quality Model), was developed by incorporating into the Hg chemistry, in-cloud transformation, and air-surface exchange of elemental mercury (Xu et al., 2000b,a). The SARMAP is a revised version of the RADM code which was applied to regional ozone air pollution in the California Central Valley in the early 1990's. A mercury mechanism containing 3 key species(Hg(0), Hg(II) and Hg(p)) were added to SAQM's CB4 mechanism and the model was refined to treat mercury processes in precipitation clouds, co-existing non-precipitating clouds and fair weather clouds. Three mercury species, Hg(0), Hg(II) and Hg(p), were included in the model. Soot particles were also considered. The aqueous chemical reaction of Hg was largely adapted from Petersen et al. (1995). The sum of dissolved and adsorbed Hg(II) in cloud water was defined as the total Hg(II) concentration produced by aqueous phase ozone oxidation of Hg(0). The wet deposition rates of Hg(II) and Hg(p) due to direct scavenging, including direct absorption of Hg(II) in cloud droplets, and impaction and interception of Hg(p) by cloud droplets, were calculated using ambient concentrations of these two species, liquid water content, precipitation amount, and scavenging ratios as defined by Petersen et al. (1995). Seasonal dry deposition rate tables developed by Walcek et al. (1986) and Wesely (1986) were used to estimate Hg(II) dry deposition rates over various surface types.

The model was tested with corresponding measurements at 8 monitoring stations in Connecticut for a summer week and a winter week in 1997 (Xu et al.,

2000a). The simulated results showed a good agreement between ambient gaseous Hg concentrations and the observations, and that the simulated concentration in precipitation fell within the range of measurements made in Connecticut and other regions.

The five mercury chemistry models including GKSS TCM, EPA CMAQ-Hg, AER/EPRI MCM, MSC-E HM and IVL CAM have been intercompared using the same data set for model initialization (Ryaboshapko et al., 2002). All five Hg chemistry models have the same basic formulation: (1) gas phase oxidation of Hg(0) to Hg(II) (which was ignored in one model for these 48-h simulations), (2) fast redox reactions of aqueous Hg(0) and Hg(II) and (3) adsorption of Hg(II) to soot particles within droplets. However, the five models differ in their detailed treatment of those basic processes. The gas-phase oxidation is treated as a slow process or ignored by four models; on the other hand, IVL CAM includes a relatively fast oxidation of Hg(0) by OH radicals. Two models (CMAQ and AER/EPRI) treat the aqueous oxidation of Hg(0) by O_3 and Cl_2 and the aqueous reduction of Hg(II) by HO_2 and SO_2. For these models, the Cl_2 reaction dominates Hg(0) oxidation and the HO_2 reaction dominates Hg(II) reduction. MSC-E HM and IVL CAM include these reactions except the aqueous oxidation of Hg(0) by Cl_2; therefore, less Hg(II) is formed during nighttime. The other model (GKSS TCM) does not treat the Cl_2 and HO_2 reactions; thus, Hg(0) aqueous oxidation is governed solely by the O_3 reaction and Hg(II) reduction is governed solely by $Hg(SO_3)_2^{2-}$ decomposition. In addition, a faster kinetics is used for that latter reaction in GKSS TCM and IVL CAM than used in the other three models.

Eulerian-type models are capable of incorporating sophisticated process-level understanding and description. They more accurately describe the complex interactions of different air parcels with different histories and the full context of in situ interactions at a given location in space. Since more powerful computer resources have been becoming available for atmospheric mercury modelling, Eulerian-type models are expected to become predominant in the future.

Modelling of atmospheric mercury has evolved along several lines, many reflecting the personal preferences of the model developers. Some models emphasize the treatment of chemical processes at the expense of being able to characterize physical atmospheric processes such as transport, turbulent diffusion, cloud-effects, and deposition processes. Some models address large (i.e., global) scales with a concomitant simplification in some physical or chemical processes. Some models treat the regional scale chemical transport and removal processes in depth, but have more limited ability to characterize the full body of knowledge regarding mercury chemistry and must make assumptions about the inflow boundary conditions. The latter limitation can be important in simulating mercury given the long atmospheric lifetimes of some Hg forms.

Further advancement of atmospheric modelling is in many aspects limited by a lack of quantitative knowledge of the atmospheric behaviour of mercury. Many of the key processes involved in the transformation and deposition of atmospheric mercury remain unidentified or unquantified, among these is the emission of mercury by natural sources.

1.2.2 Modelling of natural Hg emissions

Mercury is released into the atmosphere by both anthropogenic and natural processes. The annual global Hg emission is estimated to be about 5000 metric tons (Fitzgerald et al., 1994). Emissions from natural sources might represent the major (up to 60% of the total) contribution to the global atmospheric mercury budget.

Mercury emitted to the atmosphere from natural soils is primarily in elemental form, Hg(0) (Alberts et al., 1974; Kim and Lindberg, 1995; Rundgren et al., 1992). Based on regression analysis of experimental data, several empirical or in some cases thermodynamically-based models have been proposed for the dependence of Hg(0) emissions on parameters such as soil temperature, soil moisture and solar radiation (Carpi and Lindberg, 1998; Gustin et al., 1997; Poissant and Casimir, 1998). The fundamental basis for these relationships is not well known. This may introduce considerable uncertainty when empirical methods are used to extrapolate experimental measurements to regional, continental or global scales covering multi-year time periods. The scaling-up of mercury soil-to-atmosphere flux measurements to regional or global scales requires a credible air-surface exchange model of the physical, chemical and biochemical processes that occur in the soil (Zhang and Lindberg, 1999). The model should include the transformations between the various mercury forms (species) in the soil, as well as the influences of land-use, soil properties, meteorology and climate. Such a model would provide a tool for furthering understanding of the exchange of mercury in the soil with the atmosphere, and for making estimates of the contributions of mercury emissions from background and mercury-contaminated soils to the atmospheric load of mercury.

Few attempts have been made to estimate the natural Hg emissions by a modelling approach. Xu et al. (1999) developed an approach to estimate bidirectional air-surface exchange of elemental mercury for surfaces which calculates emission and dry deposition respectively for various types of land cover from meteorological data provided by MM5 and elemental mercury concentrations. Xu et al. (1999) modelled the emission from base soil as a function of soil temperature; the emission from plant canopies was formulated as a function of the rate of evapotranspiration (the sum of evaporation and plant transpiration) and the Hg(0) concentration in the surface soil water; the air-water exchange of Hg(0) was parameterized with wind speed, whitecap coverage and the Hg(0) concentration in air and water. The dry deposition rate is calculated using a resistance model described by Hicks et al. (1987). In order to calculate the evapotranspiration rate of plant canopies, the modified Penman-Monteith equation (Raupach, 1991) and other parameters such as minimal stomatal resistance to water vapour transfer, albedo, and canopy height were used. Some key assumptions made for the simulation include: 1) Hg(0) concentration in soil solution was assumed to be 100 ng/L for all locations. A mean concentration of 0.04 ng/L was used for dissolved Hg(0) concentration in sea water. 2) The soil water deficit was set as a constant for whole domain and simulation period. The canopy resistance is a function of soil water deficit.

Lin and Tao (2003) introduced a different method to calculate the air-water Hg exchanges, though they used methods similar to those Xu et al. (1999) used to calculate the Hg emissions from plant canopies and soils. While Xu et al. (1999) used empirical formulae of Mackay and Yeun (1983) and Asher and Wanninkhof (1995), Lin and Tao (2003) adopted the approach by Poissant et al. (2000) in which

the mass transfer coefficient of Hg(0), K_w, was treated to be correlated with the mass transfer of CO_2 across the air/water interface.

To date, very little has been known about the natural emissions and re-emissions of mercury. The great uncertainty in the natural mercury emission exists. There is still no effective way to strictly distinguish between natural emissions and re-emissions, except in cases where there is a strong natural source signal (e.g., areas geologically enriched in mercury). In addition, there are few measurements available and current estimates are to a large extent extrapolated from a few data points and constrained by global mass balance estimates.

1.3 Research Objectives

There have been a number of modelling studies on atmospheric Hg thus far. Many of them, however, either ignore or oversimplify natural Hg emissions. Only a limited number of published estimates of natural Hg emission rates exist and these estimates vary by orders of magnitude. The inventory development of natural emissions is constrained due to a lack of temporally and spatially representative flux data (Ebinghaus et al., 1999). Many factors such as Hg concentration in soil solution, soil moisture and Hg speciation in substrate, light, precipitation and temperature influence the Hg emission from the substrate. Hg concentration in the substrate might be a significant factor controlling emissions and may be used to predict emissions from the substrate. Several attempts have been made to simulate the natural mercury emissions, but none of them simulated were based on the detailed measurements of soil Hg concentration. None of them has been found to

consider the emissions from snow-covered surfaces and influence of winter.

Atmospheric Hg models should treat all important chemical and physical transformations which take place in the atmosphere and use accurate treatments of these transformations. However, the atmospheric processes incorporated in the models are far from complete. Many of the key processes involved in the transformation and deposition of atmospheric mercury remain unidentified or unquantified. Further advancement of atmospheric modelling is in many aspects limited by a lack of quantitative knowledge of the atmospheric behaviour of mercury. The pace of improvements will depend on having adequate data.

Although the behaviour of atmospheric Hg transport, transformation and deposition is directly affected by Hg emissions to the atmosphere, the emissions of some non-Hg air pollutants such as NO_x, SO_2, NH_3, CO and VOCs also play a significant role in influencing the behaviour of atmospheric Hg. Little is known about how and how much the atmospheric Hg depends on them. It is important to grasp the key roles that other atmospheric species play in the transformation and deposition processes of mercury.

This study recognizes the above limitations currently remaining in the area of atmospheric mercury modelling, takes the challenge to develop and evaluate a multiscale air quality model for mercury, and explores the behaviour of atmospheric Hg in North America. The objectives of this study are summarized as follows:

1. On the basis of the detailed substrate information, to develop a refined natural Hg emission model which is able to better estimate the natural mercury emissions from different land-use types, especially from soil, water and canopy.

The spatial and temporal variability of emission fluxes will be examined through numerical experiments.

2. To improve the CMAQ-Hg model system through the detailed treatment of natural mercury emissions, the adoption of boundary conditions from a global Hg simulation and the supplement of the dry deposition calculation of elemental mercury. The improved model system will be validated with observations and applied to simulate the atmospheric transport, transformation and deposition of mercury in North America.

3. To investigate the effects of Hg emissions, including natural and anthropogenic Hg emissions, and non-Hg emissions such as NO_x, SO_2, NH_3 and VOCs on the air concentration and deposition of atmospheric Hg. To identify the key emissions significantly influencing the behaviour of atmospheric Hg. A mitigation plan for wet Hg deposition will be advised.

Chapter 2

EPA CMAQ-Hg model system

2.1 The standard CMAQ model system

Community Multiscale Air Quality (CMAQ) is a powerful third generation air quality modelling and assessment tool developed by US EPA to support air quality modelling applications ranging from regulatory issues to science enquiries on atmospheric science processes. It employs a "one-atmosphere" approach and addresses complex interactions known to occur among multiple pollutants. The pollutants simulated by the standard version of CMAQ include tropospheric ozone, acidic and nutrient substances, and particulate matter of various composition and particle size. The components in the CMAQ modelling system includes: (1) The PSU/NCAR MM5 meteorological modelling system (MM5); (2)The Sparse Matrix Operator Kernel Emission (SMOKE); (3)The CMAQ Chemical Transport Modelling System (CCTM); (4)The Meteorology-Chemistry Interface Processor (MCIP); (5)Initial

Conditions (ICON); (6) Boundary Conditions (BCON); (7)The photolysis processor (JPROC). The relationship and purpose of each component in CMAQ modelling system framework is shown in Figure 2.1. The arrows show the flow of data through the modelling system. The MM5 and the MCIP are incorporated to provide meteorological fields data for both SMOKE and CCTM. The CCTM performs chemical transport modelling for multiple pollutants and scales using other additional data from ICON, BCON and JPROC. Each component of this system is briefly described below.

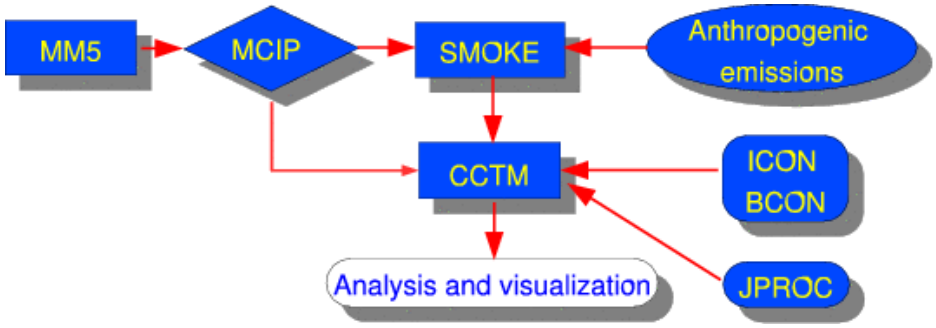

Figure 2.1: The components of the standard CMAQ modelling simulation

- **The PSU/NCAR MM5 meteorological modelling system**

The Fifth-generation NCAR/Penn State Mesoscale Model (MM5) meteorological modelling system generates the meteorological fields for CMAQ. MM5 is a complex, state-of-the-science community model, which is maintained by NCAR. It is a limited-area, nonhydrostatic, terrain-following sigma-coordinate model designed to simulate or predict mesoscale atmospheric circulation. MM5 can be used for a broad spectrum of theoretical and real-time studies, including applications of both predictive simulation and four-dimensional data assimilation to monsoons, hurricanes, and cyclones. The components of MM5 includes: (1) TERRAIN, Defining

the Simulation domain; (2) REGRID, Processing the meteorological background fields; (3) LITTLE_R/RAWINS, Objective Analysis; (4) INTERPF, Setting the initial and boundary conditions; (5) MM5, The main meteorological model; (6) Meteorology model post-processing. Terrestrial and isobaric meteorological data are horizontally interpolated (programs TERRAIN and REGRID) from a latitude-longitude grid to a mesoscale, rectangular domain on either a Mercator, Lambert Conformal, or Polar Stereographic projection. Since the interpolation of the meteorological data does not necessarily provide much mesoscale detail, the interpolated data may be enhanced (program LITTLE_R/RAWINS) with observations from the standard network of surface and rawinsonde stations using a successive-scan Cressman or multiquadric technique. Program INTERPF then performs the vertical interpolation from pressure levels to the σ-coordinate of the MM5 model. After a MM5 model integration, data can be interpolated back to pressure levels with program INTERPB. Program NESTDOWN can interpolate model level data to a finer grid to prepare for a new model integration. Graphic programs (RIP and GRAPH) may be used to view modelling system output data on both pressure and σ-levels.

- **The Sparse Matrix Operator Kernel Emission**

The MCNC Environmental Modelling Center (EMC) created the Sparse Matrix Operator Kernel Emission (SMOKE) Modelling System to allow emissions data processing methods to integrate high-performance-computing (HPC) sparse-matrix algorithms. The SMOKE system is a significant addition to the available resources for decision-making about emissions controls for both urban and regional

applications. The purpose of SMOKE is to convert the resolution of the emission inventory data to the resolution needed by an air quality model such as CMAQ, REMSAD, CAMX and UAM. Emission inventories are typically available with an annual-total emissions value for each emissions source, or perhaps with an average-day emissions value. The air quality models, however, typically require emissions data on an hourly basis, for each model grid cell (and perhaps model layer), and for each model species. Consequently, emissions processing involves transforming an emission inventory through temporal allocation, chemical speciation, and spatial allocation, to achieve the input requirements of the air quality model. SMOKE can process criteria gaseous pollutants such as carbon monoxide (CO), nitrogen oxides (NO_x), volatile organic compounds (VOCs), ammonia (NH_3), sulfur dioxide (SO_2); particulate matter (PM) pollutants such as PM2.5 microns or less (PM2.5) and PM less than 10 microns (PM10); as well as a large array of toxic pollutants, such as mercury, cadmium, benzene, and formaldehyde. Currently, SMOKE supports area-, mobile-, and point-source emissions processing and also includes biogenic emissions modelling through both a rewrite of the Biogenic Emission Inventory System, version 2 (BEIS2) and the BEIS3 system. SMOKE can process both criteria and toxic emissions data inventories. Generally, emission inventories are divided into the following source categories:

Stationary area/Nonpoint source: Sources that are treated as being spread over a spatial extent (usually a county or air district) and that are not movable (as compared to nonroad mobile and on-road mobile sources). *Nonroad mobile sources*: Vehicular and otherwise movable sources that do not include vehicles that travel on roadways. *On-road mobile sources*: Vehicular sources that travel on roadways.

Point sources: These are sources that are identified by point locations, typically because they are regulated and their locations are available in regulatory reports. *Wildfire sources with precomputed plum rise*: Traditionally, wildfire emissions have been treated as stationary area sources. More recently, data have also been developed for point locations, with day-specific emissions and hour specific plume rise being computed prior to input to SMOKE. *Biogenic land use data*: Biogenic land use data characterize the type of vegetation that exists in either county total or grid cell values.

- **The CMAQ Chemical Transport Modelling System**

The CMAQ Chemical Transport Modelling system (CCTM) is used to perform model simulations for the relevant and major atmospheric chemistry, transport and deposition processes involved throughout the modelling domain with input data. The science options available in CCTM to the user include the gas phase chemistry mechanisms, RADM2 and CB-IV, a set of numerical solvers for the mechanisms, options for horizontal and vertical advection schemes, algorithms for fine and coarse particulate matter predictions, photolysis rates, and a plume-in-grid approach. The CMAQ modelling system includes interfaces processors to incorporate the output of the meteorology and emissions processors and to prepare the requisite input information for initial, boundary and photolysis rates to the CCTM. The interfaces include:

The Meteorology-Chemistry Interface Processor (MCIP) links meteorological models such as MM5 with the Chemical Transport Model (CTM) of the Models-3 Community Multiscale Air Quality (CMAQ) modelling system to provide a com-

plete set of meteorological data needed for air quality simulation. Because most meteorological models are not built for air quality modelling purpose, MCIP deals with issues related to data format translation, conversion of units of parameters, diagnostic estimations of parameters not provided, extraction of data for appropriate window domains, and reconstruction of meteorological data on different grid and layer structures. The main functions of MCIP are: (1) Reading in meteorological model output files; (2) Extraction of meteorological data for CTM window domain; (3) Interpolation of coarse meteorological model output for finer grid; (4) Collapsing of meteorological profile data if coarse vertical resolution data is requested; (5) Computation of passing through surface and PBL parameters; (6) Diagnosing of cloud parameters; (7) Computation of species-specific dry deposition velocities; (8) Generation of coordinate dependent meteorological data for the generalized coordinate CCTM simulation; (9) Output meteorological data in Models-3 I/O API format.

Initial Conditions and Boundary Conditions (ICON and BCON) provide concentration fields for individual chemical species for the beginning of a simulation and for the grids surrounding the modelling domain, respectively. The ICON and BCON processors use data provided from previous three-dimensional model simulations or from clean-troposphere vertical profiles. Both vertical profiles and modelled concentration fields have specific chemical mechanisms associated with them, which are a function of how these files were originally generated.

The photolysis processor (JPROC) calculates temporally varying photolysis rates. JPROC requires vertical ozone profiles, temperature profiles, profiles of the

aerosol number density, and the earth's surface albedo to produce the photolysis rates for the CCTM. JPROC uses this information in radiative transfer models to calculate the actinic flux needed for calculating photolysis rates. JPROC generates a look-up table of photo-dissociation reaction rates.

2.2 Hg version of CMAQ model system (CMAQ-Hg)

The standard version of the CMAQ model system was extended (Bullock and Brehme, 2002) to simulate chemistry, transport and deposition of mercury. The CMAQ-Hg model simulates the emission, transport, transformation and deposition of atmospheric mercury in three distinct forms: Hg(0), Hg(II) and Hg(p). The atmospheric transport of these three forms of Hg is simulated in the same manner as for all other substances simulated by the CMAQ to date. Transformations of Hg are simulated with four new chemical reactions within the standard CMAQ gaseous chemistry framework and a highly modified cloud chemistry mechanism which includes a compound-specific speciation for oxidized forms of Hg, seven new aqueous-phase Hg reactions, six aqueous Hg chemical equilibria, and a two-way mechanism for the sorption of dissolved oxidized Hg to elemental carbon particles (Table 2.1). The CMAQ-Hg model simulates the partitioning of reactive gaseous Hg between air and cloud water based on the Henry's constant for mercuric chloride. Henry's Law equilibrium is assumed for elemental Hg also. Particulate Hg is assumed to be incorporated into the aqueous medium during cloud nucleation. Wet and dry

deposition is simulated for each of the three forms of Hg. Wet deposition rate is calculated based on precipitation information from the CMAQ meteorological processor and physicochemical Hg speciation in the cloud chemistry mechanism. Dry deposition rate is calculated based on dry deposition velocity and air concentration information for each of the three forms of Hg.

Reaction	k or K
Gaseous-phase reaction of Hg	
$Hg^0_{(g)} + O_{3(g)} \rightarrow PHg + RGM$	$2.11 \times 10^{-18} cm^3 molecules^{-1} s^{-1}$
$Hg^0_{(g)} + Cl_{2(g)} \rightarrow RGM$	$2.6 \times 10^{-18} cm^3 molecules^{-1} s^{-1}$
$Hg^0_{(g)} + H_2O_{2(g)} \rightarrow RGM$	$8.5 \times 10^{-19} cm^3 molecules^{-1} s^{-1}$
$Hg^0_{(g)} + OH_{(g)} \rightarrow PHg + RGM$	$7.7 \times 10^{-14} cm^3 molecules^{-1} s^{-1}$
Aqueous-phase reactions of Hg	
$Hg^0_{(aq)} + O_{3(aq)} \rightarrow Hg^{2+}_{(aq)} + products$	$4.7 \times 10^7 M^{-1} s^{-1}$
$HgSO_{3(aq)} \rightarrow Hg^0_{(aq)} + products$	$Texp((31.971T) - 12595T) T s^{-1}$
$Hg(OH)_{2(aq)} + h\nu \rightarrow Hg^0_{(aq)} + products$	$6.0 \times 10^{-7} s^{-1} (maximum)^a$
$Hg^0_{(aq)} + OH_{(aq)} \rightarrow Hg^{2+}_{(aq)} + products$	$2.0 \times 10^9 M^{-1} s^{-1}$
$Hg^{2+}_{(aq)} + HO_{2(aq)} \rightarrow Hg^0_{(aq)} + products$	$4.7 \times 10^7 M^{-1} s^{-1}$
$Hg^0_{(aq)} + HOCl_{(aq)} \rightarrow Hg^{2+}_{(aq)} + products$	$2.09 \times 10^6 M^{-1} s^{-1}$
$Hg^0_{(aq)} + OCl^-_{(aq)} \rightarrow Hg^{2+}_{(aq)} + porducts$	$1.99 \times 10^6 M^{-1} s^{-1}$
Aqueous-phase chemical equilibria for Hg	
$Hg^{2+} + SO_3^{2-} \rightleftharpoons HgSO_3$	$2.0 \times 10^{-13} M$
$HgSO_3 + SO_3^{2-} \rightleftharpoons Hg(SO_3)_2^{2-}$	$4.0 \times 10^{-12} M$
$Hg^{2+} + 2Cl^- \rightleftharpoons HgCl_2$	$1.0 \times 10^{-14} M^2$
$Hg^{2+} + OH^- \rightleftharpoons HgOH^+$	$2.51 \times 10^{-11} M$
$HgOH^+ + OH^- \rightleftharpoons Hg(OH)_2$	$6.31 \times 10^{-12} M$
$HgOH^+ + Cl^- \rightleftharpoons HgOHCl$	$3.72 \times 10^{-8} M$
Henry's equilibria for Hg	
$Hg^0_{(g)} \longleftrightarrow Hg^0_{(aq)}$	$1.1 \times 10^{-1} M atm^{-1}$
$HgCl_{2(g)} \longleftrightarrow HgCl_{2(aq)}$	$1.4 \times 10^6 M atm^{-1}$

[a] Rate constant is scaled to the cosine of solar zenith angle

Table 2.1: Reactions and rate constants used by the latest CMAQ-Hg model (Bullock et al., 2002)

All major species known to react with mercury in the atmosphere are already present in this version of the CMAQ model. The latest CMAQ-Hg system (version 4.3) was used in this study.

The CMAQ-Hg V4.3 system includes components shown in Figure 2.2. Compared to the standard CMAQ modelling system, the CMAQ-Hg system includes one more component called the Natural Mercury Emission Model (NMEM) which was specifically developed in this study for the CMAQ-Hg modelling system to estimate the natural mercury emissions. The detailed description of NMEM is documented in Section 3.2. MCIP, ICON and BCON were modified in this study to generate dry deposition velocities of elemental mercury, and to provide initial and boundary conditions for mercury modelling simulation.

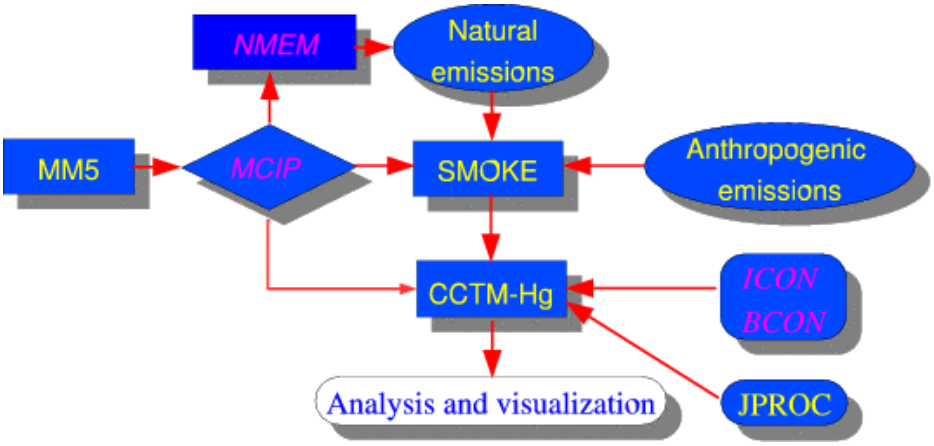

Figure 2.2: The components of improved CMAQ-Hg modelling simulation

2.3 Additions to CMAQ-Hg model system

2.3.1 Calculation of dry deposition of Hg(0) and Hg(II)

There are two options in MCIP to calculate dry deposition velocities for all pollutant species whose dry deposition process is considered to be important: (1) Models-3 dry deposition method; (2) RADM dry deposition method. The main advantage of Models-3 dry deposition method over the many similar models used in air quality modelling is the coupling of land surface model for description of stomatal pathway. This is important for certain chemical species which have been shown experimentally to have strong stomatal pathway components. Models-3 dry deposition option was configured for all simulations in this study .

In CMAQ V4.3, dry deposition of Hg(0) was assumed to be negligible in comparison to that of Hg(II) and Hg(p), therefore was ignored. Also dry deposition of Hg(II) was referenced to that of nitric acid. Although its dry deposition velocity is small, Hg(0) is the most abundant mercury species in the atmosphere, so we have included its dry deposition in our simulations. This was done by modifying the Meteorological Chemistry Interface Processor (MCIP) program, which calculates dry deposition using the physical properties of the compound and meteorological variables. For the Henry's law constant and diffusivity of Hg(0) we chose 0.11 M/atm (Lin and Pehkonen, 1999) and 0.1194 cm^2/s (Massman et al., 1999) respectively. Also, a leaf mesophyll resistance R_m (s/cm), was added for Hg(0), according to

Equation 1 (Lindberg et al., 1992).

$$R_m = 1208.5e^{-0.109T} \tag{2.1}$$

where T is ambient temperature (°C). For RGM, we used the deposition properties of $HgCl_2$. We assumed a Henry's law constant of 1.4×10^6 M/atm (Lin and Pehkonen, 1999) and a diffusivity of 0.05 cm^2/s (Scholtz et al., 2003).

2.3.2 Natural mercury emissions

In order to estimate the emissions of mercury from soil, water and vegetation, a natural mercury emission model was developed in this study based on the grid-specific substrate information and meteorology data. The detailed information about algorithm, validation and application of this model is documented in Chapter 3. The Natural Hg Emission Model requires many meteorology field data and land surface data as input to estimate the natural Hg emissions. To facilitate the Natural Mercury Emission Model runs, MCIP was modified in this study to integrate the algorithm of Natural Mercury Emission Model so that meteorological data required by Natural Hg Emission Model can be easily obtained from MM5 output. The estimated natural Hg emissions were then stored in a netCDF-formatted file which can be directly accessed by SMOKE for the purpose of merging with anthropogenic Hg emissions. The incorporation of the Natural Hg Emission Model into MCIP is illustrated in Figure 2.3.

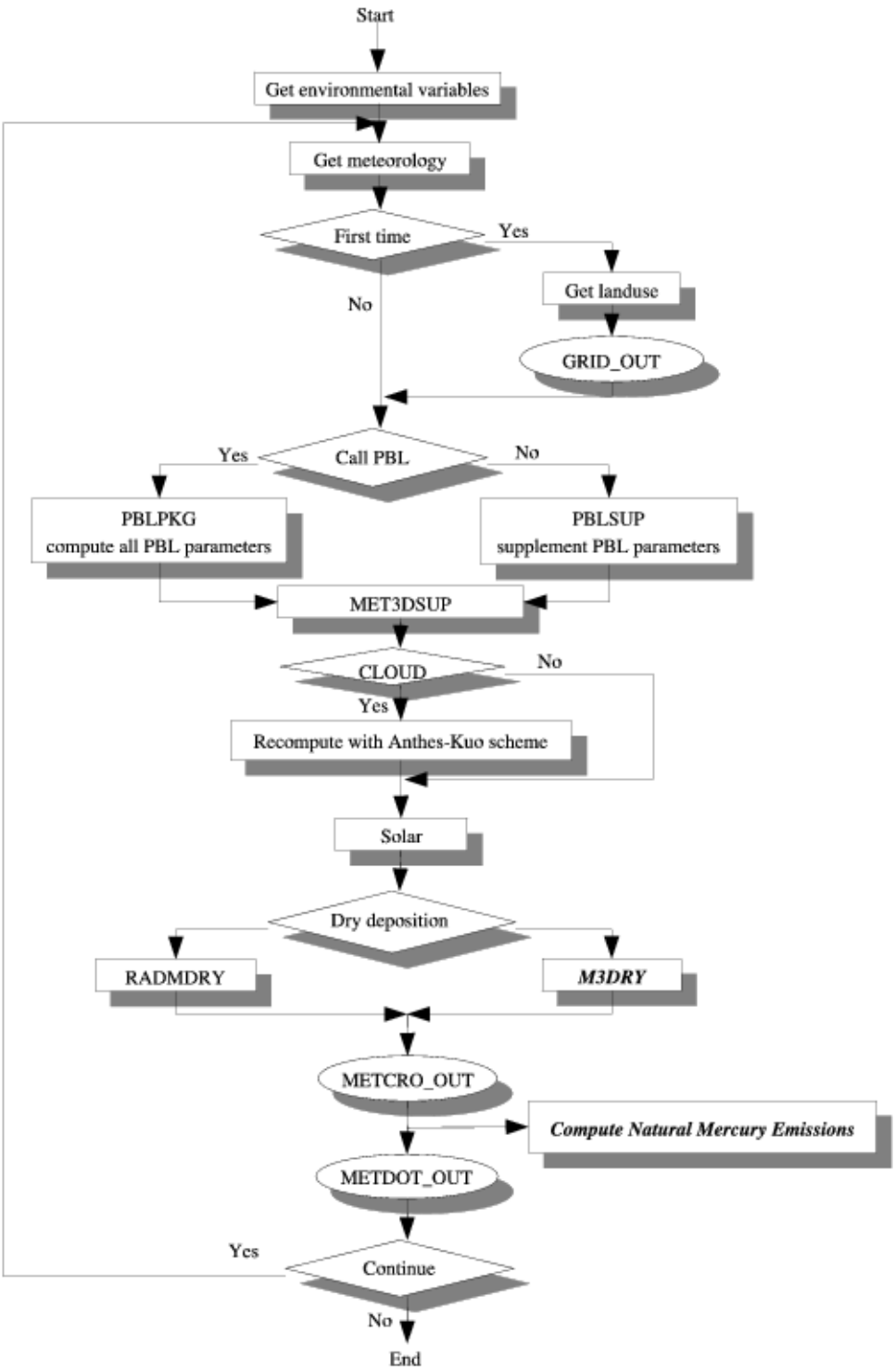

Figure 2.3: The flow chart of the standard CMAQ modelling simulation and the incorporation of Natural Mercury Emission Model into MCIP

Chapter 3

Development of a natural mercury emission model

3.1 Introduction

Mercury emission originates from both natural and anthropogenic sources. Seigneur et al. (2004) estimated that global anthropogenic Hg emissions amounted to 2143 Mg/yr, but global natural Hg emissions amounted to 4268Mg/yr.

To better understand the behaviour of mercury emission, transport, transformation and deposition in the atmosphere, one important task is to build good regional or global emission inventories. Good atmospheric Hg modelling requires the emission inventories to be refined and extended to include natural sources. Up to now, reasonably accurate anthropogenic Hg emissions have been quantified and already used by a number of models to understand the behaviours of atmospheric mercury.

However, natural Hg emission was ignored or oversimplified by most of atmospheric models. Only a limited number of published estimates of natural mercury emission rates exist and these estimates vary by orders of magnitude (Seigneur et al., 2004; Bergan et al., 1999). Inventory development of natural emissions is confined due to a deficiency of temporally and spatially representative flux data (Ebinghaus et al., 1999) and a lack of knowledge of the natural emission processes. More definitive data are urgently required to better estimate Hg emission from natural sources/surfaces. Several attempts have been made to develop detailed treatments of natural Hg emission from vegetation, water and soil. Xu et al. (1999) developed a model to estimate bi-directional air-surface exchange of elemental mercury for natural surface. This approach calculates emission and dry deposition of Hg(0) for various types of land cover and can be used to provide lower boundary conditions for regional/global atmospheric transport and deposition models. Lin and Tao (2003) introduced a different method to calculate the air-water Hg exchanges, though they used methods similar to those Xu et al. (1999) used to calculate the Hg emissions from plant canopies and soils. Xu et al. (1999) used the empirical formulae of Mackay and Yeun (1983) and Asher and Wanninkhof (1995). Lin and Tao (2003) adopted the approach (Poissant et al., 2000) in which the mass transfer coefficient of Hg(0), K_w, was treated to be correlated with the mass transfer of CO_2 across the air/water interface. Moreover, Lin and Tao (2003) also started to use location-dependent Hg concentration in surfaces in the model. Lin and Tao (2003) assumed that the Hg(0) content in surface soil water at a concerned location would be proportional to the product between the strength of a contributing anthropogenic RGM/Hg(p) source and the squared reciprocal of the distance between

the contributing source and the concerned location. In order to obtain more reasonable estimates of natural mercury emissions, a natural Hg emission model should be more mechanism-refined and built up on the basis of real Hg concentrations in soil and water.

The objective of this study is to develop a more detailed natural Hg emission model to achieve better estimates of natural Hg emission from different land uses for different seasons. Base on the methods used by Xu et al. (1999) and Lin and Tao (2003), this model included more refined parameterization of processes and more realistic substrate information. Emissions from canopy and from soil under canopy were treated differently. Natural Hg emissions from frozen surfaces and snow cover were taken into account in order to obtain emissions in winter and in northern regions. This model also considered the effect of precipitation on Hg emission from the canopy. More realistic substrate information such as measurements of soil Hg concentration, reported Hg concentration in sea and lakes, soil moisture, snow cover fraction and leaf area index from MM5 output were processed and incorporated into the model simulation for improving the accuracy of natural Hg emission estimation.

3.2 Theoretical consideration

Naturally emitted mercury is predominantly Hg(0). Natural mercury emission was modelled for three major sources: vegetation, soil and water.

- **Emission from Vegetation**

Recent studies indicate that plants emit mercury to the atmosphere (Hanson et al., 1995; Lindberg et al., 1998; Siegel et al., 1987). Mercury flux measurements over vegetation have indicated that foliar emission of Hg is more significant than emission from soil or water. Hg is thought to be transported from the soil to mesophyll cells of the leaf interior via the transpiration stream, where it volatilizes into the intercellular space of the leaf interior as elemental Hg. From the intercellular space of the leaf interior, Hg(0) follows the same pathway as water vapour, diffusing through the stomata into the atmosphere. The diffusion of any gas from the leaf interior to the atmosphere is governed by the chemical potential gradient and the conductivity of the diffusive pathway. The conductivity of the diffusive path is largely a function of the stomata, given that the boundary layer conductance is maximum. Environmental factors (e.g., irradiance, temperature) or biological processes (e.g., genetics, development) exert control over the flux of a gas by influencing either the chemical potential gradient or conductivity of the diffusive path. It has been suggested (Hanson et al., 1995; Leonard et al., 1998) and also observed that Hg emissions from vegetation are related to the transpiration rates (Lindberg et al., 2002). Equation (3.1) is used to estimate Hg transpiration from vegetation canopy (Xu et al., 1999)

$$F_c = E_c C_s \tag{3.1}$$

where, F_c is the Hg(0) flux (units of ng/m^2/s), E_c is the canopy transpiration (m/s), and C_s is the concentration of Hg(0) in the surface soil solution (ng/m^3). E_c was calculated using a simplified canopy-atmosphere model (SCAM) (Raupach, 1991) based on Penman-Monteith equation (Monteith and Usworth, 1990), a combi-

nation method of the energy balance and mass transfer to compute the evaporation from an open water surface. Monteith (1965) introduced the effects of the architecture and the stomatal regulation of the canopy on the water vapour diffusion from a cropped surface. These effect were modelled through the bulk canopy resistance (r_c) and the aerodynamic resistance (r_a). Bulk canopy resistance represents the total mechanical resistance encountered by diffusion from inside a leaf to outside, while aerodynamic resistance represents the resistance to air flux over vegetative surfaces. An important assumption of this model is the whole canopy can be considered as a "big leaf" from which heat and vapour escape. This "big leaf" is located at d + z_{0m} height, where d is the zero-plane displacement height and z_{0m} is the roughness length for momentum.

The SCAM model uses meteorological parameters (e.g., solar radiation, vapour pressure, wind speed) and canopy characteristics (e.g., height, albedo, and canopy resistance) to calculate the transpiration rate E_{cs}

$$E_{cs} = \frac{\Delta(R_n - G) + \rho c_p D_0 / r_{ac}}{\Delta + \gamma(1 + r_c/r_{ac})}(1/\lambda) \tag{3.2}$$

In contrast to previous works (Xu et al., 1999), where transpiration (or Hg(0) emission) was assumed to be zero when there is rain, in the study, we multiplied the transpiration rate (E_{cs}) by a factor α given by Mo et al. (2004)

$$\alpha = 1 - W_{fr} \tag{3.3}$$

so the transpiration rate used in this study is given by

$$E_c = \alpha E_{cs} \tag{3.4}$$

where W_{fr} is a power function of the moisture content of the interception reservoir. When it rains, the surfaces of vegetation become covered with a film of water before drip through and stem flow carries water to the ground. This water can then evaporate to the air, but at the same time transpiration is suppressed from the wet green leaves. Similarly, the formation of nighttime dew can keep foliage cool in the morning and likewise suppress transpiration. W_{fr} is parameterized as following by Deardorff (1978)

$$W_{fr} = (\frac{W_r}{W_r^{max}})^{2/3} \tag{3.5}$$

where W_r is the interception of rainfall which is given by

$$W_r = \delta p \tag{3.6}$$

p is the precipitation above the canopy. δ is fraction of vegetation (Mo et al., 2004)

$$\delta = 1 - exp(-0.5LAI) \tag{3.7}$$

W_r^{max} is water holding capacity of the canopy which is a function of leaf area index (LAI).

$$W_r^{max} = \mu LAI \tag{3.8}$$

and μ is a constant with reported values of between 0.05 and 0.2 (Dickinson, 1983).

In this study $W_r^{max}(mm) = 0.2LAI$ was used according to Dickinson (1985) After introducing the factor, the transpiration rate is given by

$$E_c = \frac{\Delta(R_n - G) + \rho c_p D_0 / r_{ac}}{\Delta + \gamma(1 + r_c/r_{ac})}(\frac{1 - W_{fr}}{\lambda}) \tag{3.9}$$

where:

1. $\Delta(kPa/^\circ C)$ is the first-order derivative of saturation vapour pressure with temperature which is given by Allen et al. (1998)

$$\Delta = \frac{4098\{0.6108exp(\frac{12.27T}{T+237.3})\}}{(T + 237.3)^2} \tag{3.10}$$

R_n is the net radiation above the canopy.

2. $\lambda(MJ/kg)$ is given by

$$\lambda = 2.501 - 2.36 \times 10^{-3} \times T_h \tag{3.11}$$

where: $T_h(^\circ C)$ is air temperature at height of h

3. G is soil heat flux and R_n is the net radiation. $R_n - G$ is given by Raupach (1991)

$$R_G - G = F_{A1} = f_G\{(1 - \alpha_c)R_s \downarrow + \varepsilon_c R_L \downarrow - \varepsilon_c \sigma T_1^4\} \tag{3.12}$$

α_c is the canopy albedo and the canopy emissivity ε_c is 1. f_G is a dimensionless number accounting for the heat flux density G into the ground and its value is set to 0.8. $T_1(^\circ C)$ is air temperature at z_1. $R_s \downarrow, R_L \downarrow$ are the short-wave and long-wave downward irradiance at the surface. σ is the Stefan-Boltzman constant.

4. D_0 is vapour pressure deficit of the air ($= e_s - e_a$).

5. ρ is mean air density at constant pressure.

6. c_p is specific heat of the air which has a value of $1.013 \times 10^{-3} MJ°C/kg$

7. $\gamma(kP_a/°C)$ is psychrometric constant which was given by Allen et al. (1998)

$$\gamma = 0.665 \times 10^{-3} P \tag{3.13}$$

where P is atmospheric pressure kP_a

8. r_{ac} is aerodynamic resistance of canopy which describes the resistance from the vegetation upward and involves friction from air flowing over vegetative surfaces. The transfer of heat and water vapour from evaporating surface into the air above the canopy is determined by the aerodynamic resistance:

$$r_{ac} = ln(\frac{z-d}{z_{om}})ln(\frac{z-d}{z_{oh}})/(\kappa^2 u_a) \tag{3.14}$$

where u_a is wind speed at reference height z. κ is von Karman's constant with a value of 0.41. d is zero-displacement height. z_{om} is roughness length for momentum transfer. z_{oh} is roughness length for heat and water vapour transfer. For crop and grass, $z_{om} = 0.123h_c$ and $d = 0.67h_c$ according to Monteith. Several empirical equations for the estimation of d, z_{om} and z_{oh} have been developed. In this study, $z_{om} = 0.10h_c$ and $d = 0.70h_c$ are used for forest (Verseghy et al., 1993). The relation

of z_{om} and z_{oh} is assumed (Brutsaert, 1979; Garrat and Hicks, 1973) as follows

$$z_{oh} = \begin{cases} z_{om}/2.0, & \text{Forest} \\ z_{om}/7.0, & \text{Crops} \\ z_{om}/12.0, & \text{Grass} \end{cases} \tag{3.15}$$

9. r_c is canopy resistance which describes the total mechanical resistance encountered by diffusion from inside a leaf to outside. Water vapour inside leaves is maintained at or very near its saturated value, for otherwise the mesophyllic cells of the leaf would desiccate and the leaf wilt. The stomata are pores which when open are the main conduits for transpirated water. Hence, the net resistance to water passing from the inside to the outside of the leaf depends largely on the stomata. However, some water diffusion also occurs through leaf cuticles, which can be the primary route for transpiration when the stomata are closed. In this study the more flexible approach of Noilhan and Planton (1989) was used. Canopy resistance was expressed as :

$$r_c = \frac{R_{smin}}{LAI} F_1 F_2^{-1} F_3^{-1} F_4^{-1} \tag{3.16}$$

where R_{smin} is the minimum stomatal resistance. LAI is leaf area index.

F_1 is the effect of photosynthetically active radiation on surface resistance r_c (Sellers et al., 1986). It was parameterized as (Dickinson, 1985; Noilhan and Planton, 1989)

$$F_1 = \frac{1+f}{f + \frac{R_{smin}}{R_{smax}}} \tag{3.17}$$

Category	h_c (m)	R_{GL} (W/m^2)	R_{smin} (s/m)
Crop	1.0	100.0	50.0
Deciduous	10.0	30.0	150.0
Coniferous	7.0	30.0	250.0
Mixed forest	8.5	30.0	200.0
Grass	0.1	100.0	50.0
Mixed agriculture and grass	0.5	100.0	50.0

Values of h_c and R_{smin} from Xu et al. (1999)

Table 3.1: Vegetation types and parameter values in the model

with

$$f = 0.55 \frac{R_G}{R_{GL}} \frac{2}{LAI} \tag{3.18}$$

where R_G is flux of visible solar radiation, and R_{GL} the visible solar radiation flux for which F_1 is about double its minimum value. It has a limiting value of 30 W/m^2 for forest and 100 W/m^2 for crop and grass. R_{smax} is the cuticular resistance of the leaves with a value of 5000 s/m (Noilhan and Planton, 1989).

F_2 takes into account the effect of soil water stress on the canopy resistance. F_2 depends on the soil moisture and the ability of plant roots to take water readily from the soil for a given level of root moisture. It varies between 0 and 1 when θ varies between θ_{wilt} and a critical value θ_{cr} of $0.75\theta_{sat}$ (Thompson et al., 1981)

$$F_2 = \begin{cases} 1, & \text{if } \theta > \theta_{cr} \\ \dfrac{\theta - \theta_{wilt}}{\theta_{cr} - \theta_{wilt}}, & \text{if } \theta_{wilt} \leq \theta \leq \theta_{cr} \end{cases} \tag{3.19}$$

θ is mean volumetric water in the root zone. θ_{cr} is the moisture content(θ) below which transpiration is stressed by soil moisture. It is assumed to be 0.75 times the saturated soil moisture (θ_{sat}) which is set as 0.4. The wilting point (θ_{wilt}) is set to 0.1.

F_3 represents the effect of the vapour pressure deficit (δq) on the canopy resistance and was given by Javis (1976)

$$F_3 = 1 - b\delta q \tag{3.20}$$

where b is a coefficient and set as -0.12 in this study according to reported data (Javis, 1976)

F_4 represents the effect of air temperature (T_a) on the canopy resistance. It was parameterized by Dickinson (1985)

$$F_4 = 1 - 0.0016(298 - T_a)^2 \tag{3.21}$$

The concentrations of Hg(0) in soil water were assumed to be constant in any location in the work of Xu et al. (1999). Lin and Tao (2003) assumed the concentration based on the closeness of that location to anthropogenic RGM and Hg(p) emission sources. The Hg(0) in the transpiration stream in this study was assumed to be dependent on the total Hg concentration in the soil. The information about data source, data processing and spatial distribution of Hg concentration in soil can be found in Section 3.4.5. Total Hg concentration in soil water is obtained by multiplying Hg concentration in soil by a soil-water partition coefficient of 0.215

g/L calculated using data from two independent studies reported in Lyon et al. (1997). The total Hg concentration in soil water was used as the Hg concentration in the transpiration stream, since plants are known to reduce dissolved oxidized Hg species (Rugh et al., 2000). Laboratory experiments by Leonard et al. (1998) showed that about 70% of Hg taken up by roots was emitted into the atmosphere. Recent experiments by Schwesig and Krebs (2003) indicated that 70-94% loss from the soil of potted plants was due to volatilization from both soil and plant, but the contribution from each source was unknown.

- **Emission from Soil**

Recent research suggests that Hg(0) emissions from soil depend on soil temperature and solar radiation (Kim and Lindberg, 1995; Carpi and Lindberg, 1998). In this study, Hg emission from soil was classified into emission from bare soil and emission from soil under vegetation canopy. For emission from bare soil, the common flux-temperature relationship was extended to include Hg concentration in soil. The Hg flux from soil (F_s) can be expressed as:

$$F_s = k[Hg]_s^n \tag{3.22}$$

where k is a rate constant and $[\mathrm{Hg}]_s$ is Hg soil concentration. The above Equation can be simplified to obtain:

$$lnF_s = -\frac{\beta}{T_s} + nln[Hg]_s + \eta \tag{3.23}$$

where β and η are constants and T_s is the soil temperature. β is a measure of the activation energy. We obtained a value of $12589K^{-1}$ for this from Xu et al. (1999). Using additional data on Hg flux for different $[Hg]_s$ (Carpi and Lindberg, 1998; Frescholtz and Gustin, 2004), we obtained n as 1.0 and γ as 38.67. Emission from soil under a canopy was neglected in previous work. Since a large part of our domain is forested, we included emission from beneath the canopy, based on a Hg flux-solar radiation relationship, since solar radiation was found to correlate better with Hg flux from soils under a canopy (F_{sc}) than temperature. Using measurements of mercury flux from forest soil and artificially shaded background soil (Carpi and Lindberg, 1998) and expressing the mercury flux and solar radiation relationship in a form similar to Equation 3.23, we obtained

$$lnF_{sc} = aR_{Gc} + bln[Hg]_s + b \tag{3.24}$$

where, a is 3.5×10^{-3} , b is 0.28 and c is -1.24. R_{Gc} is the solar radiation reaching the soil under the canopy, is given as:

$$R_{Gc} = R_G e^{-\lambda LAI} \tag{3.25}$$

The value for λ is taken to be 0.65 (Monteith and Usworth, 1990).

- **Emission from Water**

Dissolved gaseous Hg (DGM) is composed primarily of Hg(0), and its formation, distribution, and air-water exchange have been investigated in a variety of

freshwater and marine environments (Fitzgerald et al., 1991; Poissant et al., 2000; Gardfeldt et al., 2001). These studies have shown that dissolved Hg(0) measured as DGM can be produced in surface waters through biotic (bacteria and phytoplankton) and abiotic (photo-induced) processes, or by bacteria in light deficient waters. Such processes lead to supersaturation of volatile Hg(0) and subsequent evasion to the atmosphere across the water-air interface. Abiotic Hg(0) formation appears related principally to photolysis reactions in natural waters. Proposed mechanisms for Hg(0) formation include photochemical reactions involving dissolved organic matter (DOM) and/or Fe or Mn (Nriagu, 1994; Amyot et al., 1994; Zhang and Lindberg, 2001). Direct and/or secondary photoreduction of Hg(II) complexes by DOM to Hg(0) was reported in lacustrine surface waters (Nriagu, 1994) and it was suggested that aqueous organic matter is probably involved in sunlight-induced reduction of Hg(II) complexes to Hg(0). Presumably, given sufficient solar radiation, abiotic production of Hg(0) in aqueous systems can be enhanced as DOM increases.

In this study, emission flux of Hg(0) from water (F_w) is given by

$$F_w = K_w C_w \tag{3.26}$$

where, K_w is the mass transfer coefficient and C_w is the concentration of dissolved gaseous mercury (DGM) in the water. The mass transfer coefficient K_w is calculated with an approach used by Lin and Tao (2003) in which K_w can be correlated with the mass transfer of CO_2 across the air-water interface through

$$K_w = (0.45U_{10}^{1.64})[Sc_w(Hg^0)/Sc_w(CO_2)]^{-0.5} \tag{3.27}$$

where U_{10} is the wind speed (m/s) at 10m and Sc's are the Schmidt numbers for CO_2 and Hg(0) in water, respectively. The Schmidt number of CO_2 is calculated using the temperature-corrected dependency (Hornbuckle et al., 1994; Bidleman and McConnell, 1995).

$$Sc_w(CO_2) = 0.11T^2 - 6.16T + 644.7 \tag{3.28}$$

with T in ℃. The Schmidt number of Hg(0) is directly derived from its definition

$$Sc = \nu/D \tag{3.29}$$

where the temperature (℃) dependent ν (kinetic viscosity of water, cm^2/s) and D (diffusivity of Hg^0 in water, cm^2/s) are estimated by

$$\nu = 0.017exp(-0.025T) \tag{3.30}$$

$$D = 6.0 \times 10^{-7}T + 10^{-5} \tag{3.31}$$

A number of reports indicated that the concentration of DGM in water followed a diurnal pattern. The concentration of DGM(C_w, pg/L) has been found to correlate with time-shifted solar radiation ($R_{G(tminprior)}$, kW/m^2) (O'Driscoll et al., 2003).

$$C_w = aR_{G(tminprior)} + b \tag{3.32}$$

The optimum time, *tminprior* was found to be 75 minutes (R=0.9). A time of 60 minutes was used in this study since we have hourly meteorology data and also the

correlation observed by the authors was good for *tminprior*=60 minutes (R=0.85). Measurements indicate that concentration of DGM in the great lakes is usually higher (20-130 pg/L) than that in the ocean (10-50 pg/L). Therefore, for lakes this study used a=10 and $b = 82$ (O'Driscoll et al., 2003) and for the ocean this study used a=10 and b=40.

- **Emission from snow and frozen soil**

There is a special case that arises in natural Hg emission estimation. That is that we must take into account frozen surfaces and snow cover in wintertime for northern areas in our simulation domain (see Figure 3.1). To account for the effect on natural emission of snow cover and low temperatures during the winter months, we followed the approach used for NO emissions from soil in the Biogenic Emission Processing System (BEIS) of the SMOKE program (Byun and Ching, 1999) and set the emission of mercury from the soil and water to be zero when soil or water temperature is less than 0°C. Emission is also set to zero if the surface is completely covered with snow. For surfaces that are partially covered with snow, the emission flux is multiplied by the fraction of surface not covered with snow. These assumptions are consistent with recent measurements that indicate average mercury emission flux from background soils covered with snow is less than 0.1 ng/m^2/h (Schroeder et al., 2005). Figure 3.1 shows average snow cover in January, 2002 in North America in the simulation domain. About 63% of grid cells in the simulation domain (132×90) were partly or totally covered by snow in January, 2002.

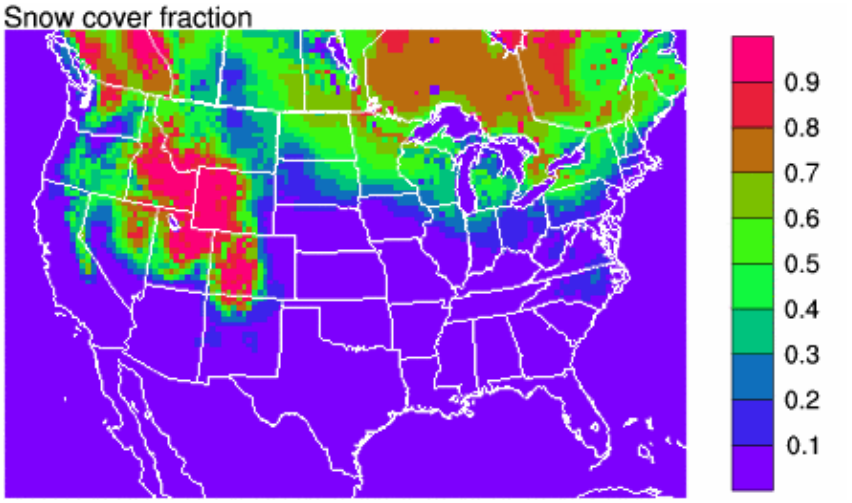

Figure 3.1: Average snow cover fraction in January, 2002

3.3 Generation of natural mercury emission

To implement the estimation of natural mercury emissions, we ran MCIP twice. The first run was a temporary run to obtain the solar radiation field from MM5 output. After that, solar radiation data were reconstructed into one-hour backwardly shifted solar radiation data required to compute natural Hg emission from water. The second run of MCIP was a normal run to estimate natural mercury emission fluxes from various land uses in the domain, including emission from water using one-hour shifted solar radiation data.

3.4 Simulation procedure

3.4.1 Domain of simulation

The modelling domain represents the geographical bounds of the area to be modelled. It should include the area of interest with local emissions and an external extra area sufficient to represent the transported emissions according to the wind pattern. In order to investigate atmospheric behaviour of mercury emission, transport, transformation and deposition in North America, especially in South Ontario region, the modelling domain was chosen to be centered at 40°N, 100°W and cover the main portion of North America (Figure 3.2). The Lambert-conformal projection was used in the mapping procedure. To minimize the effect of big anthropogenic mercury emissions, the west and east bounds were extended into oceans. The domain includes 132×90 grid cells with a grid size of 36km×36km, and vertically there are 15 layers in half sigma coordinates extending from the ground to 100 mb. The simulation period covers the whole year 2002.

3.4.2 Land use data

There are ten basic land use types in the simulation domain according to MM5 land use classification. The distribution of land uses in the simulation domain is presented in Figure 3.3. The statistical information on land uses in the modelling domain is also listed in Table 3.2. For urban grids, 25% of the area was treated as mixed forests, 25% treated as bare soil for emission estimation. Rocky open areas with low shrubs grids were treated as range. Non-forested wetland grids were

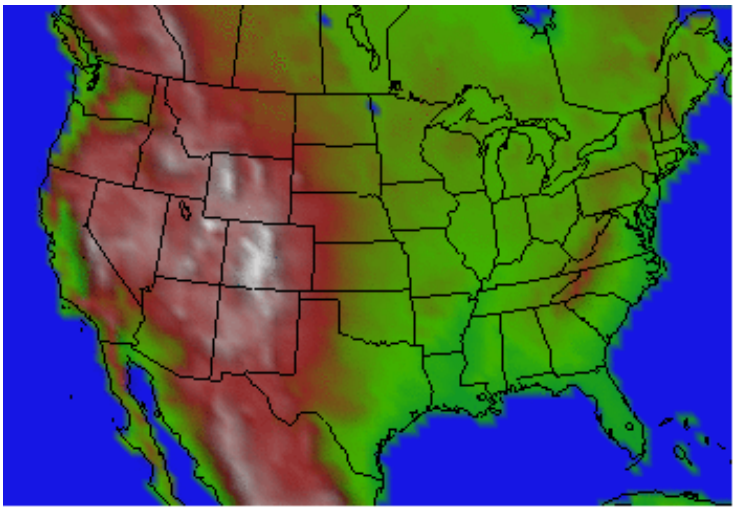

Figure 3.2: The modelling domain

treated as water during this estimation.

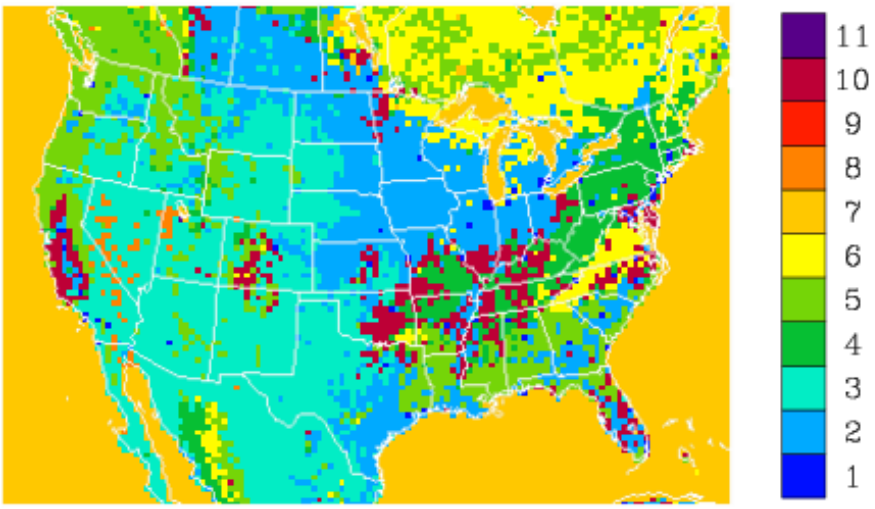

1. Urban 2. Agriculture 3. Range 4. Deciduous forest
5. Coniferous forest 6. Mixed forest wetland 7. Water
8. Barren land 9. Non-forested wetland 10. Mixed agriculture/rangeland
11. Rocky open areas with low shrubs

Figure 3.3: Land uses in modelling domain

Landuse	Number of grids	%
Urban	73	0.61
Agriculture	1836	15.45
Range	2494	20.99
Deciduous forest	729	6.13
Coniferous forest	1517	12.77
Mixed forest wetland	1000	8.41
Water	3583	30.16
Barren land	72	0.61
Non-forested wetland	0	0.00
Mixed agricultural/rangeland	575	4.84
Rocky open areas with low shrubs	1	0.00

Table 3.2: Land uses and the fraction of each land use in the simulation domain

3.4.3 Meteorology conditions

The Fifth-generation NCAR/Penn State Mesoscale Model (MM5) version 3.6 was employed to generate meteorological field data using a nested domain technique. The centre of coarse domain is at 40°N, 100°W and the coarse domain includes 63×79 grid cells with a resolution of 108km. The fine domain has 103×154 grid cells with a resolution of 36km. 22 vertical half-sigma layers extending from ground to 100mb were defined for MM5 simulation for the whole year 2002. Overlapping parabolic interpolation handles the mapping of terrain heights, vegetation fractions, and land use characteristics from the USGS 25-category, 10-minute resolution datasets to the specified coarse grid, 5-minute resolution datasets for the finer grid. Additional field datasets such as 17-category global soil data, 10-minute global vegetation fraction data, 1-degree annual deep soil temperature required for the implementation of the land surface model were selected within the TERRAIN preprocessor. First-guess fields were established through the NCEP/NCAR six-hourly

analysis data. The NCEP Global Tropospheric Analysis datasets were processed within PREGRID to incorporate observed Sea Surface Temperature (SSTs). The physical parameterization selections employed for MM5 runs in this study were summarized in Table 3.3.

Physical option	Configuration
Explicit moisture scheme	Simple ice
Cumulus scheme	Grell
Planetary boundary layer	Pleim-Chang
Atmospheric radiation	Cloud radiation
Multi-layer soil temperature model	Pleim-Xiu LSM
Shallow convection	No

Table 3.3: Physical options and configurations in MM5 simulation

Pleim-Xiu Land-Surface Model (ISOIL=3) was configured as surface scheme and Pleim-Chang PBL (IBLTYP=7) as PBL scheme in MM5 simulation to obtain land-surface information for estimating natural mercury emissions.

3.4.4 Snow cover

MM5 was run with Noah Land Surface Model to generate snow cover data, and then it was run again with Pleim-Xiu Land Surface Model to obtain the meteorology data for MCIP and CMAQ-Hg models. The reason to run MM5 twice is that MCIP only takes the output of MM5 run with Pleim-Xiu Land-Surface Model as input, but with this setup MM5 is not able to generate snow cover data needed by natural mercury emission model for estimating natural Hg emission.

3.4.5 Hg(0) concentrations

The Hg(0) in the transpiration stream was assumed to depend on the total Hg concentration in the soil in this study. Figure 3.4 shows the spatial distribution of Hg concentration in soil over the simulation domain, which was generated from soil Hg concentration measurements from USA and Canada. Hg concentration measured at 20 cm, or the B horizon for the United States was obtained by Boerngen and Shacklette (1981) from 1267 sample sites spread all over USA. For Canada, a value (40 ppb) was assigned to locations in Ontario and BC in our domain, and 30 ppb to locations in other provinces to produce a data density similar to that of the US. 40 ppb was also assumed to locations in Mexico. The value assigned corresponded to the median of Hg measurements done by the Geological Survey of Canada for Southern Ontario (Garrett, 2004). The data were gridded over the simulation domain to produce a Hg distribution similar to that reported by Gustavsson et al. (2001). Total Hg concentration in soil water is obtained by multiplying Hg concentration in soil by a soil-water partition coefficient of 0.215 g/L calculated using data from two independent studies reported in Lyon et al. (1997). Since plants are known to reduce dissolved oxidized Hg species (Rugh et al., 2000), total concentration of Hg in soil water was used as Hg(0) concentration in the transpiration stream in the calculation of Hg emission from vegetation.

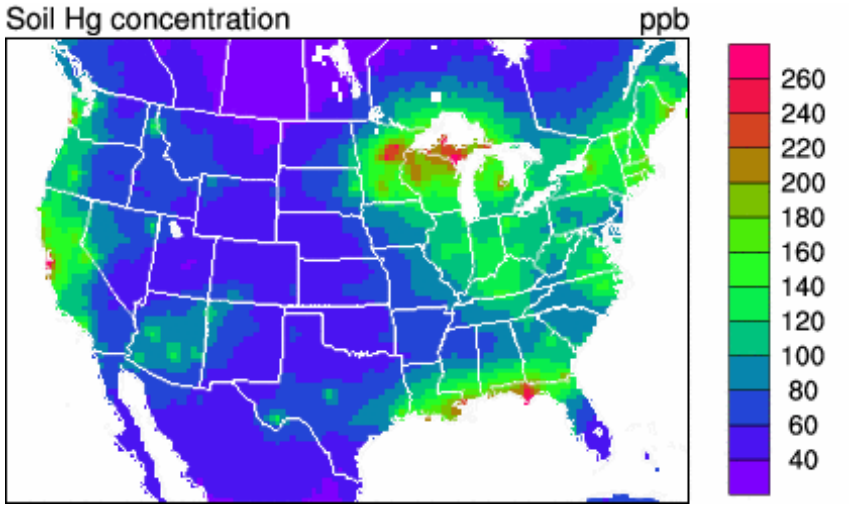

Figure 3.4: Spatial distribution of soil Hg concentration in the simulation domain

3.5 Results and discussions

3.5.1 Validation

Figure 3.5 shows the mercury emission flux averaged across the domain for different land covers. This average emission flux is greater for vegetation than water and soil. The modelled fluxes lie within the values reported in the literature, which are shown in Table 3.4. Note that some of these flux measurements were taken near contaminated sites (Lindberg et al., 1998) and these far exceed those at clean sites, indicating the importance of soil Hg concentration in the estimation of natural Hg emission.

3.5.2 Characteristics in modelled natural Hg emission

3.5.2.1. Spatial patterns in modelled Hg(0) emissions

Vegetation		Soil		Water	
Location	Hg $ng/m^2/h$	Location	Hg $ng/m^2/h$	Location	Hg $ng/m^2/h$
Matured Hardwood, TN	8-66 (Lindberg et al.,1998)	Shade Forest Soil, TN	2-7 (Carpi and Lindberg,1998)	Swedish Coast	0-8.8 (Gardfeldt 2001)
Young small Pine, TN,	1-35 (Lindberg et al.,1998)	Shade Forest Soil, MI	1.4±1.4 (Zhang et al. 2000)	Lakes NS	0-13 (Boudala et al.,2001)
Cattail Canopy, FL	17±43 (Lindberg et al.,2002)	Agricultural Soil, PQ	3±2.2 (Poissant and Casimir,1998)	Lake Ontario	0-9 (Poissant et al., 2000,calculated)

Table 3.4: Some measured natural mercury emission fluxes

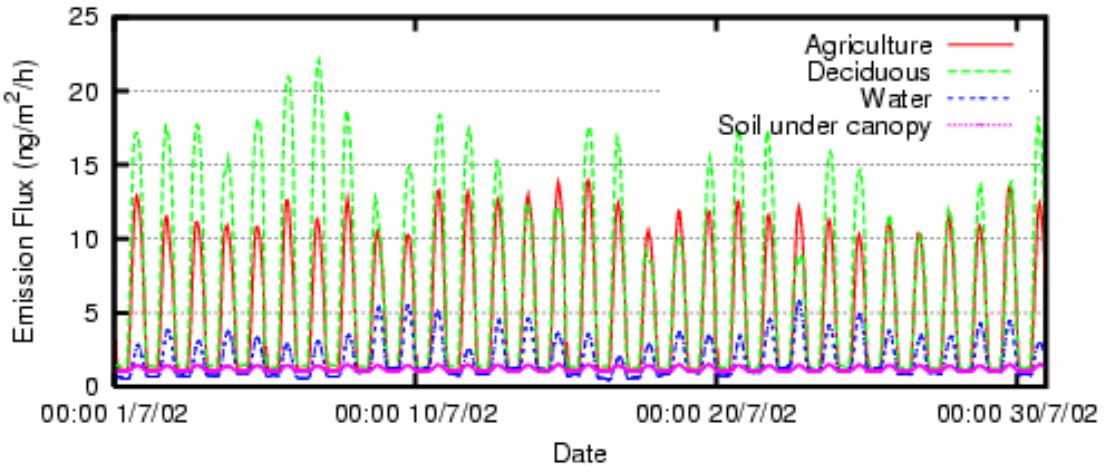

Figure 3.5: Average natural Hg emission fluxes in the domain for different land covers in July, 2002

3.5.2.1.1 Horizontal distribution of modelled Hg emission

Figure 3.6 shows the spatial variation of natural Hg emission fluxes averaged over the entire simulation period. The fluxes vary within a range of 0.5 - 8.5 ng/m^2/h. The emission flux is generally high in the west coast of U.S. and Eastern North America. This is similar to the distribution of soil mercury concentration (Figure 3.2). A relatively strong correlation between emission flux and soil Hg concentration (Figure 3.7) suggested soil Hg concentration as a key factor governing the Hg emission distribution across the simulation domain. However, the distribution of natural Hg emission flux is not identical to that of soil mercury concentration because the natural emission is also dependent on a number of factors such as land cover, soil moisture deficit, temperature, solar radiation, wind speed and water vapour pressure.

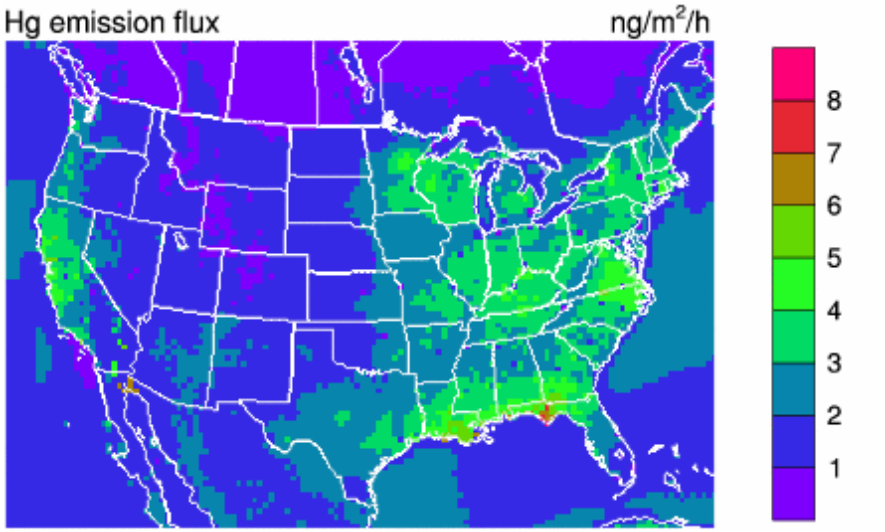

Figure 3.6: Spatial distribution of annual average natural Hg emission flux for 2002

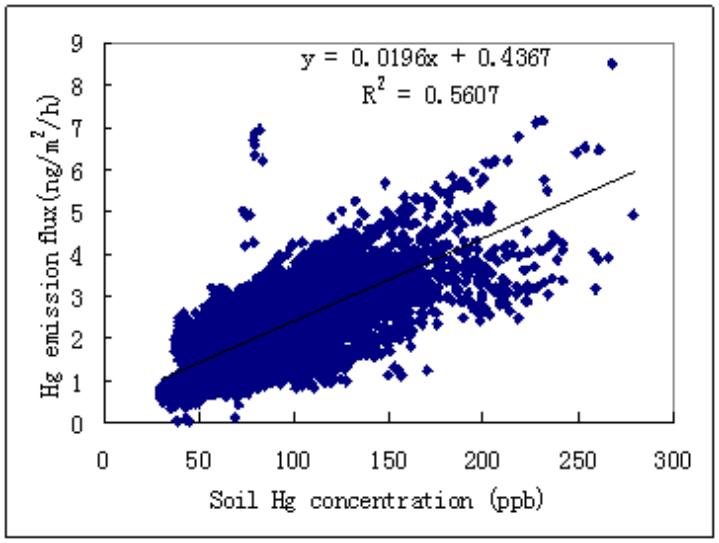

Figure 3.7: Correlation between soil Hg concentration and annual average flux of natural Hg emission for 2002

3.5.2.1.2 Variation of modelled Hg(0) emissions from south to north

Modelled Hg emission fluxes averaged along a west-east direction over the simulation domain show a variation of emission with latitude (Figure 3.8). It is of interest to note that high emission flux occurs in an area band between around 30°N to 45°N. This may be caused by high annual average temperature, large portion of vegetation and high soil Hg concentration in this region. Regions outside this band demonstrate low natural Hg emission fluxes. Generally, soil temperature and air temperature in the region above 45°N are lower than other regions, and there snow covers a large portion of area for most of the time of a year. All of these factors limit the Hg emissions from soil, water and vegetation. Lower emission flux in low latitude area results from a large area of water, which has a lower emission flux than vegetation.

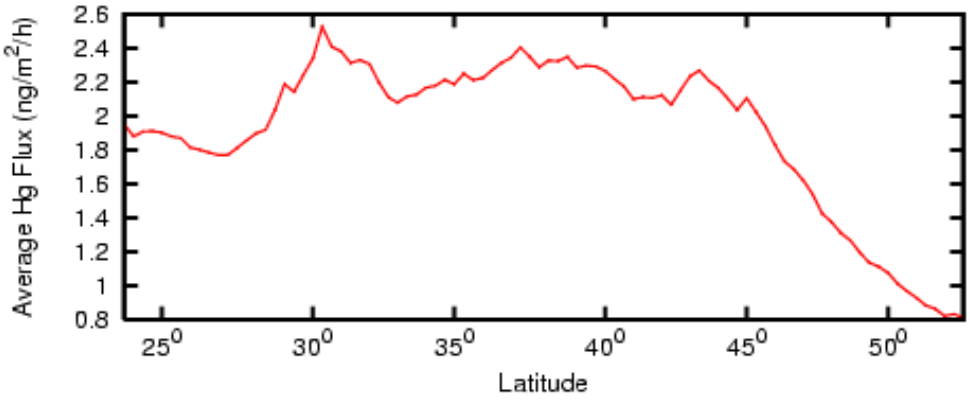

Figure 3.8: Natural Hg emission flux averaged along longitude direction in the simulation domain

3.5.2.2. Temporal pattern in modelled Hg(0) emissions

3.5.2.2.1 Daily variation

The modelled natural mercury emissions from vegetation, water and soil under canopy show strong daily diurnal cycle during the simulation period (Figure 3.9). The time-averaged cycle appears around 12:00 GMT in the morning and disappears around 24:00 GMT in the afternoon with a maximum around 19:00 GMT. No obvious emission fluctuation is observed at night for all land uses. This kind of variation pattern suggests the strong connections between natural Hg emission and some meteorological variables such as solar radiation and surface temperature, which demonstrate a strong diurnal pattern as well. The results of regression analysis (Figure 3.10 and Figure 3.11) indicate that natural Hg emission is correlated well to both surface temperature and solar radiation, especially to the latter. Solar radiation is a significant factor determining the diurnal pattern of natural Hg emission.

In water solar radiation may promote the formation of DGM via photochemical reactions and further air-water gas exchanges (Amyot et al., 1994; Poissant et al., 2000; Zhang and Lindberg, 2001). Solar radiation also greatly influences natural Hg emission because it directly affects transpiration rate of canopy. The relative importance of Hg emission from different land types can also be observed in Figure 3.9.

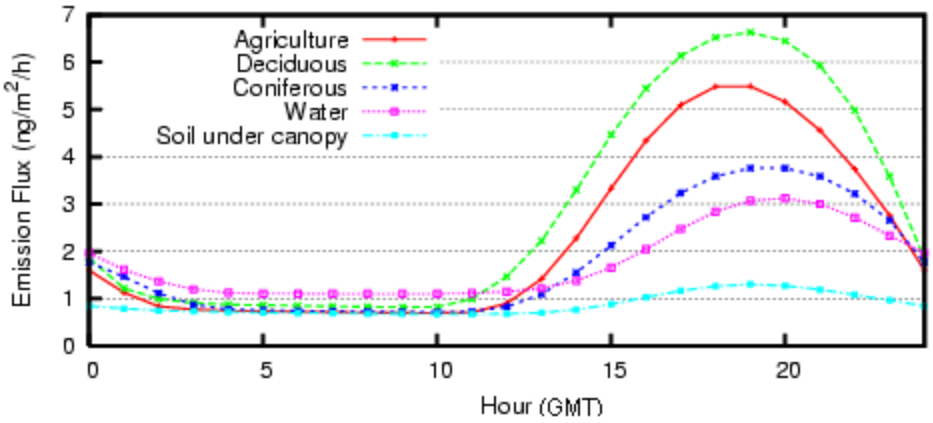

Figure 3.9: Average daily variation of natural Hg emissions for different land uses

3.5.2.2.2 Seasonal variation

Monthly total and average of natural Hg emissions over the simulation domain in 2002 are presented in Figure 3.12. The monthly total natural Hg emission obviously demonstrates an annual cycle, in which natural Hg emission reaches its maximum in July and minimum in January. The maximum is about 5 times its minimum. The same pattern is observed for monthly average emission rate as well. Since factors such as solar radiation, air temperature, leaf area index, soil moisture,

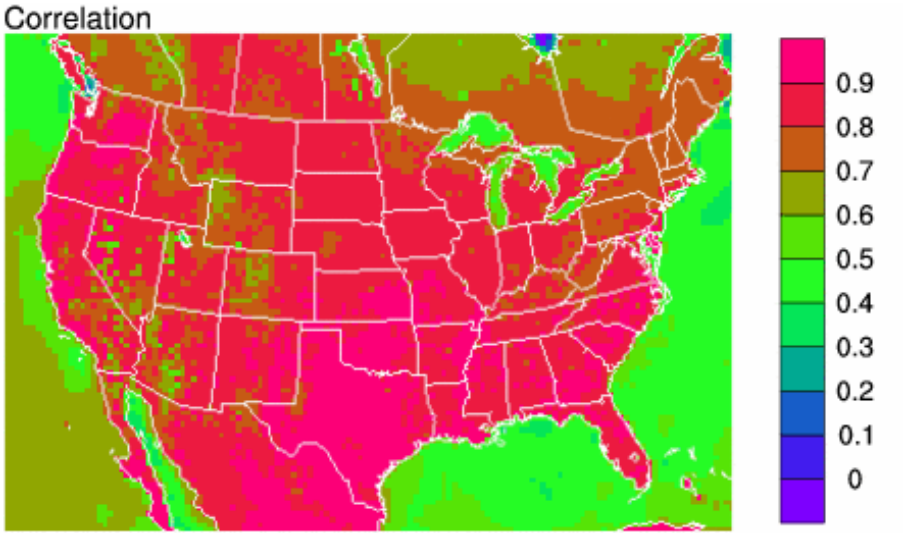

Figure 3.10: coefficients (r) between natural Hg emission fluxes and solar radiation reaching surface

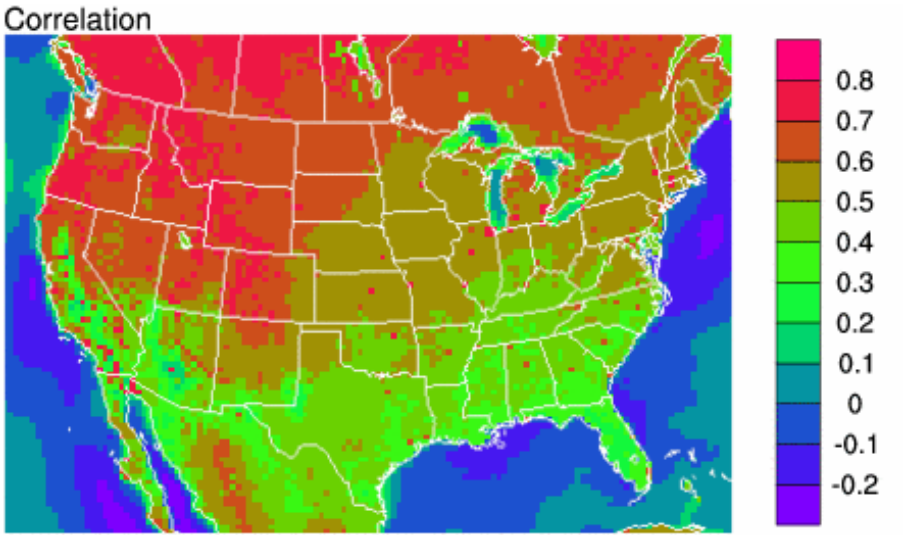

Figure 3.11: coefficients (r) between natural Hg emission fluxes and surface temperature

precipitation and snow cover fraction demonstrate an annual cycle, all of which could be the factors governing this pattern of natural Hg emission. The strongest correlation (Table 3.5) between natural Hg emission and leaf area index indicates that leaf area index might be the most important factor controlling annual natural emission variation. Other important factors include solar radiation, surface temperature, soil moisture and snow cover fraction. As expected, there is a negative correlation between natural Hg emission and snow cover fraction. In general, natural Hg emission is supposed to be positively correlated with soil moisture. The higher soil moisture, the higher transpiration rate of canopy, thus the higher natural Hg emission flux. In this study natural Hg emission is negatively correlated to soil moisture. This is possible if soil moisture is higher in winter than in summer in the simulation domain.

	Correlation coefficient (r)
Monthly surface temperature average	0.91
Monthly radiation reaching ground average	0.94
Monthly cloud fraction average	-0.08
Monthly snow cover fraction average	-0.84
Monthly leaf area index average	0.97
Monthly soil moisture average	-0.89
Monthly precipitation	0.49

Table 3.5: Correlation between monthly total natural Hg emission and other factors

3.5.2.2.3 Seasonal variations from different land uses

Similar to annual variation of total natural Hg emission, emissions from different land uses also show an obvious annual cycle pattern in which maximum occurs

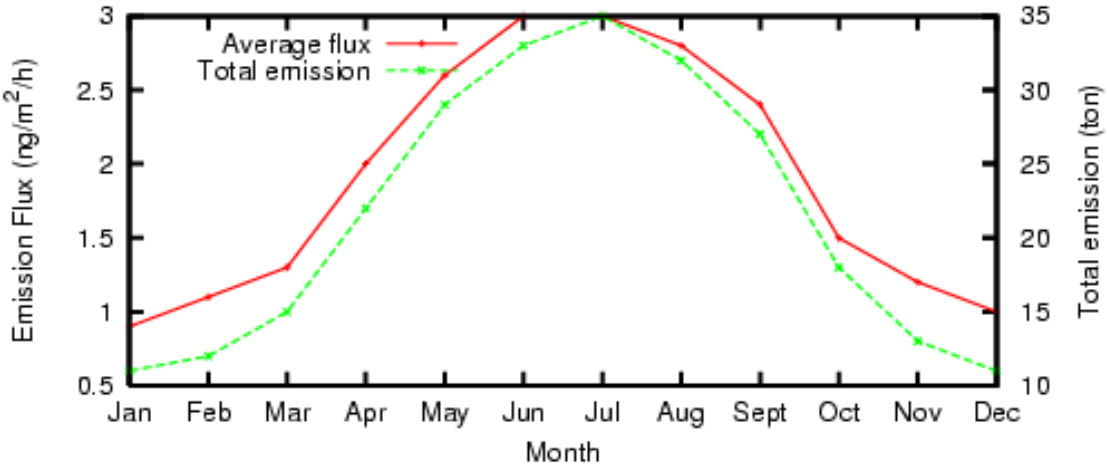

Figure 3.12: Monthly average natural Hg emission flux over the simulation domain in 2002

in July and minimum in January or in December (Figure 3.13). An exception was found for water from which no obvious annual variation is observed. The results (Table 3.6) of a regression analysis indicate that surface air temperature, solar radiation and leaf area index are all important factors determining an annual variation of natural Hg emissions from vegetation and soil. Since emission from water is not significantly affected by surface air temperature, solar radiation and solar radiation, no obvious annual variation is presented for emission from water. Figure 3.14 shows the same variation pattern as shown in Figure 3.13 for monthly total emissions from different land types. Water constitutes a major part of the domain, so even if it has a relatively small emission rate, it still exhibited high total emission for all months.

3.5.2.3. Annual total natural Hg emission

	Surface temperature	Solar radiation	Leaf area index
Agriculture	0.98	0.93	0.97
Deciduous forest	0.99	0.91	0.97
Water	0.30	0.63	
Soil under canopy	0.94	0.9	0.96

Table 3.6: Correlation coefficients (r) between natural Hg emissions from several land uses and other factors

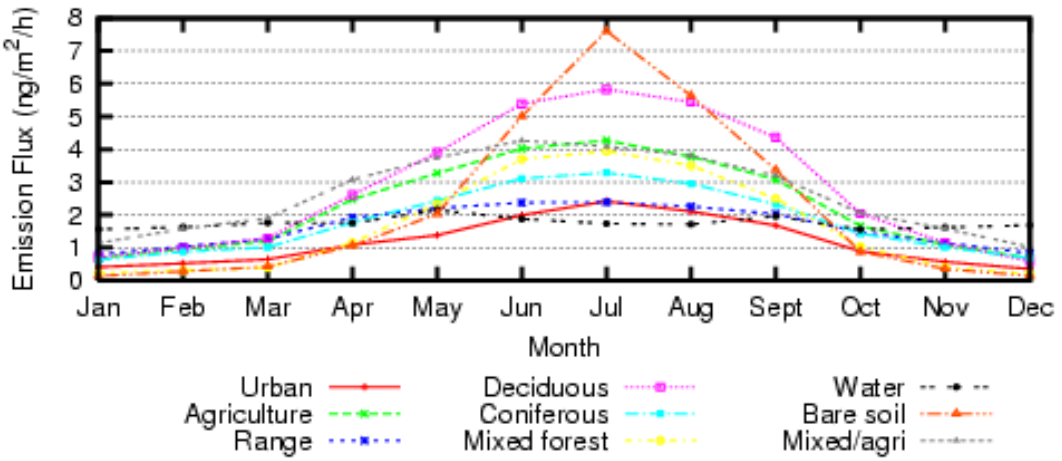

Figure 3.13: Monthly average of natural Hg emission fluxes from different land uses in the simulation domain in 2002

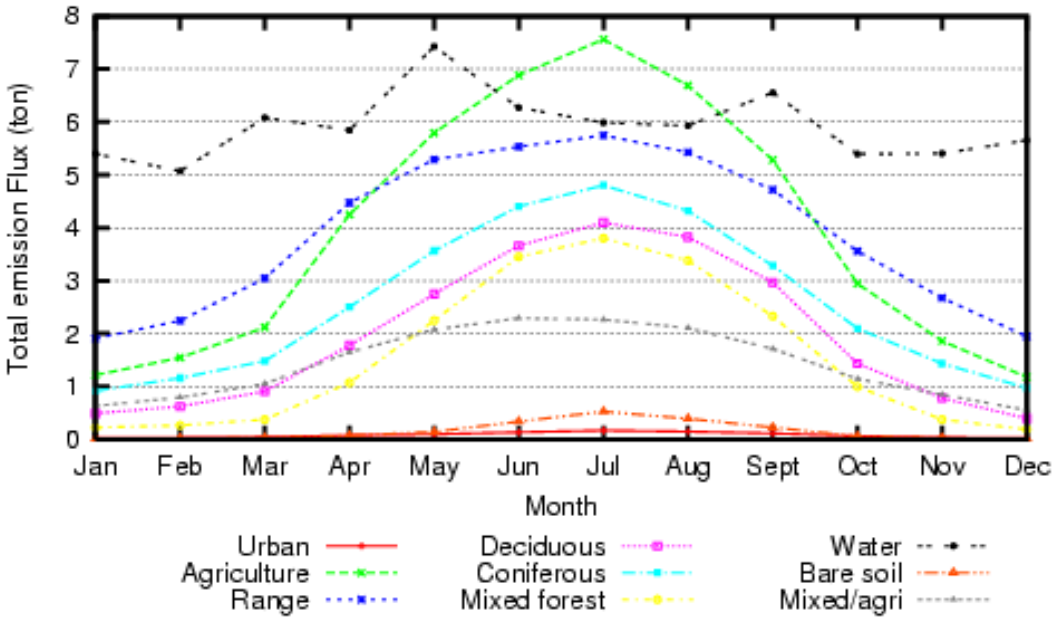

Figure 3.14: Monthly total natural Hg emissions from different land uses in the simulation domain in 2002

During the simulation period over the whole simulation domain, about 229 metric tons of Hg(0) was estimated to be naturally emitted into the atmosphere from various land uses in 2002 (Table 3.7). Water was found to be the largest natural emission source accounting for 27.5% (Figure 3.15) of total natural Hg emission. The possible reason is that the largest portion of area in the domain is water and it has high emission rates in winter (Figure 3.13). Since agriculture has large emission rate and range has a large portion of area in the domain, agriculture and range have almost the same total annual emissions in this simulation. Deciduous forest has the highest emission rate; however, its total emission is smaller than coniferous forest due to small area fraction. The smallest source is rocky open areas with low shrubs because it has only one grid in the simulation domain.

The contributions to total natural Hg emission from different months are quite different (Figure 3.16). Hg emitted in July accounts for about 13.5% of total Hg emission. On the contrary, Hg emitted in January is the least, less than 4.19% of total emission. Generally speaking, summer months contribute a larger amount of Hg(0) than winter months. Total amount of Hg emission from warm half of the year (April - September) is approximately more than 2 times total Hg emission from the cold half (October - March).

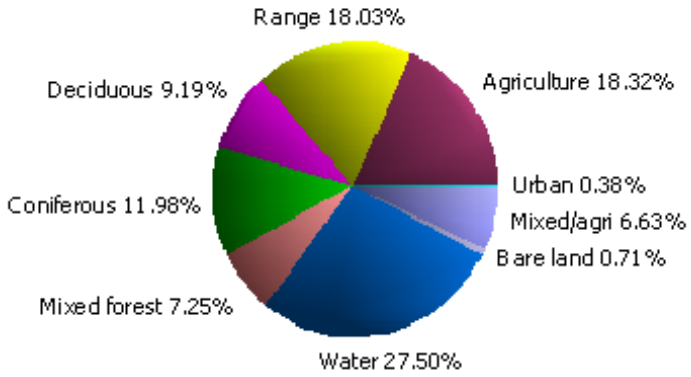

Figure 3.15: The contribution of each land use to 2002 total natural Hg emission

3.5.2.4. Emissions from summer and winter

3.5.2.4.1 Spatial distribution

Figure 3.17 shows the ratio of average natural Hg emission flux in July to that in January across the simulation domain. It is evident that emission rates across majority of the simulation domain in July 2002 are bigger than those in January,

	Number of grids	Annual total emission (tonnes)	Annual average emission flux ($ng/m^2/h$)
Urban	73	0.87	1.17
Agriculture	1836	41.95	2.28
Range	2494	41.29	1.65
Deciduous forest	729	21.05	2.87
Coniferous forest	1517	27.43	1.80
Mixed forest	1000	16.60	1.65
Water	3583	62.98	1.75
Bare land	72	1.63	2.26
Mixed/agri	575	15.18	2.63

Table 3.7: Total Hg emissions and average emission fluxes from different land covers in modelling domain for 2002

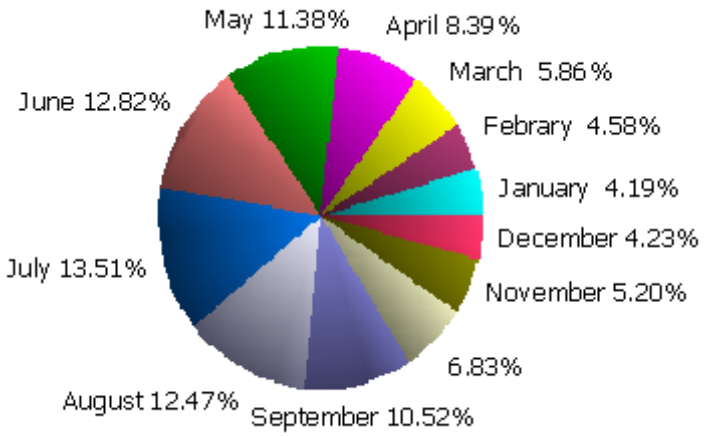

Figure 3.16: The contribution of each month to 2002 total natural Hg emission

especially in the northern part of domain where the ratios are even greater than 1000. About 92% of total grids of the domain have a ratio greater than 1. Grids with a ratio greater than 2 constitute almost 80% of the domain, and areas with a ratio greater than 100 account for 19% of domain. This phenomenon results not only from the large differences in snow cover fraction, but also from the large difference in surface temperature between summer and winter in northern part of domain. Since most of northern area in winter is covered by snow or ice, which greatly limits the natural emission of Hg(0) from surfaces, emission rates in winter should be very low. Hg emission also decreases in winter due to weakened radiation. The significant difference of emission between summer and winter indicates that any estimation only from summer emission or winter emission alone would greatly overestimate or underestimate total annual natural Hg emission.

3.5.2.4.2 Total emissions from different land uses in summer and winter

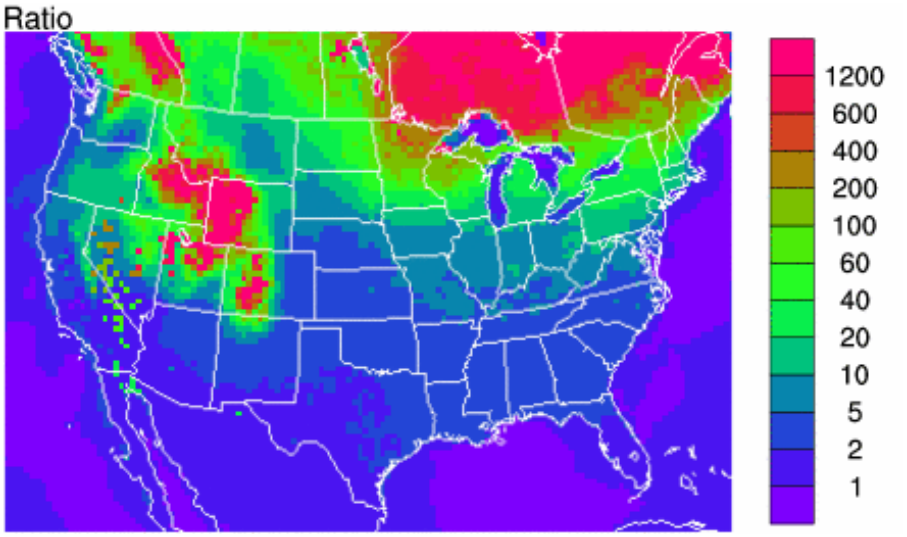

Figure 3.17: Ratio of average emission flux in July to that in January

Total natural Hg emissions from different land uses are shown in Table 3.8 for July and January, 2002. Average emission fluxes from all land uses for July and January are shown in Table 3.8 as well. As we can see, except from water, total emissions from the other land uses in July are all 3 times greater than the total emission in January (emissions from bare soil and rocky open areas with low shrubs were ignored only because there were few grids in the simulation domain). Among those different land uses, emission from mixed forest has the biggest difference between July and January because mixed forest is mainly distributed in the northernmost part of domain where the ratio of July to January is high (Figure 3.17). Deciduous forest comes next as a result of the change in leaf area index between summer and winter. As for coniferous forest, leaf area index does not vary significantly during a year, therefore, no big difference of natural Hg emission is expected between summer and winter, even if it is mainly distributed in northernmost part of the domain. Unlike other land uses in the domain, emission from water does not show

obvious seasonal change as a consequence of a relatively small annual variation of water temperature compared to land surface.

3.6 Summary and conclusions

A natural Hg emission model was developed to estimate natural Hg emissions from different land uses in the simulation domain. This model included the refined parameterization of processes related to Hg emission. It was built up on more realistic substrate information such as measurements of soil Hg concentration, reported Hg concentration in sea and lakes, soil moisture, snow cover fraction and Leaf area index from MM5 output. The influence of snow cover and low temperature on natural Hg emission in winter was also taken into account in the model. Compared with some reported natural Hg emission measurements, the results of one year's simulation demonstrated a good agreement indicating a strong simulation ability of this model.

Temporal variations of natural Hg emission from all land uses in the domain exhibit an obvious diurnal variation in which natural Hg emission rate reaches a maximum around 19:00(GMT). The ranges of variation from different land uses differ significantly.

No significant annual variation is found for natural Hg emission from water, while the variations from all other land uses demonstrate a strong annual cycle of variation, with a maximum around July and a minimum around January.

	Annual emission (tonnes)	Total emission (tonnes)		Emission flux ($ng/m^2/h$)		Ratio (Jul./Jan.)
		July	January	July	January	
Urban	0.87	0.17	0.03	2.41	0.41	5.95
Agriculture	41.95	7.56	1.22	4.27	0.69	6.22
Range	41.29	5.74	1.91	2.39	0.79	3.01
Deciduous forest	21.05	4.10	0.50	5.83	0.70	8.27
Coniferous forest	27.43	4.80	0.91	3.28	0.63	5.25
Mixed forest	16.60	3.80	0.22	3.94	0.23	17.16
Water	62.98	5.99	5.39	1.73	1.56	1.11
Bare land	1.63	0.53	0.01	7.61	0.13	56.58
Mixed/agri	15.18	2.27	0.63	4.09	1.15	3.57

Table 3.8: Monthly average and total natural Hg emissions in January and July for different land uses

The modelled total natural Hg emission in this simulation domain in 2002 is about 229 metric tons. Water is found to be the largest source accounting for about 27%. Agriculture and range are also important contributors of total natural Hg emission, both of them accounting for about 18% of total emission. Since deciduous forest has a smaller area fraction in the domain, it is not the largest source even if it has the largest average emission rate of all.

As for monthly total emission, about 40% total annual natural Hg emission is emitted in 3 summer months June, July and August, but emission in 3 winter months December, January and February only accounts for 13%. Emission in July (14% of total emission) is 3 times that in January (4% of total emission). This significant difference of natural emission between summer and winter suggests that any estimation only from summer emission rate or winter emission rate alone would greatly overestimate or underestimated total annual natural Hg emission.

Small natural Hg emission in winter results from specific winter conditions such as snow cover, low temperature, small leaf area index and frozen soil. All of these conditions greatly limit natural Hg emission.

Chapter 4

Simulation of atmospheric Hg transport, transformation and deposition in North America

4.1 Introduction

Concern about human impact on the environmental cycling of mercury is widespread due to its toxic and bio-accumulative properties. In aquatic systems mercury is often converted by bacteria to methylmercury which can be magnified up in the aquatic food chain hundreds of thousands of times, thus posing a potential risk to humans and wildlife that consume fish. It is generally believed that atmospheric deposition is the predominant pathway delivering Hg to aquatic systems. The investigation of emission, transport, transformation and deposition of atmospheric

Hg has become an active research area in recent years. Atmospheric Hg models are an effective method to investigate the atmospheric Hg emission, transport and deposition in different scales, and have undergone rapid development during recent decades. A number of models are widely used. Global mercury models include the Global Regional Atmospheric Heavy Metals Model (GRAHM, Canada) (Dastoor and Larocque, 2004); the Mercury Chemical Transport Model (CTM-Hg, USA) (Seigneur et al., 2001) and a mercury version of the Model of the Global Universal Tracer Transport In the Atmosphere (MOGUNTIA-Hg, Sweden) (Bergan et al., 1999). Regional models include the Meteorological Synthesizing Centre-East Heavy Metal Model (MSCE-Hg, Russia) (Ryaboshapko et al., 1999); a mercury version of Acid Deposition and Oxidant Model (ADOM-Hg, Germany) (Petersen et al., 2001) and a mercury version of the Community Multiscale Air Quality Model (CMAQ-Hg, USA) (Bullock and Brehme, 2002). In the previous applications of atmospheric mercury modelling, reasonably accurate estimates of anthropogenic mercury emissions were used, but natural mercury emissions were either neglected, assumed to be part of global background or oversimplified. Although the sources of natural mercury emission can be identified, estimates of the emission strengths vary widely.

This chapter presents a simulation study on the emission, transport, transformation and deposition of atmospheric Hg in North America using an improved CMAQ-Hg model system described in Chapters 2 and 3. The objective of this study is to test the improved model system and explore the behaviour of atmospheric Hg cycle in North America through one year (2002) simulation. The emphasis is on the characteristics of natural and anthropogenic emissions, comparison of modelled

ambient Hg concentration with measurements, temporal variation of ambient Hg concentration, features of dry, wet and total deposition, and Hg budget in this region.

4.2 Simulation procedures

4.2.1 Model description

The model used in this study to simulate regional atmospheric transport, transformation and deposition of Hg is a improved CMAQ-Hg model system. Details of the model were reported in Chapters 2 and 3.

4.2.2 Domain definition

The regional scale atmospheric transport, transformation, and deposition of Hg were simulated for the whole year 2002. The simulation domain covers the main portion of North America (Figure 3.2). There are 132×90 grid cells in horizontal direction with a grid size of 36km×36km. There are 15 vertical layers in sigma coordinates extending from ground to the height of 100 mb.

4.2.3 Meteorological conditions

The meteorology data used to drive the model are from the simulation of the Fifth-generation NCAR/Penn State Mesoscale Model (MM5) version 3.6. Details

of the MM5 setup for this simulation were reported in section 3.3.2. MM5 output were preprocessed by MCIP for CMAQ-Hg runs.

4.2.4 Initial and boundary conditions

The Models-3/CMAQ processors JPROC, ICON and BCON were run to generate photolysis rates, initial conditions and boundary conditions, respectively. Mercury boundary conditions, which varied from January to December, were taken from the global mercury simulation work of Seigneur et al. (2004) which included both natural and anthropogenic emissions of Hg. The global model had 9 layers. The horizontal resolution of the global model was 8 degrees latitude by 10 degrees longitude. The boundary conditions were obtained from the global model in the following manner: A layer of the model was matched to the nearest layer of the global model and the global model value was assigned to the model layer. The values for the rest of the model layers were interpolated from the values obtained by the layer-matching. For the horizontal boundaries, since CMAQ accepts one value for each boundary (South, North, East, West) the values from the global model within a model boundary were averaged and the average value obtained was assigned to the boundary. The mercury concentration values obtained from the global model were monthly averages. Each monthly average value was assigned to the middle of the month and then interpolated to get values for the other days of the year. This approach avoided a sudden change in boundary conditions from the last day of one month to the first day of the next month. Also, the boundary conditions obtained gave a better reflection of the actual seasonal variation of the boundary conditions

unlike in most simulations in which the same number is used for the boundary condition for each day. The gridded emissions output from SMOKE, along with the photolysis rates, initial and boundary conditions, were fed to the Models-3/CMAQ CTM for the simulation.

4.2.5 Emissions

Criteria pollutant emission

In this study, the 1999 National Emissions Inventory (NEI) version 3 IDA Files (U.S. EPA, 2004a) of the anthropogenic Criteria pollutants was used for the United States. The most complete Criteria inventory for anthropogenic sources in Canada is that for 1995, which was obtained from the Ontario Ministry of Environment (OMOE) (Chtcherbakov, 2004). These anthropogenic emissions were processed using Version 2.1 of the Sparse Matrix Operator Kernel Emissions (SMOKE) processor. The Criteria pollutants from biogenic sources were processed using the BEIS3 program in SMOKE V2.1 and gridded land use data for North America obtained from OMOE (Chtcherbakov, 2004).

Mercury emission

Canada and USA Hg anthropogenic emissions

Anthropogenic Hg emission data for the US and Canada were obtained from U.S. EPA (2004b). These emissions data were developed for 2001 to model the Clean

Air Mercury Rule (CAMR). The US emissions were based on the 1999 National Emissions Inventory (NEI), with the emission from 5 Medical Waste Incinerators modified to reflect 2002 emissions. The area source emissions for Canada were available as province totals, which we mapped onto counties based on population. Estimated mobile source mercury emissions for the US for 1996 are available (Bloxam, 2003). In order to obtain corresponding mobile mercury emissions for Canada, we assumed that the ratio of mobile criteria emissions to mobile mercury emissions is same for the US and Canada. The resulting total mercury emissions for the US and Canada were 107 metric tons and 9 metric tons, respectively. Anthropogenic mercury emissions from Mexico were included in the modelling as well, because mercury is transported over long distances. We used the reported 1999 anthropogenic mercury emissions from Mexico (CEC, 2001). The resulting total mercury emission from Mexico was about 31 metric tons. The major Mexican sources were gold and silver mining and refining (11 metric tons), mercury mining and refining (10 metric tons); chlor-alkali plants (5 metric tons); copper smelters (1.5 metric tons); residential wood combustion (1.2 metric tons) and carboelectric plants (0.8 metric tons). About 90 percent of these emissions (28 metric tons) were allocated to specific point sources. The rest (3 metric tons) was distributed across Mexico by population. About 8 metric tons of the emissions allocated to specific point sources were in our modelling domain. Since no stack parameters were available, all mercury emissions from Mexico were assumed to occur in the first model layer. Speciation of the Mexican mercury emissions into Hg(0), RGM and Hg(p) was done using mercury speciation data for the various sources reported in (Pacyna and Pacyna, 2002). The anthropogenic mercury emissions were processed using SMOKE

V2.1.

Natural Hg emissions

Natural Hg emissions were from the natural Hg emission model (Chapter 3) which was run for the year 2002 for this study. Natural mercury emissions were then merged with anthropogenic mercury and criteria emissions using the merge sub-program in SMOKE

Estimation of Cl_2

Hg is oxidized by molecular chlorine gas (Cl_2) in both the gaseous and aqueous phases. This oxidation of Hg makes it more subject to deposition by both wet and dry processes. Therefore Cl_2 has also been added as a modelled species in the CMAQ-Hg and its emission to air and atmospheric transport are simulated in the same manner as for all other atmospheric constitutes in the model. However, no suitable industrial emission inventory for Cl_2 was available for CMAQ-Hg applications. As an interim approach, the production of Cl_2 from sea-salt aerosol has been modelled as a continuous emission rate per unit area over all ocean surfaces. The emission rate of 4.1571×10^{-7} mol/m^2/day or 2.9476×10^{-5} g/m^2/day for CMAQ-Hg simulations was used in the CMAQ-Hg over ocean surface (Bullock and Brehme, 2002). All Cl_2 emissions were simulated to occur only in the lowest model layer. Since chlorine concentration are lower during the day (about 10 ppt) than night (100 ppt) (Seigneur et al., 2001), we assumed 90% of Cl_2 emissions occur in the

night and 10% during the day.

4.3 Simulation Results

4.3.1 Hg Emissions

Time-averaged natural Hg emission flux and anthropogenic Hg emission flux over the simulation period are presented in Figure 4.1 and Figure 4.2 respectively. As shown in Figure 4.1, natural Hg emission is much higher in west coast and eastern North America than other areas. Natural Hg emission flux seems to be heavily related to surface characteristics of land uses. Its spatial distribution is similar to that of soil Hg concentration (Figure 3.4), but it is not identical to that because it also depends on many other factors such meteorological conditions, soil moisture and vegetation conditions. Quite different from natural Hg emission, anthropogenic Hg emission shows very little dependence on characteristics of surfaces. Anthropogenic emissions are generally concentrated on specific locations where predominant anthropogenic Hg emission sources (e.g. power plants) are located. Generally, point source is the major source of anthropogenic Hg emission.

4.3.2 Natural and anthropogenic emissions in different regions

Figure 4.4 shows the relative importance of natural and anthropogenic emissions in different regions. More populated areas with higher industrial activities (Region

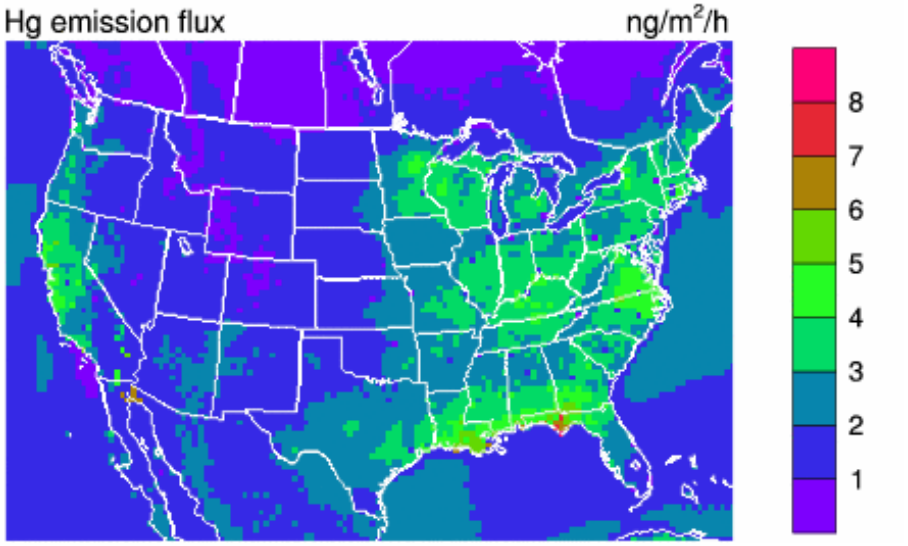

Figure 4.1: Natural mercury emission flux averaged over whole simulation period

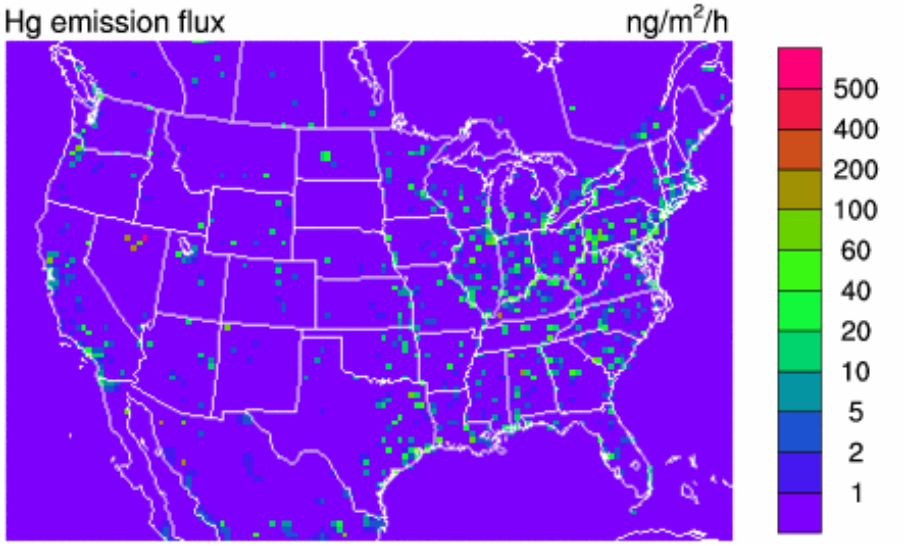

Figure 4.2: Anthropogenic Hg emission flux averaged over whole simulation period

A in Figure 4.3) have higher anthropogenic emissions (70% of the total) while natural emissions dominate (71% of the total) in more rural areas (Region B in Figure 4.3). Over the whole year 2002, natural emission is about more than twice the anthropogenic emissions within the domain. The natural and anthropogenic emissions obtained from published data for various regions are shown in Table 4.1. Clearly on the regional to global scale, natural emissions are larger than anthropogenic ones.

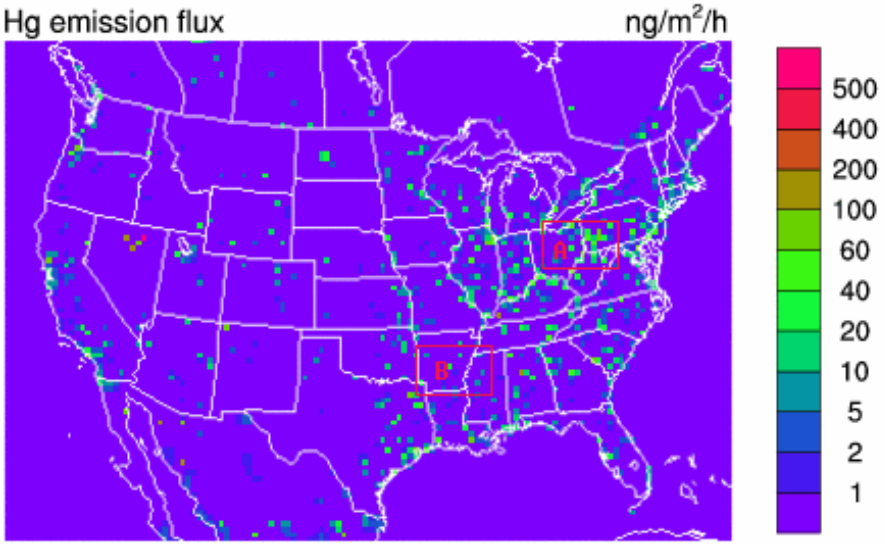

Figure 4.3: Anthropogenic Hg emission distribution

4.3.3 Ambient mercury concentration

Modelled ground TGM (Total Gaseous Mercury) concentrations were compared with measurements (Blanchard, 2005) from three Canadian Atmospheric Mercury Measurement Network (CAMNet) sites within the modelling domain, namely Point Petre, Egbert and Burnt Island, all in Ontario (Environment Canada, 2000) (Figure

Region	Period	Natural emission	Anthropogenic emission	Ratio[a]	Reference
North America Domain	1 year (2002)	230(104[b])	126	1.8	This work
North America Domain	1 year (2001)	28-127[b]	129		Lin et al. (2005)
Contiguous U.S. and Canada	1 year (Dec.,1988 - Nov.,1989)	507			Shannon and Voldner (1995)
Global	1 year	4268	2143	2.0	Seigneur et al. (2004)
Global	1 year		2144	2[c]	Dastoor and Larocque (2004)

[a]Ratio of total natural to anthropogenic mercury

[b]Vegetation only

[c]Suggested

Table 4.1: Reported anthropogenic and natural (including re-emission) mercury emissions (metric ton)

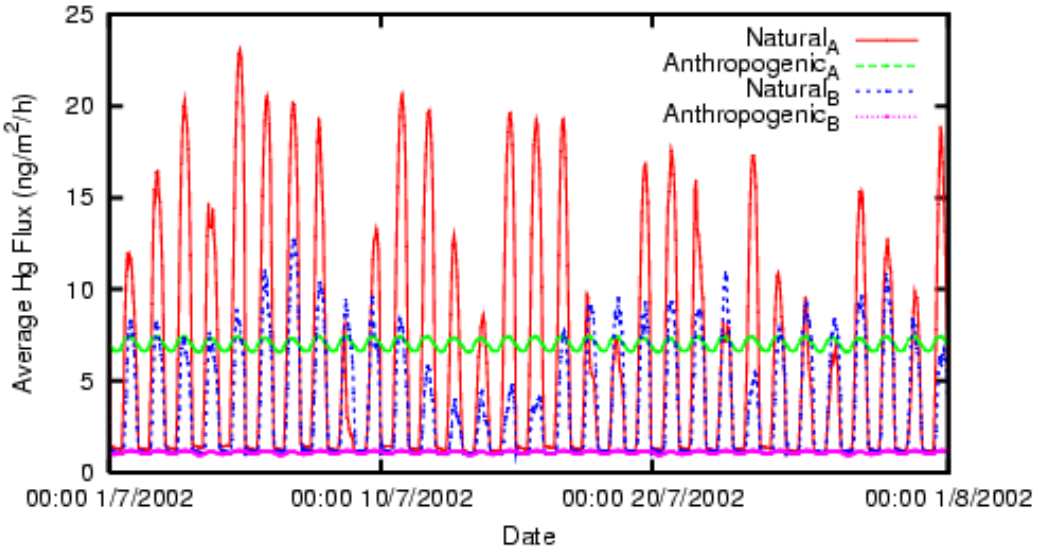

Figure 4.4: Natural Hg emission flux for regions A and B in Figure 4.3

4.6). Figure 4.5, which shows the model versus measurement comparison for Point Petre, is typical of the results obtained. The agreement between the measurement and the base case modelled result (Table 4.2) is good; the absolute values from the model simulation follow the observed trends very closely. High and low mercury episodes are also well reproduced by the model. The major difference is in the range of the diurnal variations predicted by the model, which are smaller than the observation.

Figure 4.7 shows total gaseous mercury (TGM) concentration averaged over whole simulation period in the domain. Although TGM concentrations across the simulation domain varied between 1.1 and 5.3 ng/m^3, they generally range from 1.2 to 2.2 ng/m^3. Eastern North America and west coast area have higher concentration

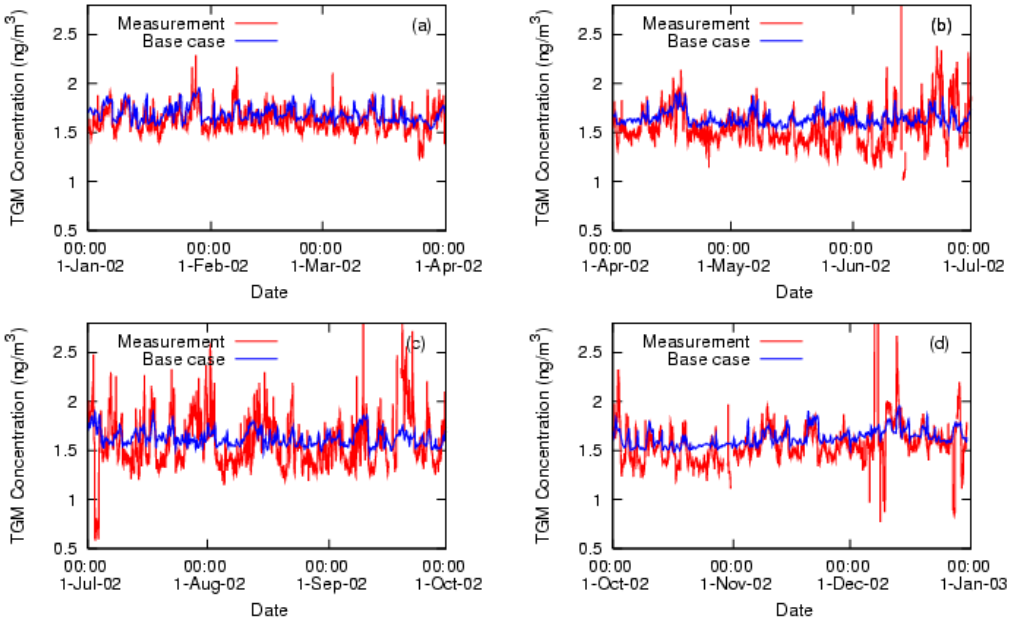

Figure 4.5: Modelled and measured hourly TGM for Point Petre for 2002. (a) January to March, (b) April to June, (c) July to September (d) October to December.

Site	Period	Case	N	Mean (ng/m^3)	Mean bias (ng/m^3)	σ	Min	Max	r^2
Point Petre	Cold season	Base	4344	1.658	0.057	0.087	1.483	1.96	0.163
		measurements	4295	1.601		0.235	0.77	6.88	
	Warm Season	Base	4393	1.634	0.067	0.074	1.465	1.89	0.088
		measurements	4320	1.567		0.247	0.58	3.56	
	all year	Base	8736	1.646	0.062	0.082	1.465	1.96	0.128
		measurements	8615	1.584		0.242	0.58	6.88	
Burnt Island	Cold season	Base	4344	1.609	-0.139	0.062	1.483	1.86	0.080
		measurements	4224	0.748		0.192	0.93	3.32	
	Warm Season	Base	4393	1.58	-0.041	0.061	1.431	1.86	0.046
		measurements	4015	1.620		0.238	0.68	3.80	
	all year	Base	8736	1.594	-0.092	0.063	1.43	1.86	0.088
		measurements	8239	1.685		0.225	0.68	3.80	
Egbert	Cold season	Base	4344	1.629	-0.106	0.087	1.472	2.04	0.428
		measurements	4163	1.735		0.209	1.2	3.25	
	Warm Season	Base	4393	1.584	-0.071	0.068	1.427	1.88	0.162
		measurements	4321	1.655		0.261	0.84	3.95	
	all year	Base	8736	1.606	-0.088	0.081	1.427	2.05	0.283
		measurements	8484	1.694		0.241	0.84	3.95	

Cold season is January to March and October to December.

Warm season is April to September.

Table 4.2: Summary statistics for modelled and measured hourly TGM concentrations for different sites.

compared with other areas of the domain. This is quite similar to the distribution of natural and anthropogenic Hg emissions (Figure 4.1 and 4.2) illustrating the strong impact of Hg emissions on the TGM concentration in the domain. Few locations in the west region of domain (north Neveda) have exceptionally high TGM concentrations probably because anthropogenic Hg emissions (>500 ng/m^2/h) are huge at those locations (Figure 4.3).

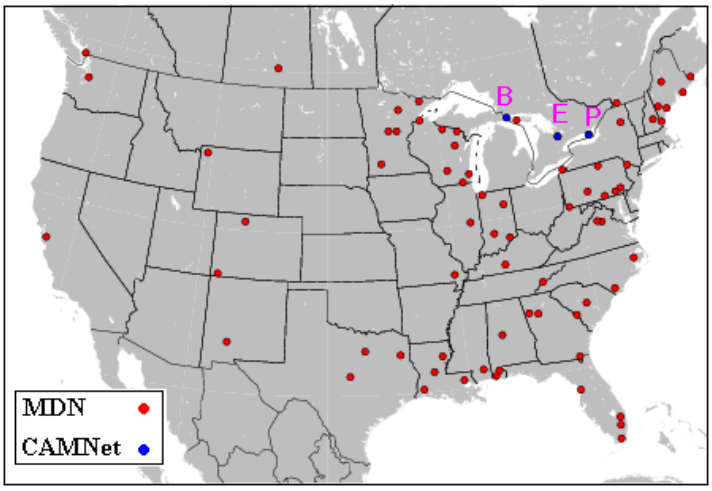

Figure 4.6: Location of sites used to compare model results with measurements. All the sites are wet mercury deposition sites used except the three sites labelled B, E and P which are TGM measurement sites. B is Burnt Island (45°49´42″/ 82°56´53″W, 184 m above sea level), E is Egbert (44°43´57″N / 79°46´53″, 251 m above sea level), and P is Point Petre (43°50´34″N / 77°09´13″W, 78 m above sea level).

4.3.4 Dry deposition

Figure 4.8 shows the spatial distribution of total dry deposition over the simulation period. Total dry deposition varies between 2.4 - 79.5 μg/m^2. Eastern North America and west coast have higher total dry deposition due to higher Hg(0) con-

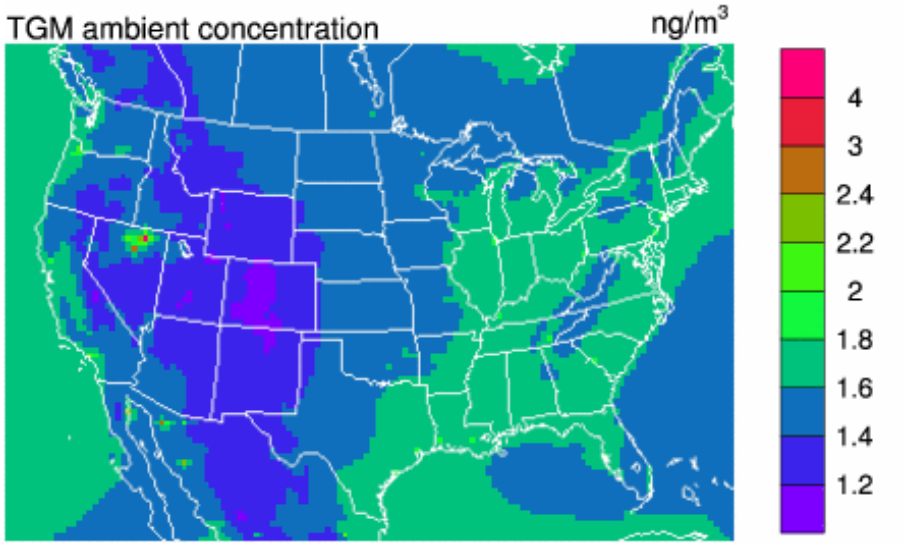

Figure 4.7: Spatial distribution of average TGM ambient concentration

centrations and dry deposition velocities of Hg(0) and Hg(II) (Figure 4.9, 4.10) in those regions. Among total dry deposition, 58% (section 4.3.8) comes from Hg(II), the biggest contributor of dry deposition. Hg(0) accounts for 39% of total dry deposition.

4.3.5 Wet deposition

Figure 4.11 shows a comparison of the simulated weekly mercury wet deposition with measurements from 47 Mercury Deposition Network (MDN) sites (Figure 4.6). The correlation between modelled and measured wet deposition was not strong. This poor agreement has been noted previously (Bullock and Brehme, 2002) and has been ascribed to the difference between the precipitation depth used by CMAQ and the actual precipitation measured at the monitoring site. Since MM5 averages the precipitation depth within the 36 km grid cell, it is possible that local differences

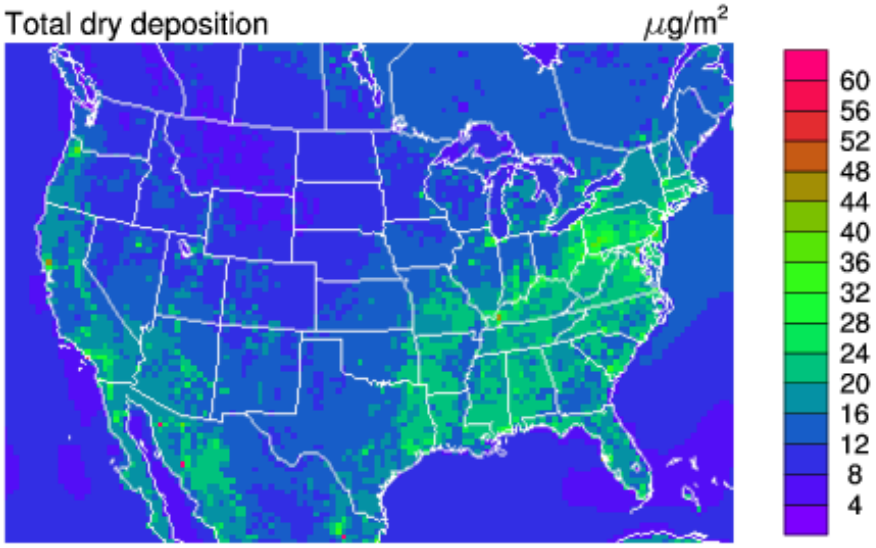

Figure 4.8: Spatial distribution of annual total dry deposition

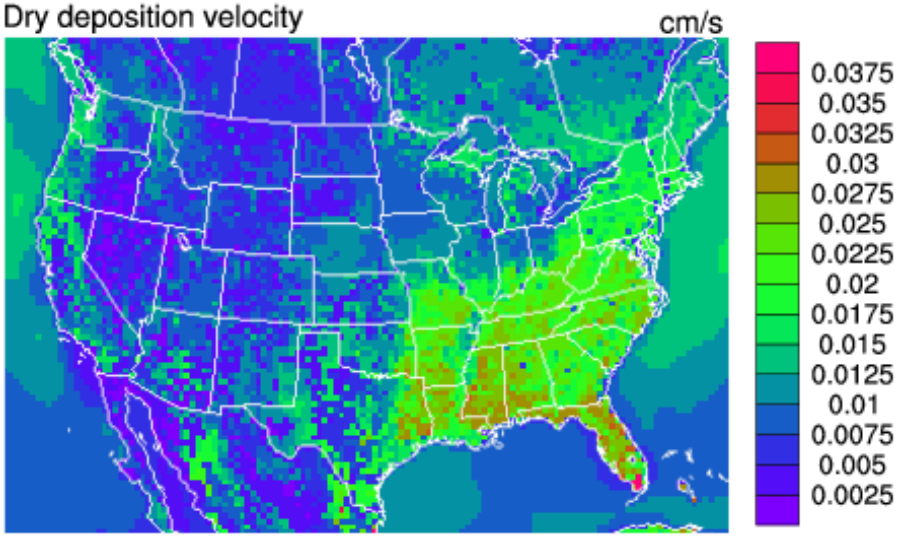

Figure 4.9: Average dry deposition velocity of Hg(0)

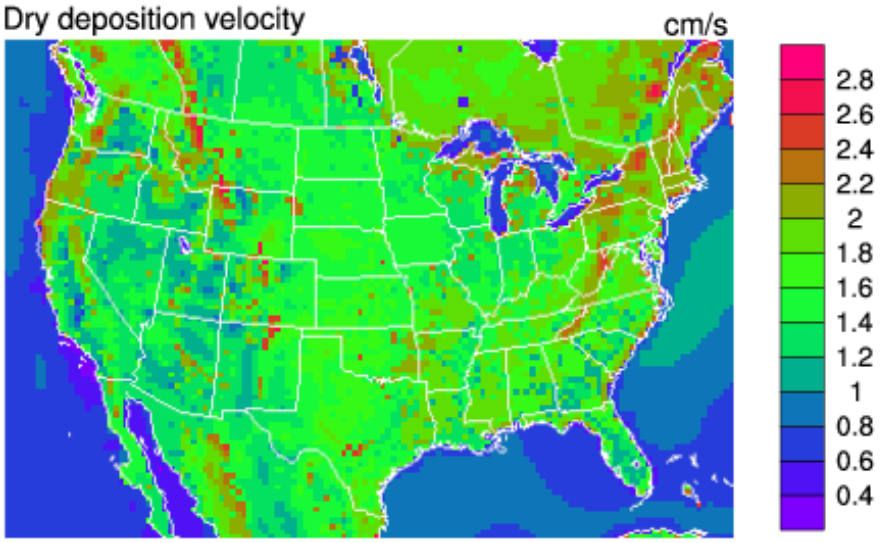

Figure 4.10: Average dry deposition velocity of Hg(II)

between modelled and measured precipitation depth will occur at the locations of the monitoring stations. Figure 4.12 compares the model results with measurements for cases where the precipitation depth used by the model was within a factor of two of the measured values. A significant improvement was observed in the correlation coefficient (from 0.4774 to 0.6524), but the model still under-predicted the deposition amounts.

Figure 4.13 and 4.14 show the total wet deposition of mercury and total precipitation for the simulation period. Wet deposition fluxes are higher in the Eastern North America and west coast. The high wet deposition fluxes on the west coast are due to the global Hg(II) concentrations at the upwind boundary (25 pg/m^3 on average) as well as high precipitation along the mountain ranges of the Cascades and Sierra Nevada. The high wet deposition fluxes in the Eastern North America result from the influence of local/regional sources and high precipitation. It

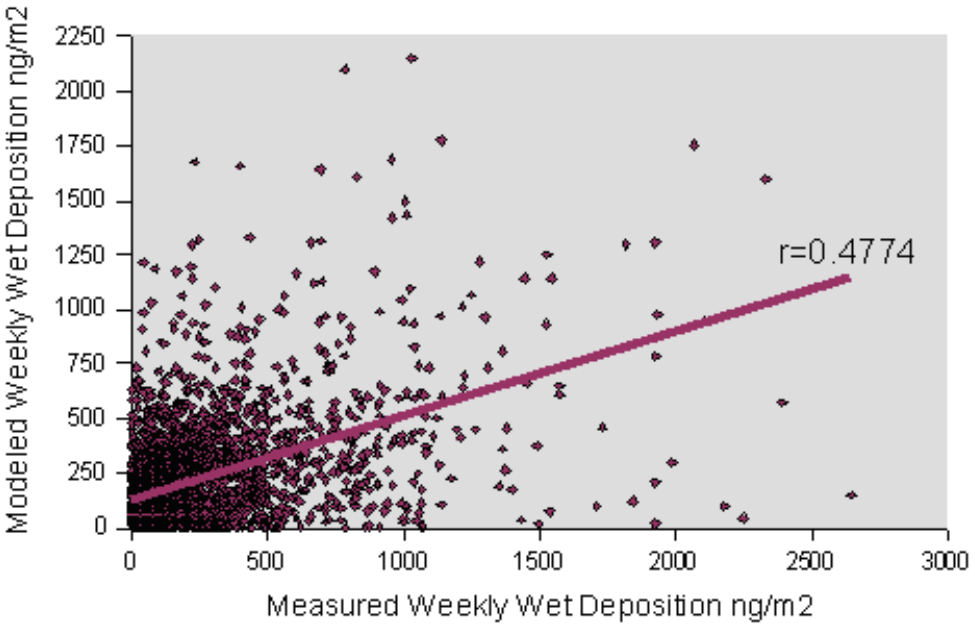

Figure 4.11: Correlation between model and measurements for weekly mercury wet precipitation for all data

can be seen that the wet deposition distribution is mainly determined by the total precipitation pattern.

4.3.6 Total deposition

Figure 4.15 shows spatial distribution of total Hg deposition over the simulation period. Total Hg deposition varies from 5.0 to 90.0 μg/m^2 across the domain. Total Hg deposition is high in southeast North America and west coast area. The total deposition fluxes reflect the characteristics mentioned above for the wet and dry deposition fluxes.

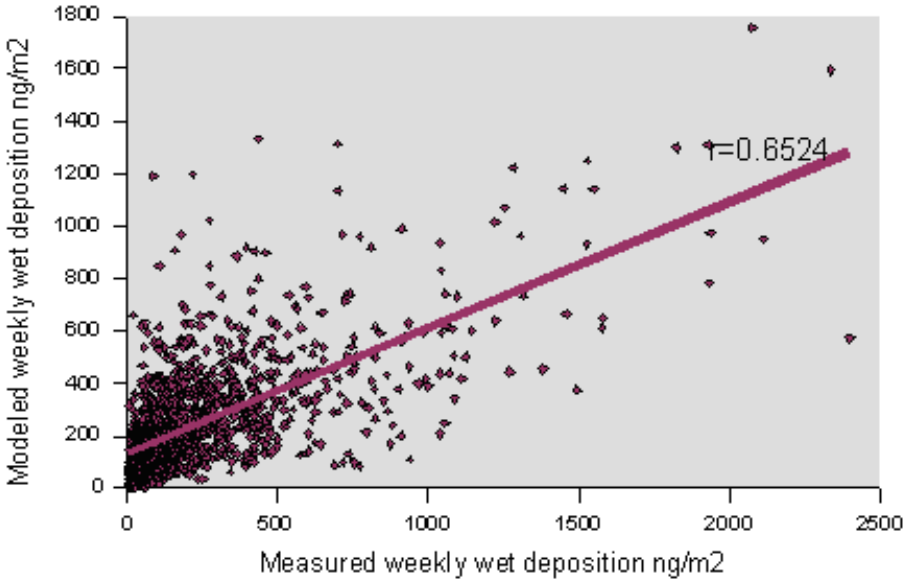

Figure 4.12: Correlation between model and measurements for weekly mercury wet precipitation for data for which model precipitation depth is within a factor of two of measurement

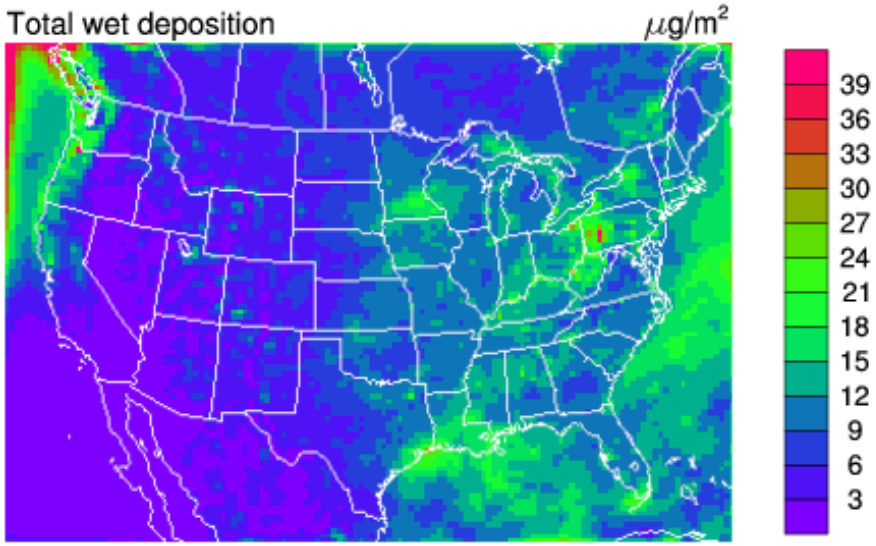

Figure 4.13: Total wet deposition during the simulation period (2002)

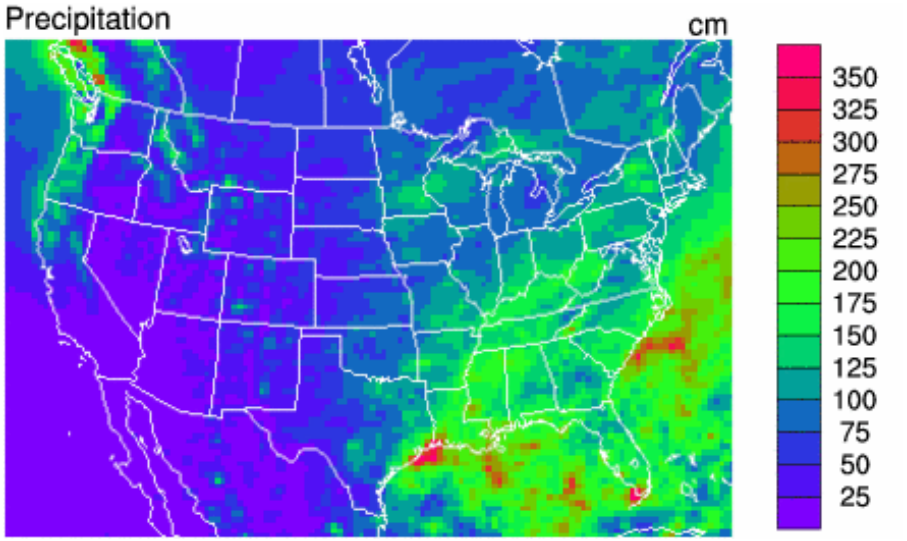

Figure 4.14: Total precipitation during the simulation period (2002)

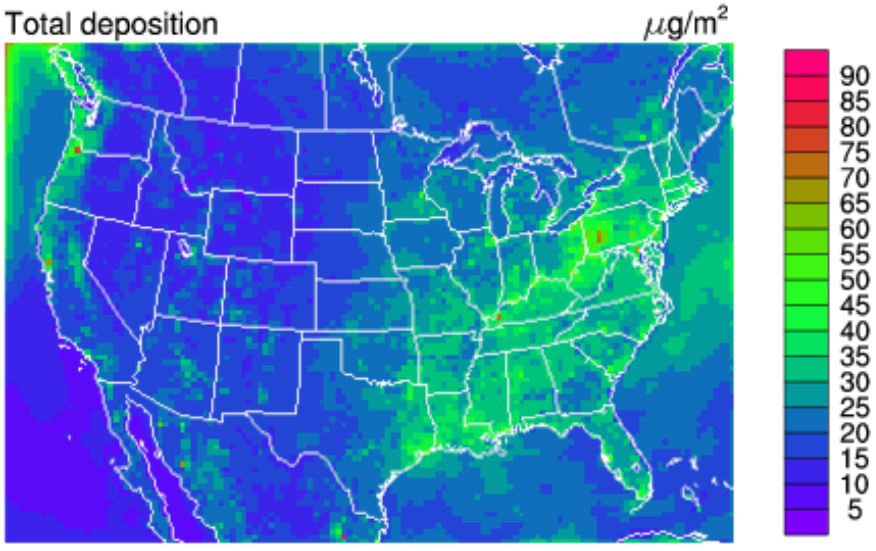

Figure 4.15: Total deposition of Hg during the simulation period

4.3.7 Net Evasion

The distribution of annual average net Hg emission flux is shown in Figure 4.16. Net Hg emission flux here is referred to the difference between natural Hg emission flux and Hg dry deposition flux. It is estimated that about 62% of total grid cells in the whole simulation domain and about 64% of total grid cells in land have positive net Hg evasion (emission greater than dry deposition) over the modelling period. There are about 31 metric tons of net Hg emission during modelling period over whole domain, which means natural Hg emission is predominant over dry deposition of Hg. This phenomenon was observed by field measurements (Lindberg and Stratton, 1998).

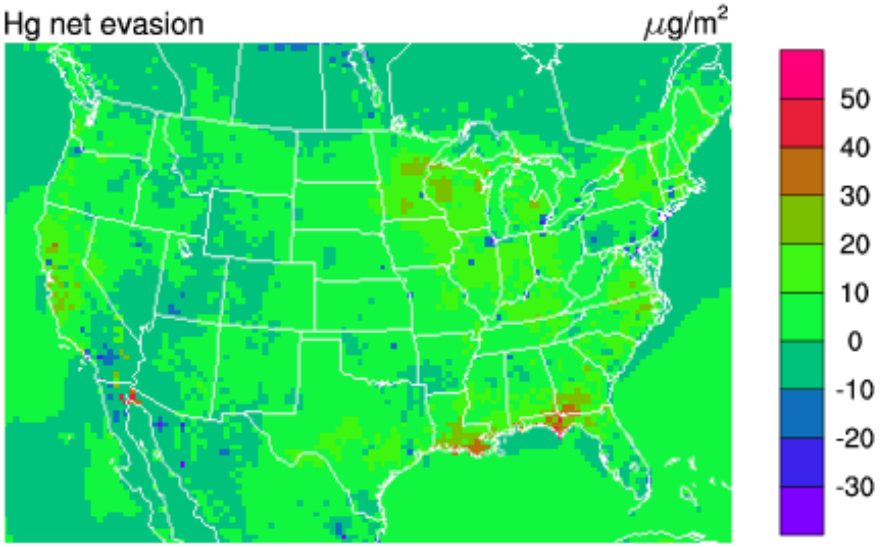

Figure 4.16: Annual net Hg emission flux over whole simulation period

4.3.8 Regional Hg budget

To investigate the regional Hg budget, Hg dry and wet depositions, natural and anthropogenic emissions over the entire domain were calculated for the simulation period of 2002. The results are presented in Table 4.3 for total Hg and its three species. It can be seen that anthropogenic Hg emission is minor compared to natural emissions which account for about 65% of total Hg emissions or about 1.8 times anthropogenic Hg emission. This is close to the results calculated by Lin and Tao (2003). Among 335 metric tons of total Hg deposition, dry deposition accounts to 198 metric tons accounting form 59% of total Hg deposition. Total amount of Hg emission is about 355 metric tons. About 335 metric tons of Hg in the atmosphere is deposited back to the surfaces through dry and wet scavenging processes. The difference between total Hg emission and total Hg deposition (about 20 metric tons of Hg) indicates that the modeling domain acts as a net source of atmospheric Hg in the simulation period. As for Hg species, Hg(0) is a major component of Hg emission but a minor component of Hg deposition. Hg(II) is the major component both in wet and dry depositions. The big difference between emission and deposition of Hg(II) suggests that the transformation of Hg(0) and Hg(p) to Hg(II) could be the main source of Hg(II) deposition.

4.4 Summary and conclusions

The improved CMAQ-Hg model was applied to North America for the year 2002 to simulate the emission, transport, transformation and deposition of atmospheric

Total Hg emission over entire domain (metric ton)				Total Hg deposition over entire domain (metric ton)					
354.99				335.43					
Natural	Anthropogenic			Dry			Wet		
228.99	126.00			198.17			137.26		
Hg(0)	Hg(0)	Hg(II)	Hg(p)	Hg(0)	Hg(II)	Hg(p)	Hg(0)	Hg(II)	Hg(p)
228.99	78.77	35.08	12.15	76.97	114.93	6.27	0.10	105.13	32.03
Total emission of each Hg species (Metric ton)				Total deposition of each Hg species (Metric ton)					
Hg(0)		Hg(II)	Hg(0)	Hg(0)		Hg(II)		Hg(p)	
307.76		35.08	12.15	77.07		220.06		38.30	
Percentage of each Hg species				Percentage of each Hg species					
86.70		9.88	3.42	22.98		65.61		11.41	

Table 4.3: Hg budget modelled within entire domain over the simulation period

Hg. The comparisons between modelled and measured hourly TGM for 3 sites were presented in this study. This is the first time that a comparison of the hourly model results versus measurement relationship has been reported for a CAMNet site. The good agreement between them demonstrated that the modified CMAQ-Hg systems had a good ability to model the behaviour of emission, transport, transformation and deposition of atmospheric Hg.

Compared to anthropogenic Hg emission, natural Hg emission flux is heavily dependent on the characteristics of surfaces such as soil Hg concentration, soil moisture and vegetation conditions. Geographical distribution of anthropogenic Hg emission is mainly determined by the distribution of point source because point source is generally predominant among anthropogenic emission sources of Hg.

The ratio of natural to anthropogenic Hg emissions is quite different for different modelling areas. More populated areas with higher industrial activities have higher anthropogenic emissions but natural emissions dominate in more rural areas.

In contrast to wet deposition which is mainly controlled by the amount of precipitation, dry deposition is primarily determined by dry deposition velocity, and therefore its geographical distribution reflected to some extent its dependence on the characteristics of surfaces. Dry deposition is greater than wet deposition and more significant to govern total Hg deposition distribution.

During the simulation period over the whole simulation domain, there were about 355 metric tons of Hg in total released in the atmosphere, among which natural Hg emission accounts for 65% of total Hg emissions or about 1.8 times anthropogenic emissions. There are about 335 metric tons of Hg deposited back to earth. The modeling domain acts as a net source of atmospheric Hg during the simulation period.

Chapter 5

A sensitivity analysis

5.1 Introduction

The toxic effects of mercury depend on its chemical form and the route of exposure. Methylmercury, formed and biomagnified in many aquatic systems, is believed to be the most toxic form of Hg exposed largely to wild animals and humans through the food chain. The primary source of Hg in fish in many locations around the world is now believed to be atmospheric deposition of Hg (Bullock, 2000b). There are a large number of factors affecting the deposition of atmospheric Hg, many of which are inextricably coupled through the complex chemical and physical processes in the atmosphere. As a result, a perturbation in one factor can lead to significant changes in others and to feedbacks that can either amplify or damp the original perturbation. While it may seem clear that human activities have perturbed the mercury cycle (Mason et al., 1994; Hudson et al., 1995; Pacyna and Pacyna, 1996),

it is not clear how each of them perturbed the deposition of atmospheric Hg and the mercury cycle. Modelling studies have been rapidly developed to analyze and predict the transport, transformation and deposition of atmospheric Hg (Rajar et al., 2000; Xu et al., 2000a; Kallos et al., 2001; Petersen et al., 2001; Bullock and Brehme, 2002; Travnikov and Ryaboshapko, 2002; Cohen et al., 2004). Some studies have analyzed the effects of some input parameters on the behaviour of atmospheric Hg (Pai et al., 1999; Lohman et al., 2000; Xu et al., 2000b; Hedgecock et al., 2005). However, no attempt has been made so far to quantitatively examine the sensitivity of atmospheric Hg to emissions, especially non-Hg emissions such as NO_x, SO_2, NH_3 and VOCs. Nitrogen oxides and volatile organic compounds affect ozone and a variety of oxidants (e.g., OH) in the atmosphere as well as secondary aerosol particulates, and SO_2 affects particulate and gaseous sulphur compounds. A change in these emissions may have a significant impact on atmospheric Hg.

This chapter presents the results of a sensitivity analysis of atmospheric Hg to emissions including Hg emissions and non-Hg emissions such as NO_x, SO_2, NH_3 and VOCs, with a special emphasis on the effects of non-Hg emissions. This sensitivity analysis was conducted with the improved CMAQ-Hg model (Chapters 2, 3 and 4).

5.2 Model description

The air quality model used in this study is the improved CMAQ-Hg model. The detailed description of this model can be found in Chapters 2, 3 and 4.

5.3 Sensitivity simulations

The selected simulation period is from July 1 to August 1, 2002. The simulation domain is the same as the one used in section 3.4.1 (Figure 3.3). The model input and meteorological conditions are described in Chapter 4.

For the sensitivity analysis, the default conditions for the simulation period were used as the base case. The sensitivity cases for various emission adjustments used in this study are shown in Table 5.1.

Simulation	input
Hg_{nat}	±50% changes in natural Hg emission of base case
Hg_{anth}	±50% changes in anthropogenic Hg emission of base case
NO_x	±50% changes in NO_x emission of the base case
SO_2	±50% changes in SO_2 emission of the base case
NH_3	±50% changes in NH_3 emission of the base case
VOCs	±50% changes in VOCs emission of the base case

Table 5.1: The design of the sensitivity study

For simulations with input change applied to the whole region, the regional average value for concentrations and total amount for dry and wet deposition for the simulation period were calculated and compared with those of the base case. All sensitivities were determined from ±50% input changes and were expressed as the percent change in model output from the base case simulation.

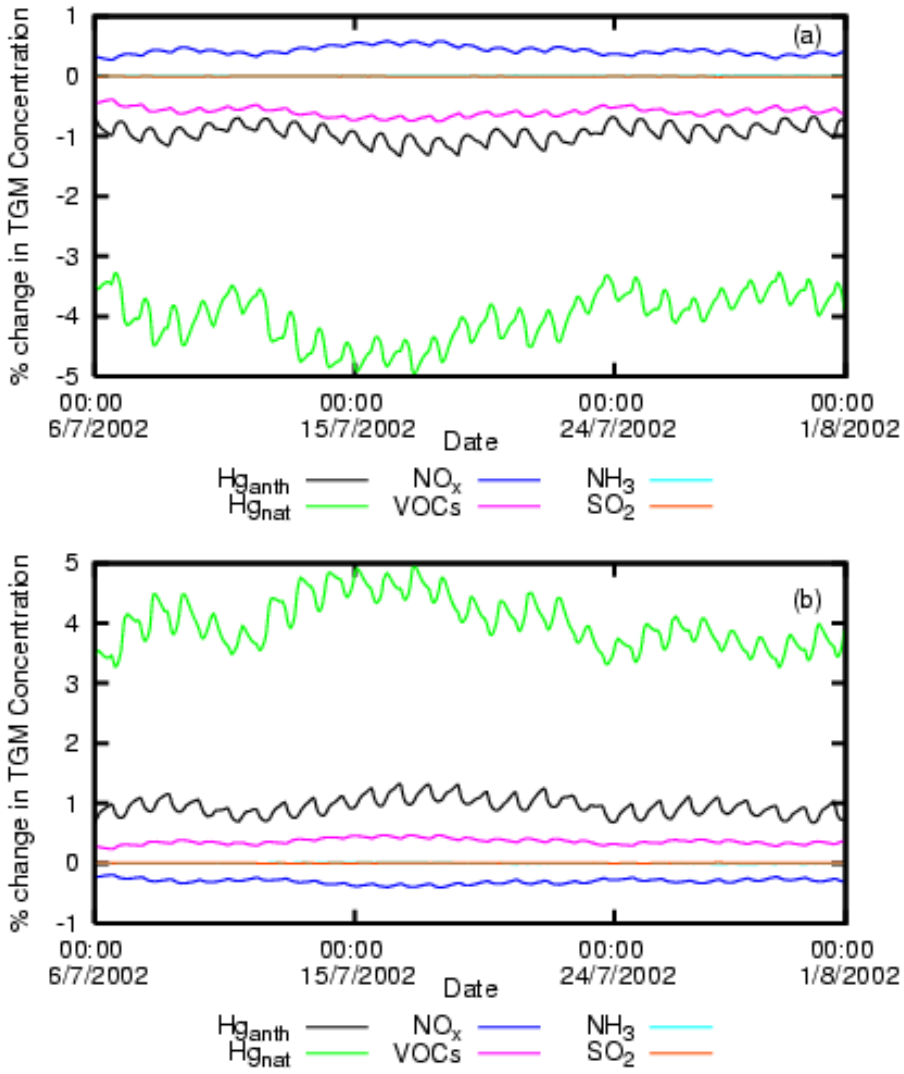

Figure 5.1: Percentage changes in domain-averaged surface TGM concentration resulting from (a) -50% emissions changes, and (b) +50% emissions changes.

5.4 Results of sensitivity analysis

5.4.1 Sensitivity of TGM

The modelled ambient air concentrations for Total Gaseous Mercury (TGM) for the adjusted emissions scenarios were compared with those for the base case. The percentage changes in domain-wide averaged TGM concentration for the emissions scenarios were calculated and presented in Figure 5.1. TGM concentration decreases by 4% with a 50% natural Hg emission reduction, and increases by 4% with a 50% natural Hg emission increase. This is the greatest effect on TGM air concentration, suggesting natural Hg emission is the most significant factor influencing TGM concentration among the emissions investigated here. This is possible because natural Hg emission directly releases Hg into the atmosphere in the form of Hg(0) which is chemically inactive and easy to accumulate. This result not only illustrates natural Hg emission as a key factor influencing the level of TGM air concentration, but also indicates the importance of natural Hg emission inventory to Hg modelling. Modelled Hg level should be obviously underestimated if natural Hg emission is neglected.

Although both anthropogenic and natural Hg emissions directly release Hg into the atmosphere, the simulation results show that anthropogenic Hg emission has a much smaller effect on TGM concentration than natural emission. This is not surprising because anthropogenic Hg emission is smaller than natural Hg emission (Seigneur et al., 2004; Gbor et al., 2006; Lin et al., 2005). According to the simulation results of the base case in this study, anthropogenic Hg emission is only 0.5

times natural Hg emission. Moreover, anthropogenic Hg emission always has a fraction of Hg(II) which can be easily scavenged by wet and dry deposition processes in the atmosphere.

Emissions of non-Hg pollutants such as NO_x, VOCs, SO_2 and NH_3, have small effect on TGM level. All percentage changes caused by these emissions are less than 1%. The influences of SO_2 and NH_3 are even negligible. Emissions of non-Hg pollutants, unlike anthropogenic and natural Hg emissions which direct emit Hg species into the atmosphere, affect ambient TGM concentration mainly through Hg(0) oxidation and Hg(II) reduction processes which generally cannot significantly alter the concentration of Hg(0) due to their small rate constants and low concentrations of related reactants (Bullock and Brehme, 2002; Lin and Pehkonen, 1999).

The trend change in ambient TGM concentration with adjusted emissions is presented in Figure 5.2. The trend of changes in two components of TGM, Hg(0) and Hg(II), are also presented in Figure 5.2. Obviously, percentage change in ambient TGM concentration (Figure 5.2a) is quite similar to that in Hg(0), one of the TGM components (Figure 5.2b). This similarity indicates that a change in ambient TGM concentration due to adjusted emissions is significantly determined by Hg(0). Hence, Hg(0) is a primary contributor to the change in TGM concentration. From Figure 5.2, we also see an inverse effect of NO_x emission on both TGM and Hg(0) concentration even if it is small. VOCs and SO_2 emissions have an inverse effect on Hg(II) concentration.

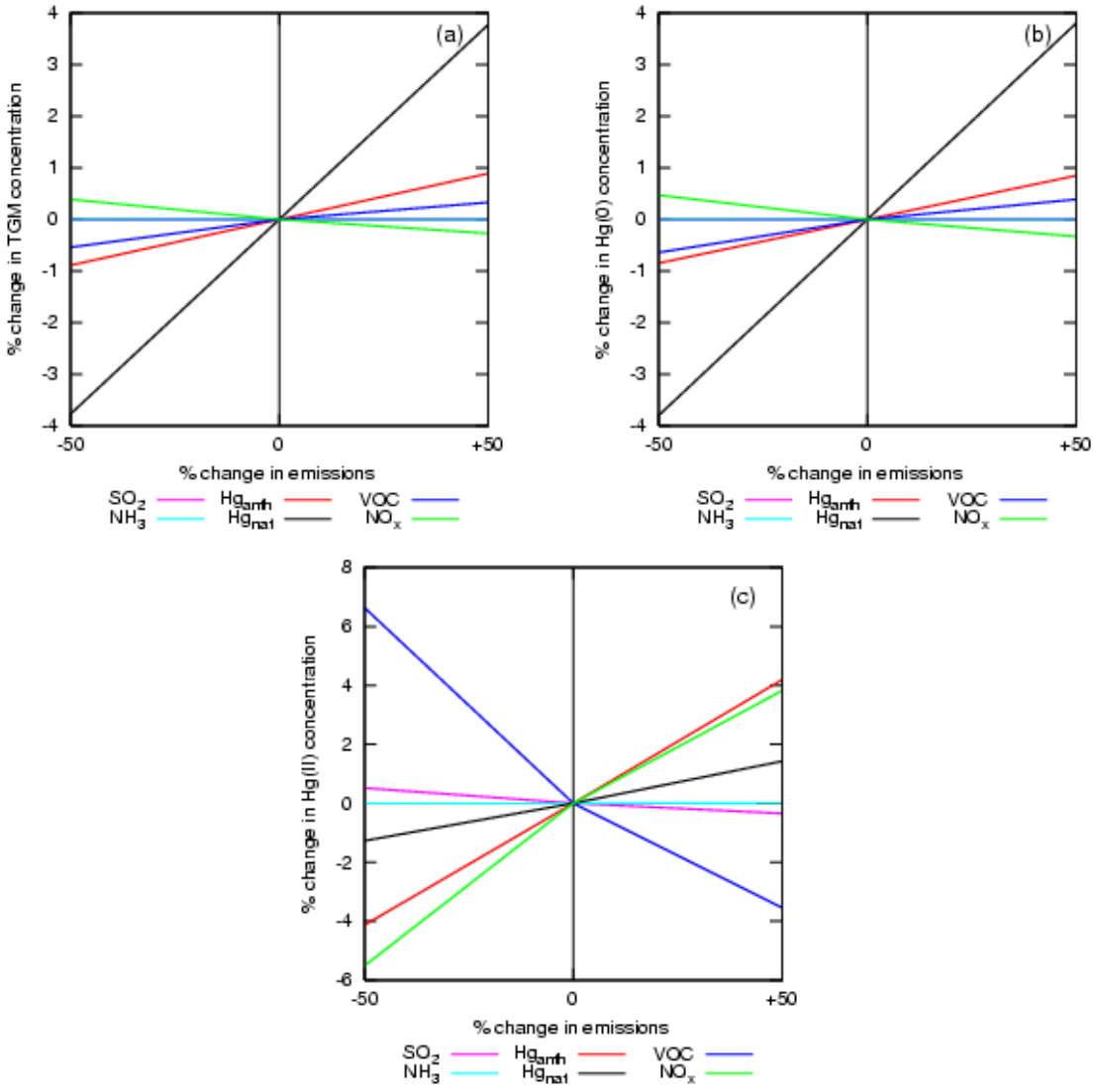

Figure 5.2: Percentage changes in average (a) TGM, (b) Hg(0) and (c) Hg(II) concentration resulting from ±50% emissions changes

The spatial variability of sensitivity of TGM concentration to natural Hg emission change is presented in Figure 5.3. TGM concentration increases everywhere in the simulation domain if natural Hg emission increases by 50%, and decreases everywhere if natural Hg emission decreases by 50%. Since natural Hg emission fluxes are different for different parts of the domain, the sensitivity of TGM concentration spatially varies. Eastern North America has much higher sensitivity than other areas in the domain.

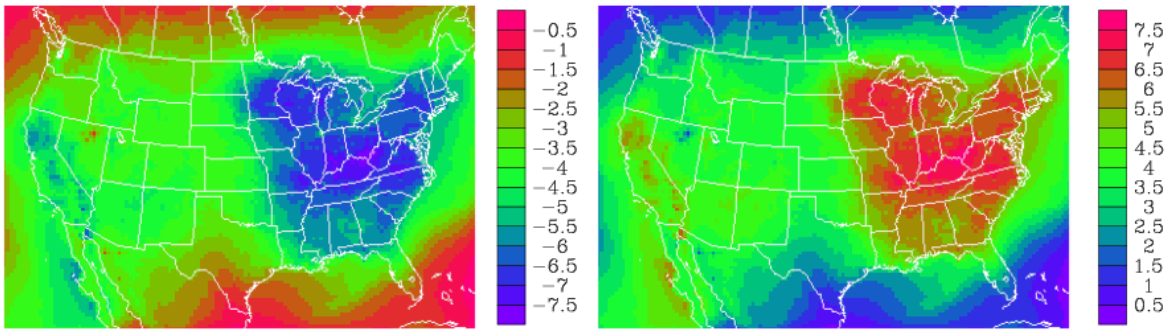

Figure 5.3: Spatial distribution of percentage changes in TGM concentration resulting from (a) -50%, and (b) 50% natural Hg emissions changes

5.4.2 Sensitivity of Hg dry deposition

Modelled sensitivity of Hg dry deposition is presented in Figure 5.4. Roughly speaking, Hg dry deposition is not only sensitive to Hg emissions but also to non-Hg emissions such as VOCs and NO_x. Hg emissions, including natural and anthropogenic, and NO_x emission have almost the same effect on total dry deposition. ±50% changes in these emissions lead to approximate ±3% change in total dry deposition. VOCs has the strongest effect on total dry deposition of Hg; however,

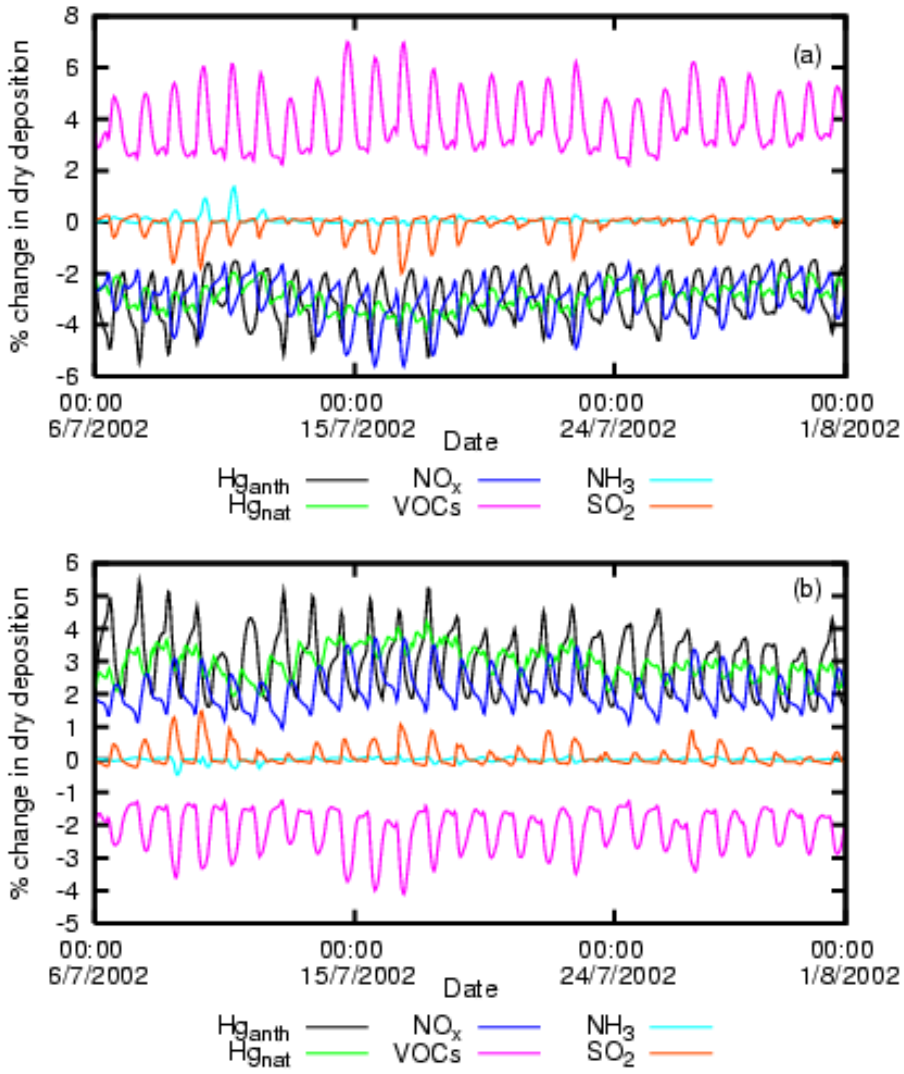

Figure 5.4: Percentage changes in total dry deposition for the whole domain resulting from (a) -50% emissions changes, and (b) +50% emissions changes.

the effect is inverse. Moreover, VOCs demonstrates a non-linear impact on dry deposition. SO_2 and NH_3 have the least affect on total dry deposition.

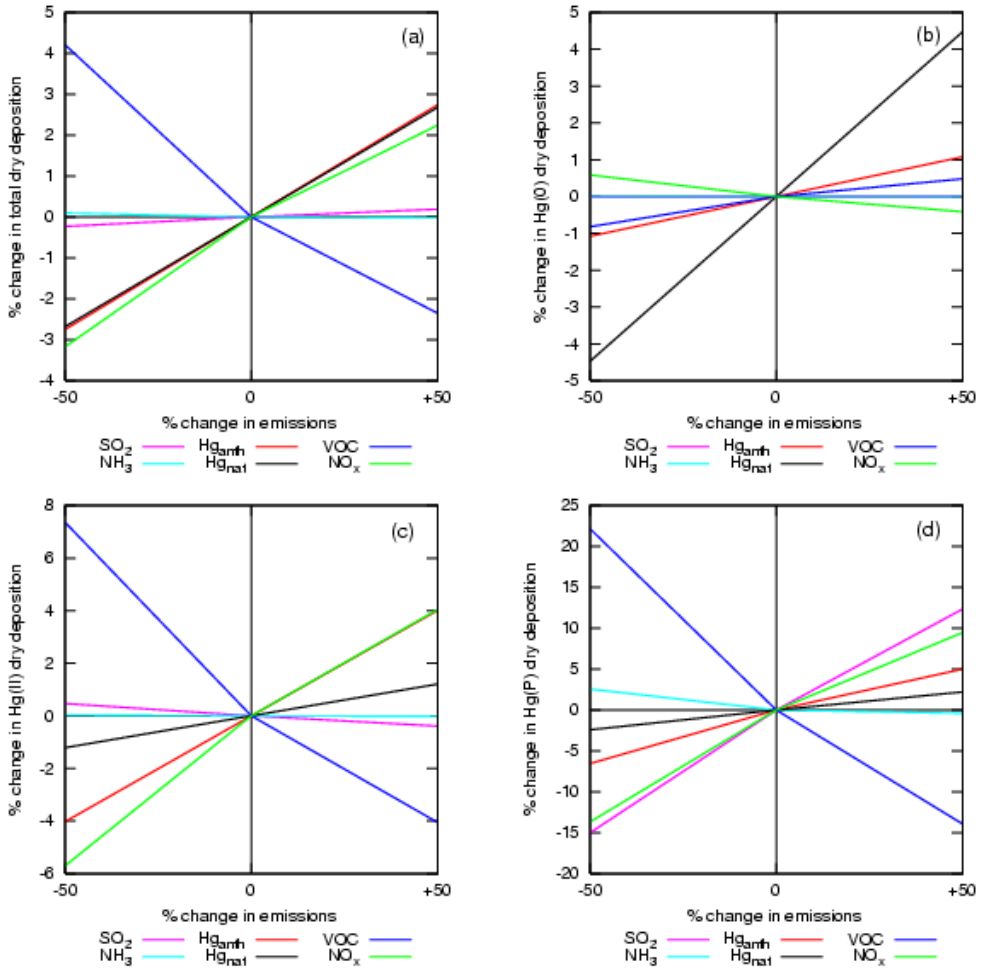

Figure 5.5: Percentage changes in total (a) TGM, (b) Hg(0), (c) Hg(II) and (d) Hg(p) dry deposition resulting from ±50% emissions changes

The changes in total dry deposition of Hg and its three species, Hg(0), Hg(II) and Hg(p), with adjusted emissions are presented in Figure 5.5. By comparing the change in dry deposition between Hg and its species shown in Figure 5.5, it

can be found that a change in total dry deposition due to non-Hg emissions such as VOCs and NO_x is mainly contributed by Hg(II) and Hg(p) (or else the trend change in Hg(0) dry deposition (Figure 5.5b) should be consistent with that in total dry deposition (Figure 5.5a). This result suggests that both emission and transformation of Hg are important for total Hg dry deposition, unlike TGM air concentration whose percentage change is mainly controlled by direct Hg emissions. The base case simulation in this study shows that the ratio of Hg(0) dry deposition to Hg(II) dry deposition is about 2:3.

The spatial variability of sensitivity of Hg dry deposition to the changes in anthropogenic Hg emission, natural Hg emission, NO_x emission, and VOCs emission is presented in Figure 5.6, 5.7, 5.8 and 5.9 respectively. Hg dry deposition is more sensitive to natural and anthropogenic Hg emissions in Eastern North America due to high natural and anthropogenic Hg emissions there. However, Hg dry deposition is much more sensitive to NO_x emission in central US, especially in Kansas and Oklahoma. Due to nonlinear relationship between atmospheric Hg and VOCs, spatial variability of sensitivity of Hg dry deposition is more complicated to VOCs emission change. The high sensitive area for VOCs emission reduction is quite different from that for VOCs emission increase. The most sensitive area for VOCs emission reduction is in northern border of Mexico, however, the most sensitive area for VOCs emission increase is in eastern North America.

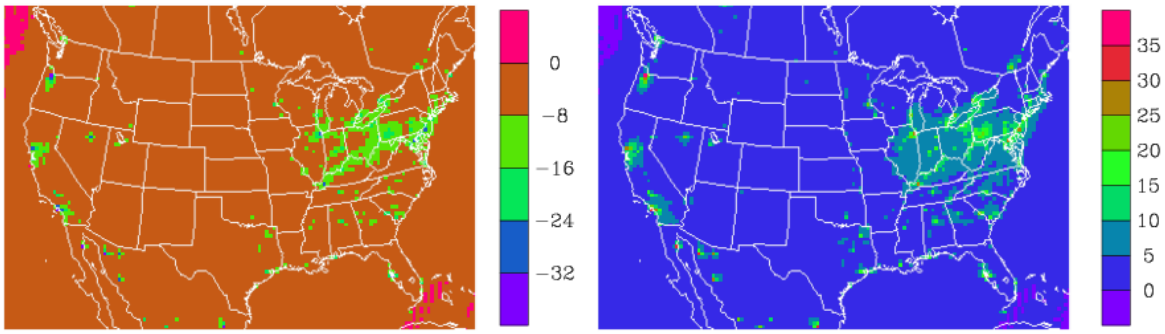

Figure 5.6: Spatial distribution of percentage changes in dry deposition of Hg resulting from (a) -50%, and (b) 50% anthropogenic Hg emissions changes

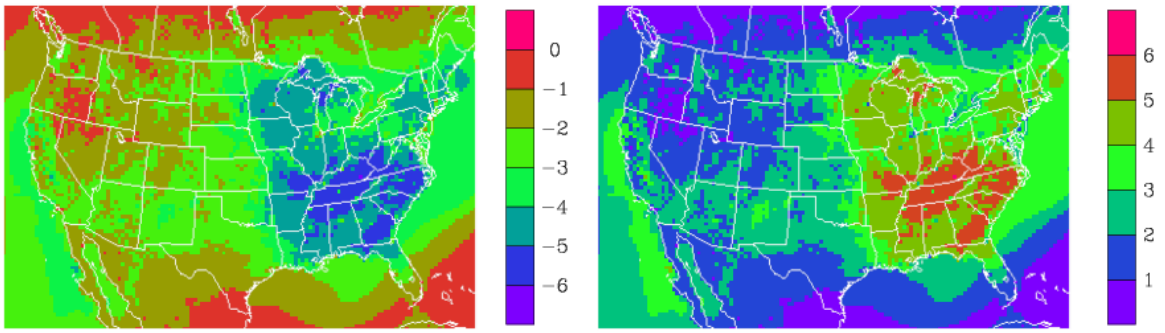

Figure 5.7: Spatial distribution of percentage changes in dry deposition of Hg resulting from (a) -50%, and (b) 50% natural Hg emissions changes

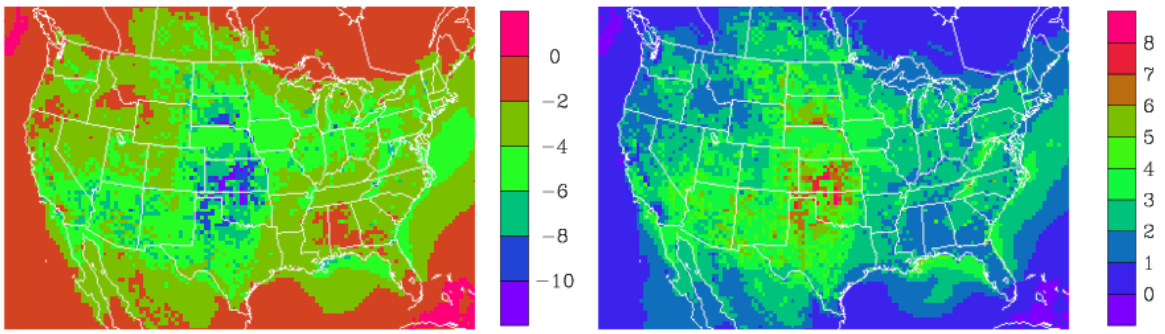

Figure 5.8: Spatial distribution of percentage changes in dry deposition of Hg resulting from (a) -50%, and (b) 50% NO_x emissions changes

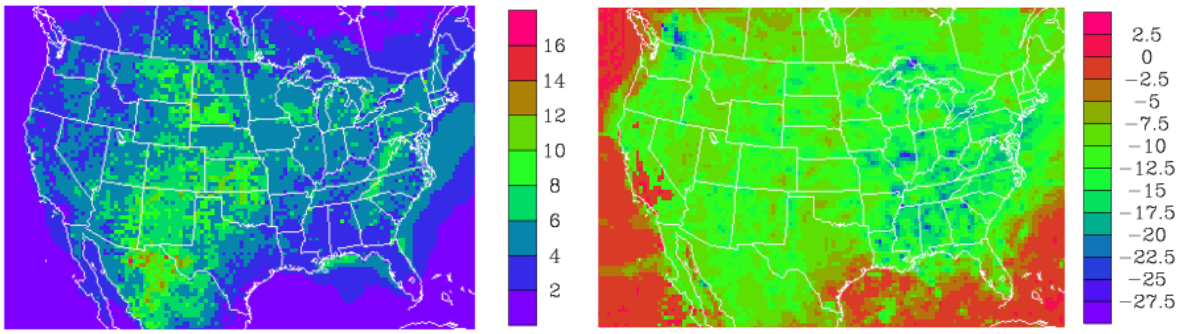

Figure 5.9: Spatial distribution of percentage changes in dry deposition of Hg resulting from (a) -50%, and (b) 50% VOCs emissions changes

5.4.3 Sensitivity of Hg wet deposition

Modelled sensitivity of Hg wet deposition is presented in Figure 5.10. Quite different from Hg dry deposition, Hg wet deposition is not so sensitive to Hg emissions including natural and anthropogenic, but is highly sensitive to VOCs emission and NO_x emission. Only non-Hg emissions such as NO_x and VOCs can significantly affect the total Hg wet deposition, especially of VOCs emission. This is very important for guiding the mitigation of Hg wet deposition. According to this result, reducing Hg emissions including natural and anthropogenic is not an effective way to reduce Hg wet deposition. Only controlling NO_x and VOCs emissions can achieve a significant reduction of wet deposition.

VOCs emission has a strong effect on Hg wet deposition, even stronger than NO_x; However, the effect is inverse. As shown in Figure 5.10, reducing VOCs emission by 50% leads to about 15% increase of Hg wet deposition; increasing VOCs emission by 50% results in about 10% reduction of Hg wet deposition. This inverse effect of

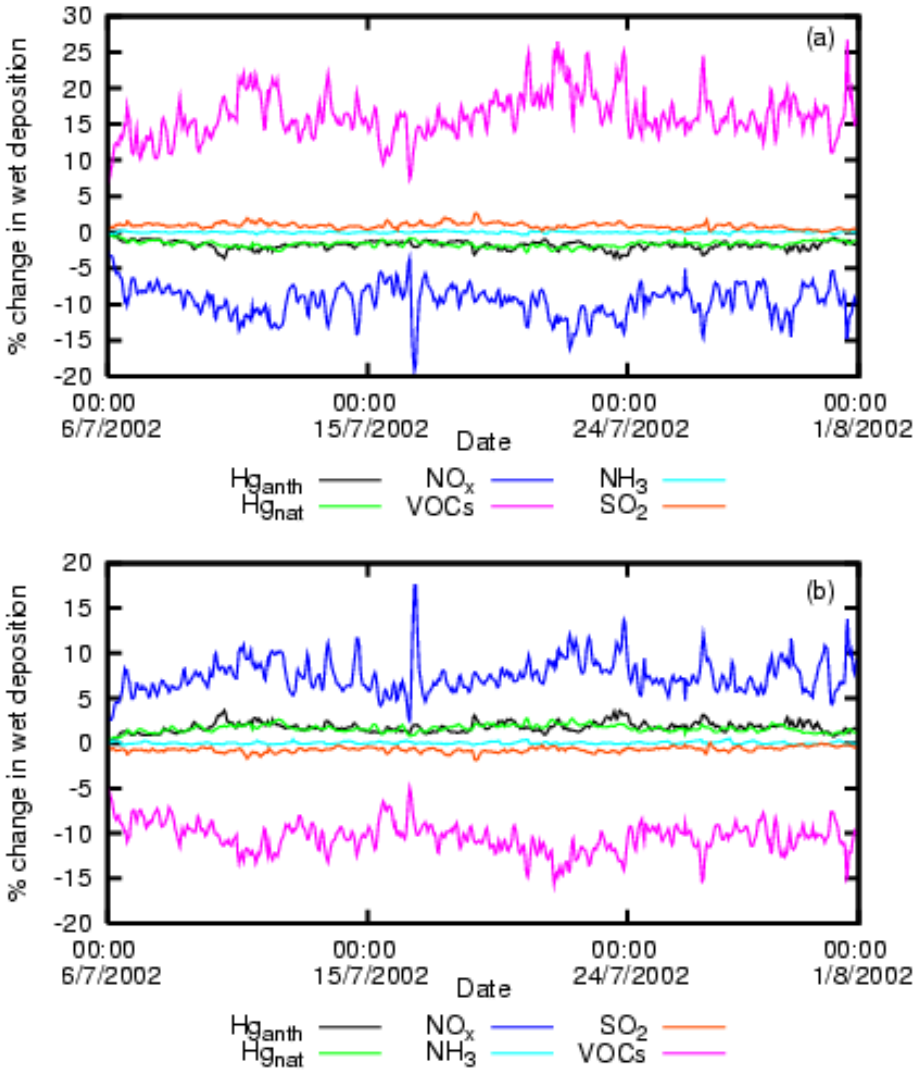

Figure 5.10: Percentage changes in total wet deposition for the whole domain resulting from (a) -50% emissions changes, and (b) +50% emissions changes.

VOCs implies that Hg wet deposition reduction can be significantly reduced at the cost of a great increase of VOCs emission. From this point, VOCs is not a good option to reduce Hg wet deposition. Modelled results show that increasing NO_x emission by 50% results in about 5% increase of Hg wet deposition, but reducing NO_x emission by 50% leads to about 10% reduction of Hg wet deposition. Since lowering NO_x emission leads to efficient mitigation of Hg wet deposition, controlling NO_x emission should be the best way to abate Hg wet deposition through the way of emission control.

The trend changes in wet deposition of Hg and its three species, Hg(0), Hg(II) and Hg(p), with changes in emissions are presented in Figure 5.11. Since the trend change in wet deposition of Hg(0) is opposite to that in wet deposition of Hg, Hg(0) should be a small contributor to the change in total wet deposition or else it should have a similar trend as wet deposition of Hg has. In addition, the similarity between Figure 5.11(a) and Figure 5.11(c) suggests that Hg(II) is the only important contributor to the change in total wet deposition.

Figure 5.12 and 5.13 show the spatial variability of sensitivity of Hg wet deposition to NO_x emission change and VOC emission change respectively. Eastern North America is the most sensitive area for NO_x emission change and for VOCs emission change. The possible reason is that both precipitation and Hg concentration are high in this region.

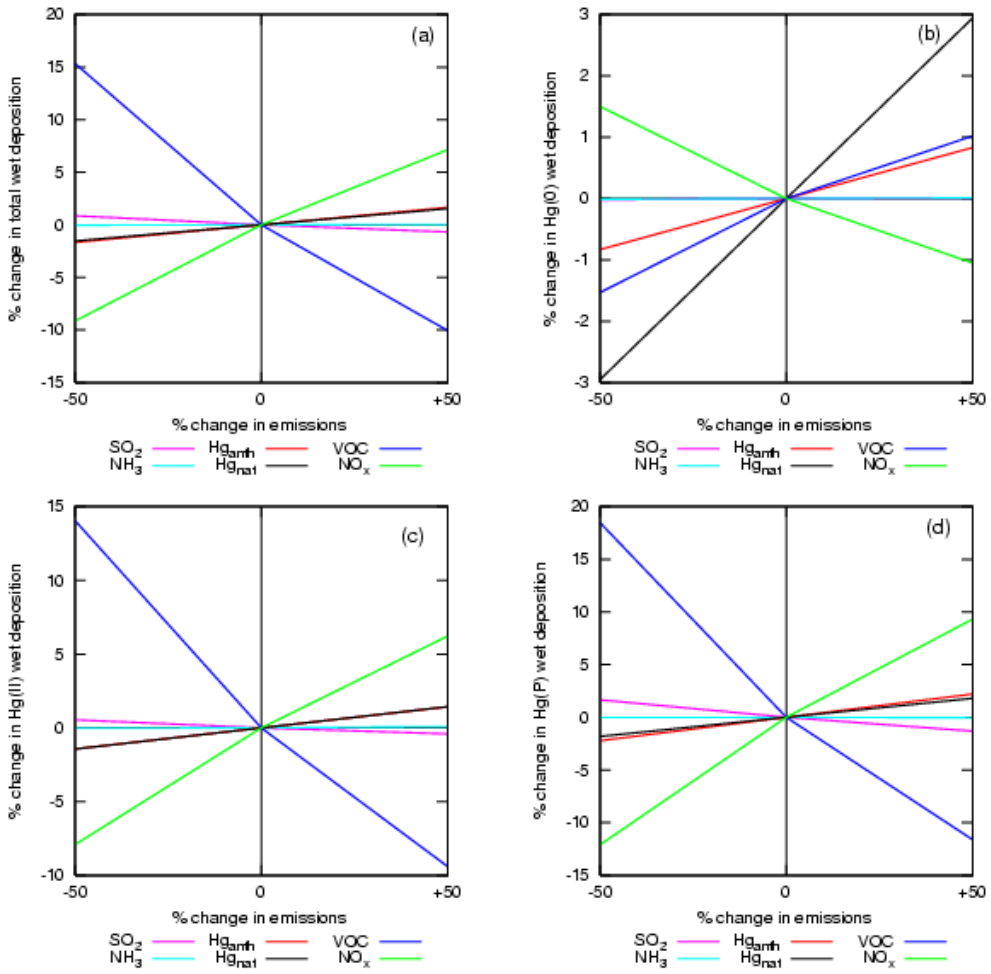

Figure 5.11: Percentage changes in total (a) TGM, (b) Hg(0), (c) Hg(II) and (d) Hg(p) wet deposition resulting from ±50% emissions changes

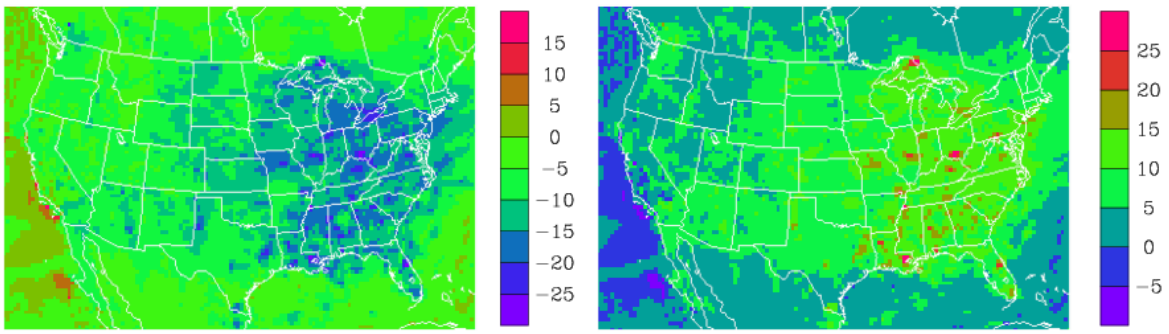

Figure 5.12: Spatial distribution of percentage changes in wet deposition of Hg resulting from (a) -50%, and (b) 50% NO_x emissions changes

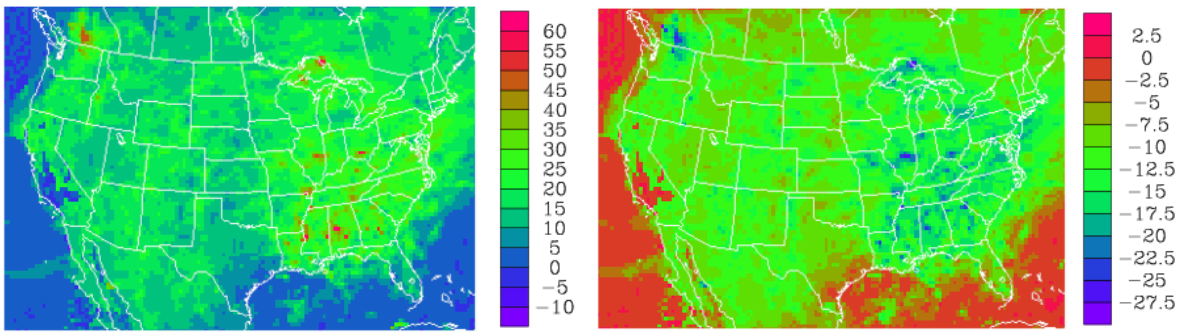

Figure 5.13: Spatial distribution of percentage changes in wet deposition of Hg resulting from (a) -50%, and (b) 50% VOCs emissions changes

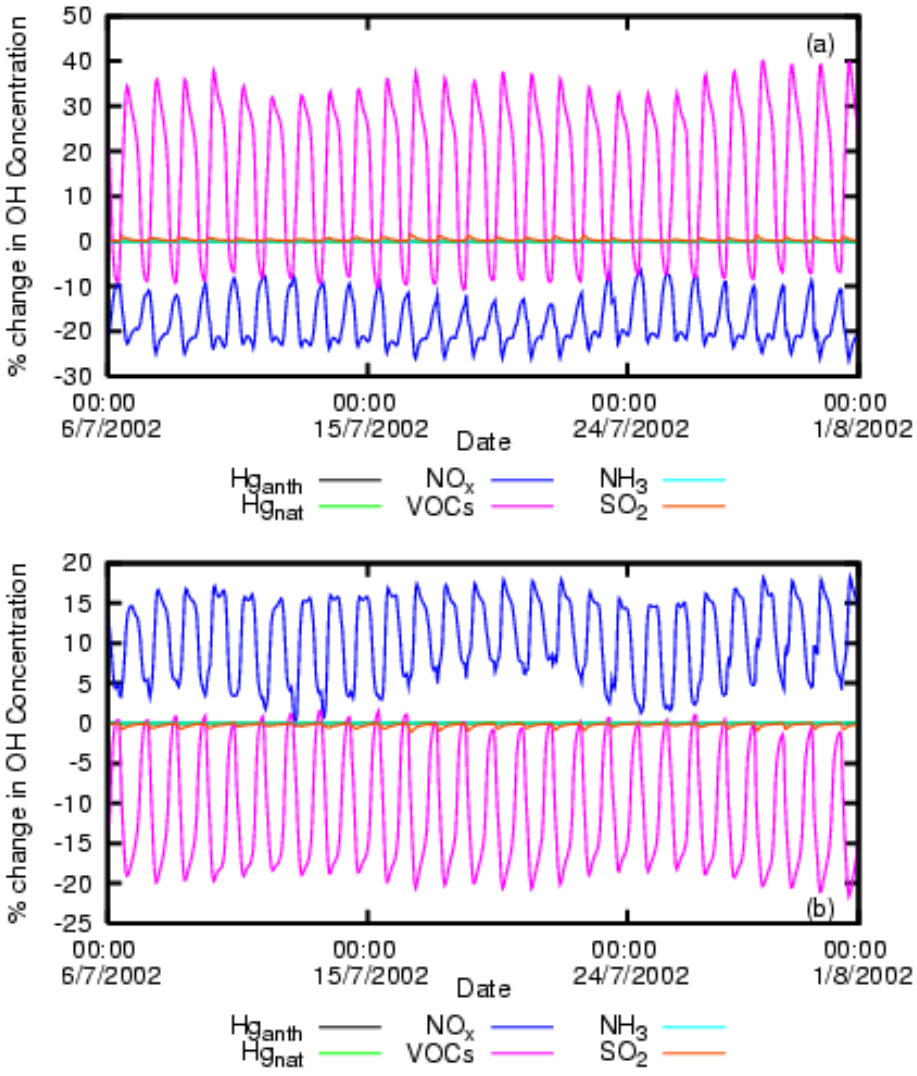

Figure 5.14: Percentage changes in average OH concentration for the whole domain resulting from (a) -50% emissions changes, and (b) +50% emissions changes.

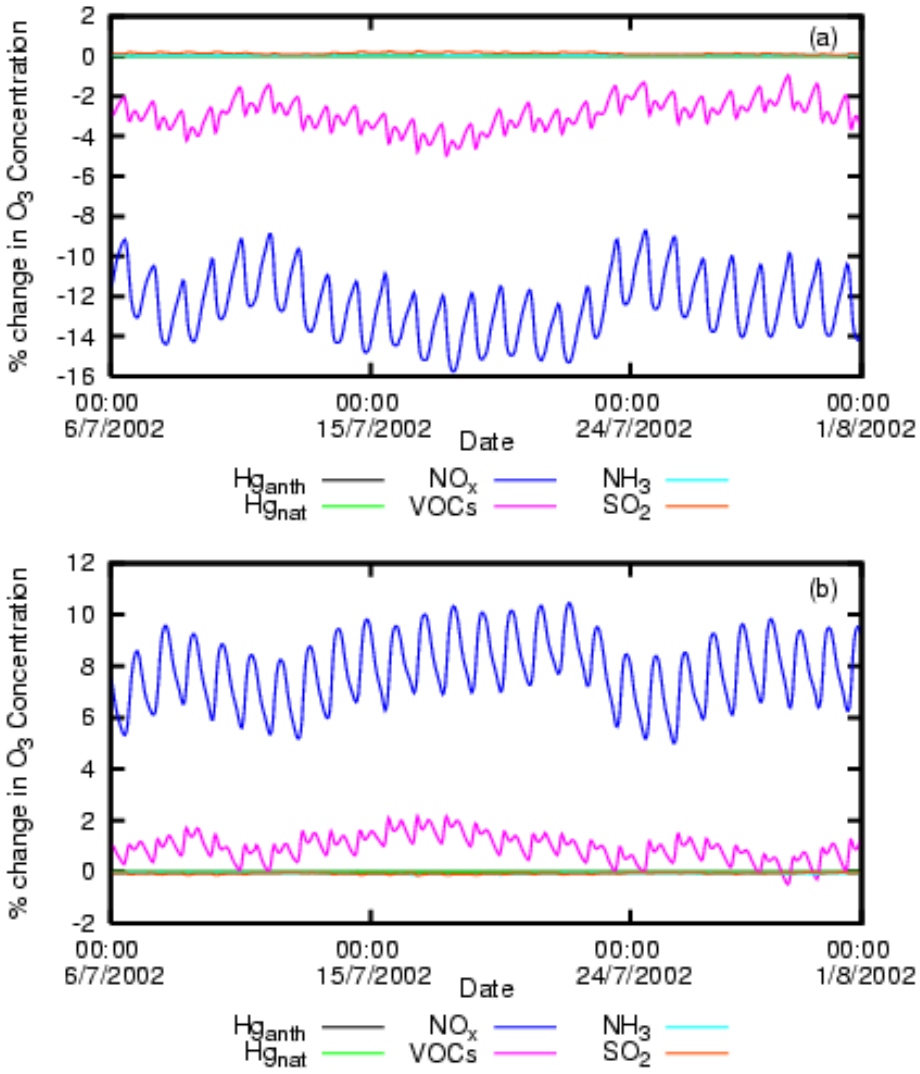

Figure 5.15: Percentage changes in average O_3 concentration for the whole domain resulting from (a) -50% emissions changes, and (b) +50% emissions changes.

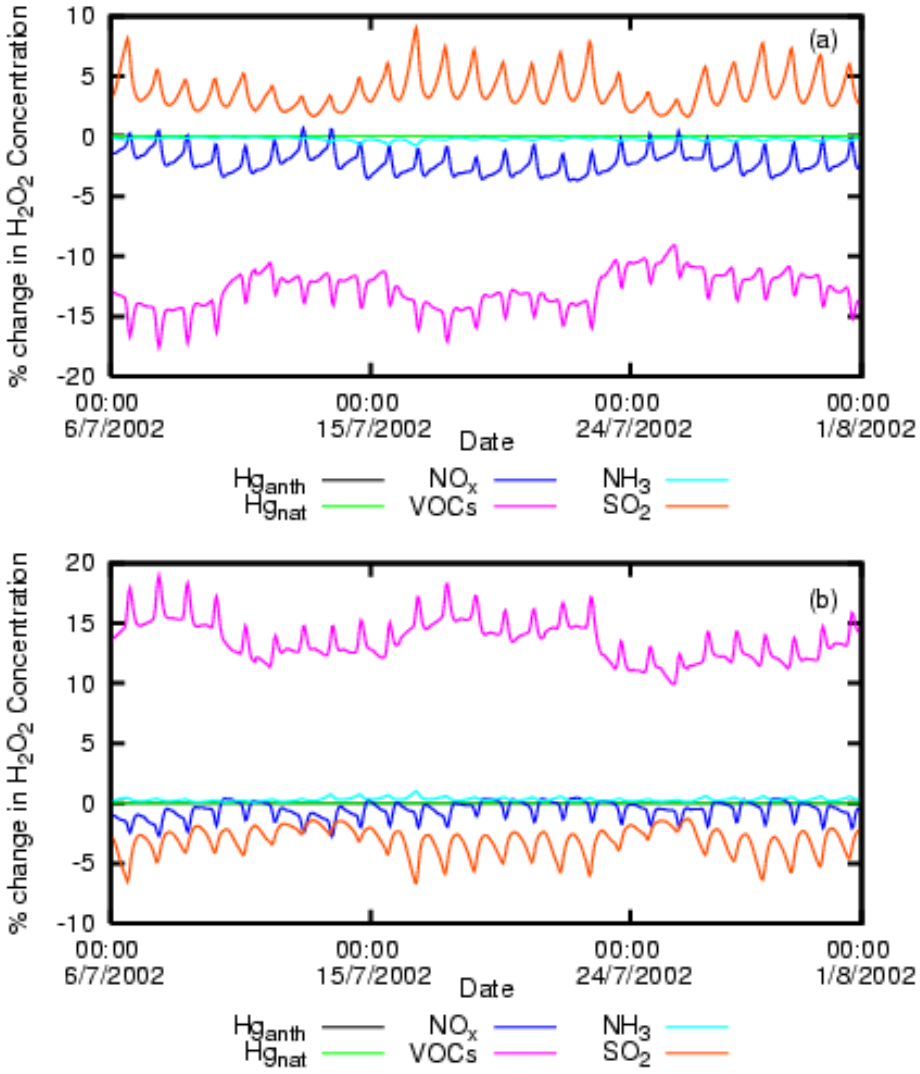

Figure 5.16: Percentage changes in average H_2O_2 concentration for the whole domain resulting from (a) -50% emissions changes, and (b) +50% emissions changes.

5.4.4 Discussion

From the above results, it is clear that non-Hg emissions (especially VOCs and NO_x) play an important role in affecting, Hg dry deposition and wet deposition. Since they do not directly emit Hg into the air, the only way to affect atmospheric Hg should be through chemical processes which link non-Hg emissions and atmospheric Hg together. In order to better understand the impacts of the emissions on atmospheric Hg, it is essential to identify the key pathway through which atmospheric Hg is mainly affected by the emissions.

The reactions between Hg and OH, and O_3 and H_2O_2, were found to be important for atmospheric chemistry of Hg (Lin and Pehkonen, 1999; Bullock and Brehme, 2002). The effects of these species on atmospheric Hg were examined in this study. Figure 5.14, Figure 5.15 and Figure 5.16 show their percentage changes in response to all emission changes investigated here. From Figure 5.14, we can see that OH concentration increases with a reduction of VOCs emission and decreases with an increase of VOCs emission, while it increases with an increase of NO_x emission and decreases with a reduction of NO_x emission. Meanwhile, we also can see that Hg(II) concentration and wet and dry deposition of Hg all change in a similar way to OH concentration. This phenomenon indicates that OH is most important among OH, O_3 and H_2O_2 because its concentration is significantly determined by non-Hg emission such as VOCs and NO_x, and at the same time its concentration heavily affects the concentration, dry and wet deposition of atmospheric Hg. Thus, the possible pathway through which atmospheric Hg is significantly affected by emission

change might be emissions of pollutants, especially VOCs and NO_x, that affect the level of OH in the atmosphere. It is OH, not O_3 and H_2O_2, that primarily control the concentration and deposition of Hg by affecting the gas phase reaction between Hg(0) and OH. This reaction converts Hg(0) into Hg(II) and Hg(p) (Bullock, 2005).

Since VOCs emission inversely and nonlinearly affects OH concentration in the atmosphere and further affects the conversion of Hg(0) into Hg(II) and Hg(p), it is no wonder that VOCs emission has some nonlinear effects on Hg and its species. Similarly, NO_x has some inverse and nonlinear effect on Hg and its species because NO_x nonlinearly affects OH and further influences the conversion of Hg(0) into Hg(II) and Hg(p).

5.5 Conclusions

The results of a sensitivity analysis shows that ambient concentration of TGM is much more sensitive to Hg emissions, including anthropogenic emission and natural emission, than non-Hg emissions such as NO_x, VOC_x, NH_3 and SO_2. As for Hg emissions, natural Hg emission is more significant than anthropogenic Hg emission in affecting ambient concentration of TGM. This result not only illustrates natural Hg emission is a key factor influencing the level of TGM air concentration, but also indicates the importance of natural Hg emission inventory to Hg modelling. Ambient concentration change in TGM due to emissions changes is mainly contributed by Hg(0).

Hg dry deposition is not only sensitive to Hg emissions but also to non-Hg emissions such as VOCs and NO_x. Anthropogenic and natural Hg emissions have almost the same effect on percentage change in total dry deposition. Both Hg emission and transformation of Hg are important for total Hg dry deposition.

Different from dry deposition, Hg wet deposition is not so sensitive to Hg emissions including natural and anthropogenic, but is highly sensitive to VOCs emission and NO_x emission. Only non-Hg emissions such as NO_x and VOCs can significantly affect the total Hg wet deposition, especially of VOCs emission. Hg(II) is the only important contributor to the change in total wet deposition. Because of the inverse effect of VOCs on Hg wet deposition, reducing NO_x emission is an effective solution to the mitigation of Hg wet deposition.

Hg emissions affect the concentration and deposition of atmospheric Hg mainly through direct input of Hg species into the atmosphere. Emissions of non-Hg pollutants, especially VOCs and NO_x, greatly affect the level of OH in the atmosphere. Consequently, by affecting the gas phase reaction between Hg(0) and OH, they significantly act on the concentration and deposition of atmospheric Hg.

Chapter 6

Conclusions and recommendations

This thesis presents a systematic study on the emission, transport, transformation and deposition of atmospheric Hg in North America. In this study, a detailed natural Hg emission model was developed to estimate Hg emissions from water, soil and vegetation. One year's simulation of natural Hg emissions in North America was conducted and the characteristics of Hg emissions from this region was investigated. The CMAQ-Hg model was improved by incorporating the natural Hg emission model, calculating dry deposition of Hg(0) and adopting boundary conditions from a global model. The improved model was then applied to North America for the whole year 2002; The regional budget was estimated. The behaviour of emission, transport, transformation and deposition of atmospheric Hg in North America was explored. Finally, a sensitivity analysis was performed to assess the effects of emissions on Hg concentration and deposition in North America.

6.1 Conclusions

A detailed natural Hg emission model was developed to estimate natural Hg emissions from different land uses in the simulation domain based on information such as meteorological data, location-specific soil Hg concentration and soil moisture content. The influence of snow cover and low temperature on natural Hg emission was also taken into account in the model. The model was applied to North America for the whole year 2002. The results of one year's simulation, compared to some reported natural Hg emission measurements, indicated that the parameterization of natural Hg emissions from different land uses was acceptable based on current knowledge. The modelled natural Hg emissions from all land uses in the simulation domain exhibited an obvious daily diurnal variation which differs significantly for different land uses. Except for water, which emission did not show an obvious seasonal variation, modelled Hg emissions from all land uses followed an annual cycle pattern with a maximum in July and a minimum in January. Modelled total natural Hg emission in this simulation domain in 2002 was about 228 tonnes, among which about 27% was from water, the largest source. Agriculture and range were also two important contributors. Temporally, about 40% of total natural Hg emission came from 3 summer months June, July and August. Emission from 3 winter months December, January and February only accounted for 13% of total annual emission. About 13% of total emission came from July and about 4% from January. The significant difference in natural emissions between summer and winter suggest that any attempt to estimate natural emission only from emission rate in summer or winter alone would significantly overestimate or underestimate

total annual natural Hg emission. Small emission in winter resulted from winter conditions such as snow cover, low temperature, low leaf area index and frozen soil, all of which greatly limited Hg emission from water, soil and vegetation.

Modelled natural Hg emission flux demonstrated a strong connection with the characteristics of surfaces, while anthropogenic Hg emission had no apparent relationship to it. Natural emission depended on many factors such as meteorological conditions, soil Hg concentration, soil moisture and vegetation conditions. Geographical distribution of anthropogenic Hg emission was mainly determined by the distribution of point sources because point sources were predominant among anthropogenic emission sources of Hg. Natural and anthropogenic Hg emissions played different roles in different modelling areas. More populated areas with higher industrial activities had higher anthropogenic emissions while natural emissions dominated in less populated areas with lower industrial activities.

Improved CMAQ-Hg was applied to North America for the whole year 2002. The comparisons between modelled and measured hourly TGM for 3 sites were presented in this study and this is the first time that a comparison of the hourly modelled results versus measurement has been reported for a CAMNet site. The good agreement between them demonstrated that improved CMAQ-Hg systems had a good performance modelling the behaviour of emission, transport, transformation and deposition of atmospheric Hg. The modelled results from base case and no natural Hg emission case indicated that neglecting natural emissions of Hg would greatly underestimate Hg ambient concentration but not significantly affect wet deposition. In contrast to wet deposition, mainly determined by the amount of

precipitation, dry deposition was primarily determined by dry deposition velocity and concentration, therefore, to some extent, its geographical distribution reflects its dependence on the characteristics of surfaces (which influence dry deposition velocity). Hg dry deposition was greater than wet deposition and mainly governed the distribution of total Hg deposition over the modelling domain. The modelled total Hg emission for 2002 was about 355 metric tons, 65% of which is natural emission, about 1.8 times anthropogenic emissions. It was estimated that about 335 metric tons of Hg in total was deposited back to earth in this simulation, about 59% via dry processes and 41% via wet processes. The modeling domain acts as a source of atmospheric Hg in the simulation period.

A sensitivity analysis was also conducted for a summer month, July 2002, to examine the effects of emissions changes on atmospheric Hg. The investigated emissions included natural Hg emission, anthropogenic Hg emission and non-Hg emissions such as NO_x, SO_2, VOCs and NH_3. The results showed that ambient concentration of TGM was much more sensitive to Hg emissions than non-Hg emissions. Natural Hg emission had a more significantly affect on ambient concentration of TGM than anthropogenic emission, illustrating natural Hg emission as a key factor influencing the level of TGM air concentration. Ambient concentration changes in TGM due to emissions changes mainly come from the contribution of Hg(0). Unlike TGM concentration, Hg dry deposition was not only sensitive to Hg emissions but also to non-Hg emissions such as VOCs and NO_x. Anthropogenic and natural Hg emissions and NO_x emission had almost the same effect on total dry deposition of Hg. Both direct Hg emission and transformation of Hg were important for total Hg dry deposition. Hg wet deposition was only sensitive to non-Hg

emissions such as NO_x and VOCs, especially of VOCs emission. Because of the inverse effect of VOCs on Hg wet deposition, reducing NO_x emission should be an ideal solution to the mitigation of Hg wet deposition. The results suggested that through significantly affecting OH concentration, non-Hg emissions greatly influence the concentration and deposition of atmospheric Hg.

6.2 Recommendations for future research

Since a significant portion of North America, especially Canada, is covered with snow for extended periods of time (Figure 3.2), natural Hg emission from snow-covered surfaces should be well studied in order to build a robust natural Hg emission inventory. So far, there have been a limited number of measurements of mercury flux from natural sources and processes, and the dynamics of Hg air-snow exchange are not well known. Future work should further investigate the processes controlling natural Hg emissions from surfaces including snow-covered surfaces, and develop a parameterization of this process and apply it in estimating natural Hg emissions. Although snow cover effect was considered in this study, only a very rough assumption was made due to the lack of data.

Natural emission and dry deposition are two important pathways determining the biogeochemical cycling of Hg in the environment. In the process of estimating the natural Hg emission flux and dry deposition velocity of Hg, current natural mercury emission model and CMAQ deposition algorithm only accept the grid-dominant landuse type data and grid-averaged landuse dependent parameters like leaf area index and vegetation fraction. In order to obtain more accurate estimation

of natural emission and dry deposition velocities of Hg for each grid cell, the models should be improved and more refined surface characteristics data such as landuse type fraction, vegetation fraction and leaf area indexes for each landuse types in each cell should be applied in future studies.

New and confident findings regarding the physical and chemical processes that govern the form and concentration of Hg in air and cloud water are emerging and these findings should be incorporated into the CMAQ-Hg model continuously. For example, the reactions of Hg with atomic halogens were found to be important pathway of Hg transformation in the air, and bromine might be responsible for the mercury depletion episode in the Arctic troposphere. The current version of the CMAQ-Hg model has included the reactions of Hg with chlorine; reactions of Hg with bromine, however, are not considered in the model. Incorporation of complete and confident scientific understanding will help to draw a complete picture of the mercury chemistry in the atmosphere.

Bibliography

Alberts, J., Schindle, J.E, Miller, R. and Carr, P. (1974): Mercury Determinations in Natural-Waters by Persulfate Oxidation. Analytical Chemistry, 46(3), 434-437.

Allan, R. (1996): Long-range atmospheric transport of heavy metals, particularly mercury in Canada: Sources, Fate and Effects. NWRI Contribution. 9680.

Allen, R., Pereira, L., Raes, D. and Smith, M. (1998): Guidelines for computing crop water requirement-FAO irrigation and drainage paper 56, FAO-Food and Agriculture Organization of the United Nations, Rome. http://www.fao.org/docrep/X0490E/X0490E00.htm.

Amyot, M., Mierle, G., Lean, D. and McQueen, D. (1994): Sunlight-Induced Formation of Dissolved Gaseous Mercury in Lake Waters. Environmental Science & Technology, 28(13), 2366-2371.

Ariya, P., Khalizov, A. and Gidas, A. (2002): Reactions of gaseous mercury with atomic and molecular halogens: Kinetics, product studies, and atmospheric implications. Journal of Physical Chemistry A, 106(32), 7310-7320.

Artaxo, P., Calixto de Campos, R., Fernandes, E., Martins, J., Xiao, Z., Lindqvist, O., Fernandez-Jimenez, M. and Maenhaut, W. (2000): Large scale mercury and trace element measurements in the Amazon basin . Atmospheric Environment, 34(24), 4085-4096.

Asher, W. and Wanninkhof, R. (1995): The effect of breaking waves on the analysis of dual-tracer gas exchange measurements, in Air-Water Gas Transfer, Jahne, B. and Monahan, E. C. (Eds.), Aeon Verlag, Hanau.

Bakir, F., Damluji, S., Amin-Zaki, L., Murtadha, M., Khalidi, A., al Rawi, N., Tikriti, S., Dahahir, H., Clarkson, T., Smith, J. and Doherty, R. (1973): Methylmercury poisoning in Iraq. Science, 181, 230-241.

Baldwin, D. and Marshall, W. (1999): Heavy metal poisoning and its laboratory investigation. Annals of Clinical Biochemistry, 36, 267-300.

BC-EMEP (1994-1998): Bulgarian contribution to EMEP, Annual reports for 1994, 1995, 1996, 1997,1998. Technical report, NIMH, EMEP/MSC-E, Sofia-Moscow.

Bergan, T., Gallardo, L. and Rodhe, H. (1999): Mercury in the global troposphere: a three-dimensional model study. Atmospheric Environment, 33(10), 1575-1585.

Bidleman, T. and McConnell, L. (1995): A Review of Field Experiments to Determine Air-Water Gas-Exchange of Persistent Organic Pollutants. Science of the Total Environment, 159(2-3), 101-117.

Blanchard, P. (2005): Total Gaseous Mercury Measurements for Point Petre, Egbert and Burnt Island. Environment Canada, Processes Research, Canada, Personal Communication.

Boerngen, J.G. and Shacklette, H.T. (1981): Chemical analyses of soils and other surficial materials of the conterminous United States: U.S. Geological Survey Open-File Report 81-197, 143 p.

Brunke, E., Labuschagne, C. and Slemr, F. (2001): Gaseous mercury emissions from a fire in the Cape Peninsula, South Africa, during January 2000. Geophysical Research Letters, 28(8), 1483-1486.

Brutsaert, W. (1979): Heat and Mass-Transfer to and from Surfaces with Dense Vegetation Or Similar Permeable Roughness. Boundary-Layer Meteorology, 16(3), 365-388.

Bullock, O. (2000a): Current methods and research strategies for modeling atmospheric mercury. Fuel Processing Technology, 65, 459-471.

Bullock, O. (2000b): Modeling assessment of transport and deposition patterns of anthropogenic mercury air emissions in the United States and Canada. Science of the Total Environment, 259(1-3), 145-157.

Bullock, O. (2003): Mercury Emissions and Atmospheric Transport Sorry Charlie -Its Coming from the Atmosphere! Western Hg Workshop -Denver,Colorado.

Bullock, O. (2005): National Oceanic and Atmospheric Administration, USA, Personal Communication.

Bullock, O. and Brehme, K. (2002): Atmospheric mercury simulation using the CMAQ model: formulation description and analysis of wet deposition results. Atmospheric Environment, 36(13), 2135-2146.

Bullock, O., Brehme, K. and Mapp, G. (1998): Lagrangian modeling of mercury air emission, transport and deposition: An analysis of model sensitivity to emissions uncertainty. Science of the Total Environment, 213(1-3), 1-12.

Byun, D. and Ching, J. (1999): Science Algorithms of the EPA Models-3 Community Multiscale Air Quality (CMAQ) Modeling System, EPA-600/R-99/030.

Cain, A. (2006): Sources of Atmospheric Mercury. LADCO Workshop on Mercury Deposition in the Upper Midwest February 22, 2006.

Carpi, A. (1997): Mercury from combustion sources: A review of the chemical species emitted and their transport in the atmosphere. Water Air and Soil Pollution, 98(3-4), 241-254.

Carpi, A. and Lindberg, S. (1998): Application of a Teflon (TM) dynamic flux chamber for quantifying soil mercury flux: Tests and results over background soil. Atmospheric Environment, 32(5), 873-882.

Christensen, J. (1997): The Danish Eulerian hemispheric model -A three-dimensional air pollution model used for the Arctic. Atmospheric Environment, 31(24), 4169-4191.

Christensen, J., Brandt, J., Frohn, L. and Skov, H. (2004): Modelling of mercury in the Arctic with the Danish Eulerian Hemispheric Model. Atmospheric Chemistry and Physics, 4, 2251-2257.

Chtcherbakov, A. (2004): Ontario Ministry of Environment, Personal Communication.

Cohen, M. (1997): The Transport and Deposition of Persistent Toxic Substances to the Great Lakes. III. Modeling the Atmospheric Transport and Deposition of Persistent Toxic Substances to the Great Lakes. Prepared for the International Joint Commission s International Air Quality Advisory Board, Windsor, Ontario, 72 pp.

Cohen, M., Artz, R., Draxler, R., Miller, P., Poissant, L., Niemi, D., Ratte, D., Deslauriers, M., Duval, R., Laurin, R., Slotnick, J., Nettesheim, T. and McDonald, J. (2004): Modeling the atmospheric transport and deposition of mercury to the Great Lakes. Environmental Research, 95(3), 247-265.

Dastoor, A. and Larocque, Y. (2004): Global circulation of atmospheric mercury: a modelling study. Atmospheric Environment, 38(1), 147-161.

Deardorff, J. (1978): Efficient prediction of ground surface temperature and moisture, with inclusion of a layer of vegetation. Journal of Geophysical Research., 83(C4), 1889-1903.

Dickinson, R. (1983): Land surface processes and climate-surface albedos and energy balance. Advances in Geophysics, Vol. 25, Academic Press, 305-353.

Dickinson, R.E. (1985): Modelling evapotranspiration for three-dimensional global climate models. In Climate Processes and Climate Sensitivity. J.E. Hansen and T. Takahashi, eds., Maurice Ewing Series, Vol. 5, American Geophysical Union, Washington DC, 58-72.

Ebinghaus, R., Jennings, S., Schroeder, W., Berg, T., Donaghy, T., Guentzel, J., Kenny, C., Kock, H., Kvietkus, K., Landing, W., Muhleck, T., Munthe, J., Prestbo, E., Schneeberger, D., Slemr, F., Sommar, J., Urba, A., Wallschlager, D. and Xiao, Z. (1999): International field intercomparison measurements of atmospheric mercury species at Mace Head, Ireland. Atmospheric Environment, 33(18), 3063-3073.

Electric Power Research Institute (2000): An Assessment of Mercury Emissions from Coal-Fired Power Plants. Technical report, EPRI, Palo Alto, Ca, TR-1000608.

Environment Canada (2000): Canadian National Atmospheric Chemistry (NAtChem) Database. http://www.msc-smc.ec.gc.ca/natchem/index e.html. Meteorological Service of Canada, Ont., Canada.

Environment Canada (2006): Sources of Mercury, Canadian releases, http://www.ec.gc.ca/MERCURY/SM/EN/sm-cr.cfm?SELECT=SM. Environment Canada.

Expert Panel on Mercury Atmospheric Processes, (1994): Mercury atmospheric processes: A synthesis report.TR-104214. Electric Power Research Institute, Palo Alto, CA, USA.

Feng, X., Yan, H., Wang, S., Qiu, G., Tang, S., Shang, L., Dai, Q. and Hou, Y. (2004): Seasonal variation of gaseous mercury exchange rate between air and water surface over Baihua reservoir, Guizhou, China. Atmospheric Environment, 38(28), 4721-4732.

Fitzgerald, W. and Clarkson, T. (1991): Mercury and Monomethylmercury Present and Future Concerns. Environmental Health Perspectives, 96, 159-166.

Fitzgerald, W., Kim, J., Gill, G. and Hewitt, A. (1986): Atmospheric Cycling of Mercury Over the Pacific-Ocean. Atmospheric Environment, 20(10), 2075-2076.

Fitzgerald, W., Mason, R. and Vandal, G. (1991): Atmospheric Cycling and Air-Water Exchange of Mercury Over Midcontinental Lacustrine Regions. Water Air and Soil Pollution, 56, 745-767.

Fitzgerald, W., Mason, R., Vandal, G. and Dulac, F. (1994): Air-water cycling of mercury in lakes. In: C.J. Watras and J.W. Huckabee (eds.). Mercury as a Global Pollutant: Towards Integration and Synthesis. Lewis Press, Boca Raton, FL.

Frescholtz, T. and Gustin, M. (2004): Soil and foliar mercury emission as a function of soil concentration. Water Air and Soil Pollution, 155(1-4), 223-237.

Gardfeldt, K., Feng, X., Sommar, J. and Lindqvist, O. (2001): Total gaseous mercury exchange between air and water at river and sea surfaces in Swedish coastal regions. Atmospheric Environment, 35(17), 3027-3038.

Garrat, J.R. and Hicks, B.B (1973): Momentum, heat and water vapour transfer to and from natural and artificial surface. Quarterly Journal of the Royal Meteorological Society, 99, 680-687.

Garrett, R. (2004): Geological Survey of Canada, Personal Communication.

Gbor, P., Wen, D., Meng, F., Yang, F., Zhang, B. and Sloan, J. (2006): Improved model for mercury emission, transport and deposition. Atmospheric Environment, 40, 973-983.

Gillis, A. and Miller, D. (2000): Some local environmental effects on mercury emission and absorption at a soil surface. Science of the Total Environment, 260(1-3), 191-200.

Grigal, D., Kolka, R., Fleck, J. and Nater, E. (2000): Mercury budget of an upland-peatland watershed. Biogeochemistry, 50(1), 95-109.

Gustavsson, N., Bolviken, B., Smith, D. and Severson, R. (2001): Geochemical landscapes of the conterminous United States. New map presentations for 22 elements: U.S. Geological Survey Professional Paper 1648, Available online at: http://pubs.usgs.gov/pp/2001/p1648/

Gustin, M., Taylor, G. and Callan, R. (1997): Anthropogenic and natural sources of atmospheric mercury in central western Nevada. Abstracts of Papers of the American Chemical Society, 214, 135-ENVR.

Hanson, P., Lindberg, S., Tabberer, T., Owens, J. and Kim, K. (1995): Foliar Exchange of Mercury-Vapor -Evidence for A Compensation Point. Water Air and Soil Pollution, 80(1-4), 373-382.

Hedgecock, I., Trunfio, G., Pirrone, N. and Sprovieri, F. (2005): Mercury chemistry in the MBL: Mediterranean case and sensitivity studies using the AMCOTS (Atmospheric Mercury Chemistry over the Sea) model. Atmospheric Environment, 39(38), 7217-7230.

Hicks, B., Meyers, T. and Baldocchi, D. (1987): Sampling for Dry Deposition. Abstracts of Papers of the American Chemical Society, 193, 21-ACSC.

Hornbuckle, K., Jeremiason, J., Sweet, C. and Eisenreich, S. (1994): Seasonal-Variations in Air-Water Exchange of Polychlorinated-Biphenyls in Lake-Superior. Environmental Science & Technology, 28(8), 1491-1501.

Hsi, H., Chen, S., Rostam-Abadi, M., Rood, M., son, C., Carey, T. and Chang, R. (1998): Preparation and evaluation of coal-derived activated carbons for removal of mercury vapor from simulated coal combustion flue gases. Energy & Fuels, 12(6), 1061-1070.

Hudson, R., Gherini, S., Fitzgerald, W. and Porcella, D. (1995): Anthropogenic Influences on the Global Mercury Cycle -A Model-Based Analysis. Water Air and Soil Pollution, 80(1-4), 265-272.

Ilyin, L., Ryaboshapko, A. and Travnikov, O. (2002): Heavy Metal Contamination on European and Hemispherical Scale, EMEP Status Report 3/2002, Cooperative Programme for Monitoring and Evaluation of the Long-Range Transmission of Air pollutants in Europe. Ul. arhitektor Vlasov, Moscow, Russia.

Javis, P. (1976): The interpretation of the variations in leaf water potential and stomatal conductance found in canopies in the field. Philosophical Transactions of the Royal Society, London, Ser. B 273: 593-610.

Johnson, D. and Braman, R. (1974): Distribution of Atmospheric Mercury Species Near Ground. Environmental Science & Technology, 8(12), 1003-1009.

Kallos, G., Voudouri, A., Pytharoulis, I. and Kakaliagou, O. (2001): Modelling framework for atmospheric mercury over the Mediterranean region: Model development and applications. Large-Scale Scientific Computing, 2179, 281-290.

Kim, K. and Lindberg, S. (1995): Design and Initial Tests of A Dynamic Enclosure Chamber for Measurements of Vapor-Phase Mercury Fluxes Over Soils. Water Air and Soil Pollution, 80(1-4), 1059-1068.

Lamborg, C., Hoyer, M., Keeler, G., Olmez, I. and Huang, Z. (1994): Mercury Pollution -Integration and Synthesis, CRC Press Inc., Florida.

Leonard, T., Taylor, G., Gustin, M. and Fernandez, G. (1998): Mercury and plants in contaminated soils: 1. Uptake, partitioning, and emission to the atmosphere. Environmental Toxicology and Chemistry, 17(10), 2063-2071.

Lin, C., Lindberg, S., Ho, T. and Jang, C. (2005): Development of a processor in BEIS3 for estimating vegetative mercury emission in the continental United States. Atmospheric Environment, 39(39), 7529-7540.

Lin, C. and Pehkonen, S. (1999): The chemistry of atmospheric mercury: a review. Atmospheric Environment, 33(13), 2067-2079.

Lin, X. and Tao, Y. (2003): A numerical modelling study on regional mercury budget for eastern North America. Atmospheric Chemistry and Physics, 3, 535-548.

Lindberg, S., Dong, W. and Meyers, T. (2002): Transpiration of gaseous elemental mercury through vegetation in a subtropical wetland in Florida. Atmospheric Environment, 36(33), 5207-5219.

Lindberg, S., Hanson, P., Meyers, T. and Kim, K. (1998): Air/surface exchange of mercury vapor over forests -The need for a reassessment of continental biogenic emissions. Atmospheric Environment, 32(5), 895-908.

Lindberg, S., Meyers, T., Taylor, G., Turner, R. and Schroeder, W. (1992): Atmosphere-Surface Exchange of Mercury in A Forest -Results of Modeling and Gradient Approaches. Journal of Geophysical Research-Atmospheres, 97(D2), 2519-2528.

Lindberg, S. and Stratton, W. (1998): Atmospheric mercury speciation: Concentrations and behavior of reactive gaseous mercury in ambient air. Environmental Science & Technology, 32(1), 49-57.

Lindqvist, O., Johansson, K., Aastrup, M., Andersson, A., Bringmark, L., Hovsenius, G., Hakanson, L., Iverfeldt, A., Meili, M. and Timm, B. (1991): Mercury in the Swedish Environment -Recent Research on Causes, Consequences and Corrective Methods. Water Air and Soil Pollution, 55(1-2), 7-17.

Lindqvist, O. and Rodhe, H. (1985): Atmospheric Mercury -A Review. Tellus Series B-Chemical and Physical Meteorology, 37(3), 136-159.

Lohman, K., Pai, P., Seigneur, C. and Levin, L. (2000): Sensitivity analysis of mercury human exposure. Science of the Total Environment, 259(1-3), 3-11.

Lyon, B., Ambrose, R., Rice, G. and Maxwell, C. (1997): Calculation of soil-water and benthic sediment partition coefficients for mercury. Chemosphere, 35(4), 791-808.

Mackay, D. and Yeun, A. (1983): Mass-Transfer Coefficient Correlations for Volatilization of Organic Solutes from Water. Environmental Science & Technology, 17(4), 211-217.

Malcolm, E. and Keeler, G. (2002): Measurements of mercury in dew: Atmospheric removal of mercury species to a wetted surface. Environmental Science & Technology, 36(13), 2815-2821.

Mason, R., Fitzgerald, W. and Morel, F. (1994): The Biogeochemical Cycling of Elemental Mercury -Anthropogenic Influences. Geochimica et Cosmochimica Acta, 58(15), 3191-3198.

Massman, W. (1999): Molecular diffusivities of Hg vapor in air, O_2 and N_2 near STP and the kinematic viscosity and thermal diffusivity of air near STP. Atmospheric Environment, 33(3), 453-457.

Mo, X., Liu, S., Lin, Z. and Zhao, W. (2004): Simulating temporal and spatial variation of evapotranspiration over the Lushi basin. Journal of Hydrology, 285(1-4), 125-142.

Monteith, J. (1965): Light Distribution and Photosynthesis in Field Crops. Annals of Botany, 29(113), 17-37.

Monteith, J. and Usworth, M. (1990): Principles of Environmental Physics. 2nd Ed., E. Arnold, London.

Munthe, J., Wangberg, I., Iverfeldt, A., Lindqvist, O., Stromberg, D., Sommar, J., Gardfeldt, K., Petersen, G., Ebinghaus, R., Prestbo, E., Larjava, K. and Siemens, V. (2003): Distribution of atmospheric mercury species in Northern Europe: final results from the MOE project. Atmospheric Environment, 37, S9-S20.

Munthe, J., Xiao, Z. and Lindqvist, O. (1991): The Aqueous Reduction of Divalent Mercury by Sulfite. Water Air and Soil Pollution, 56, 621-630.

Niki, H., Maker, P., Savage, C. and Breitenbach, L. (1983a): A Fourier-Transform Infrared Study of the Kinetics and Mechanism for the Reaction Cl+CH_3HgCH_3. Journal of Physical Chemistry, 87(19), 3722-3724.

Niki, H., Maker, P., Savage, C. and Breitenbach, L. (1983b): A Long-Path Fourier-Transform Infrared Study of the Kinetics and Mechanism for the Ho-Radical Initiated Oxidation of Dimethylmercury. Journal of Physical Chemistry, 87(24), 4978-4981.

Noilhan, J. and Planton, S. (1989): A simple parameterization surface processes for meteorological models. Monthly Weather Review, 117, 536-549.

Nriagu, J. (1989): A Global Assessment of Natural Sources of Atmospheric Trace-Metals. Nature, 338(6210), 47-49.

Nriagu, J. (1994): Mechanistic Steps in the Photoreduction of Mercury in Natural-Waters. Science of the Total Environment, 154(1), 1-8.

Nriagu, J. and Pacyna, J. (1988): Quantitative Assessment of Worldwide Contamination of Air, Water and Soils by Trace-Metals. Nature, 333(6169), 134-139.

O'Driscoll, N., Beauchamp, S., Siciliano, S., Rencz, A. and Lean, D. (2003): Continuous analysis of dissolved gaseous mercury (DGM) and mercury flux in two freshwater lakes in Kejimkujik Park, Nova Scotia: Evaluating mercury flux models with quantitative data. Environmental Science & Technology, 37(10) 2226-2235.

Pacyna, J. and Pacyna, P. (1996): Global emissions of mercury to the atmosphere. Emissions from anthropogenic sources. Prepared for Report for the Arctic Monitoring and Assessment Programme (AMAP), Oslo, Norway. June.

Pai, P., Karamchandani, P. and Seigneur, C. (1997): Simulation of the regional atmospheric transport and fate of mercury using a comprehensive Eulerian model. Atmospheric Environment, 31(17), 2717-2732.

Pai, P., Karamchandani, P., Seigneur, C. and Allan, M. (1999): Sensitivity of simulated atmospheric mercury concentrations and deposition to model input parameters. Journal of Geophysical Research-Atmospheres, 104(D11), 13855-13868.

Petersen, G., Bloxam, R., Wong, S., Munthe, J., Kruger, O., Schmolke, S. and Kumar, A. (2001): A comprehensive Eulerian modelling framework for airborne mercury species: model development and applications in Europe. Atmospheric Environment, 35(17), 3063-3074.

Petersen, G., Iverfeldt, A. and Munthe, J. (1995): Atmospheric Mercury Species Over Central and Northern Europe -Model-Calculations and Comparison with Observations from the Nordic Air and Precipitation Network for 1987 and 1988. Atmospheric Environment, 29(1), 47-67.

Petersen, G., Munthe, J., Pleijel, K., Bloxam, R. and Kumar, A. (1998): A comprehensive Eulerian modeling framework for airborne mercury species: Development and testing of the Tropospheric Chemistry Module (TCM). Atmospheric Environment, 32(5), 829-843.

Pirrone, N., Costa, P., Pacyna, J. and Ferrara, R. (2001): Mercury emissions to the atmosphere from natural and anthropogenic sources in the Mediterranean region. Atmospheric Environment, 35(17), 2997-3006.

Pirrone, N., Keeler, G. and Nriagu, J. (1996): Regional differences in worldwide emissions of mercury to the atmosphere. Atmospheric Environment, 30(17), 2981-2987.

Pleijel, K. and Munthe, J. (1995): Modeling the Atmospheric Mercury Cycle Chemistry in Fog Droplets. Atmospheric Environment, 29(12), 1441-1457.

Poissant, L., Amyot, M., Pilote, M. and Lean, D. (2000): Mercury water-air exchange over the Upper St. Lawrence River and Lake Ontario. Environmental Science & Technology, 34(15), 3069-3078.

Poissant, L. and Casimir, A. (1998): Water-air and soil-air exchange rate of total gaseous mercury measured at background sites. Atmospheric Environment, 32(5), 883-893.

Poissant, L., Pilote, M., Beauvais, C., Constant, P. and Zhang, H. (2005): A year of continuous measurements of three atmospheric mercury species (GEM, RGM and Hg-p) in southern Quebec, Canada. Atmospheric Environment, 39(7), 1275-1287.

Poissant, L., Pilote, M., Xu, X., Zhang, H. and Beauvais, C. (2004): Atmospheric mercury speciation and deposition in the Bay St. Francois wetlands. Journal of Geophysical Research-Atmospheres, 109(D11), D11301.

Pollution Probe (2006): Mercury In The Environment: A Primer. www.chem.unep.ch/mercury/Report/Chapter5.htm.

Pyle, D. and Mather, T. (2003): The importance of volcanic emissions for the global atmospheric mercury cycle. Atmospheric Environment, 37(36), 5115-5124.

Rajar, R., Zagar, D., Sirca, A. and Horvat, M. (2000): Three-dimensional modelling of mercury cycling in the Gulf of Trieste. Science of the Total Environment, 260(1-3), 109-123.

Raupach, M. (1991): Vegetation-Atmosphere Interaction in Homogeneous and Heterogeneous Terrain -Some Implications of Mixed-Layer Dynamics. Vegetatio, 91(1-2), 105-120.

Rugh, C., Bizily, S. and Meagher, R. (2000): Phytoreduction of environmental mercury Poluution, in,Phytoremediation of Toxic metals: Using Plants to Clean up the Environment, by Raskin I. and Ensley B. (eds.), John Wiley and Sons, NY.

Rundgren, S., Ruhling, A., Schluter, K. and Tyler, G. (1992): Mercury in soil distribution, speciation and biological effects, Report prepared for the Nordic Council of Ministers. Copenhagen

Ryaboshapko, A., Bullock, R., Ebinghaus, R., Ilyin, I., Lohman, K., Munthe, J., Petersen, G., Seigneur, C. and Wangberg, I. (2002): Comparison of mercury chemistry models. Atmospheric Environment, 36(24), 3881-3898.

Ryaboshapko, A., Ilyin, I., Bullock, R., Ebinghaus, R., Lohman, K., Munthe, J., Petersen, G., Seigneur, C. and Wangberg, I. (2001): Intercomparison study of numerical models for long-range atmospheric transport of mercury -Stage I: Comparison of chemical modules for mercury transformations in a cloud/fog environment. MSC-East Technical Report 2/2001 (available at http://www.msceast.org/publications.html).

Ryaboshapko, A., Ilyin, I., Gusev, A., Afinogenova, O., Berg, T. and Hjellbrekke, A., (1999): Monitoring and Modelling of Lead, Cadmium and Mercury Transboundary Transport in the Atmosphere of Europe, EMEP MSC-E report 1/99.

Sakata, M. and Marumoto, K. (2004): Dry deposition fluxes and deposition velocities of trace metals in the Tokyo metropolitan area measured with a water surface sampler. Environmental Science & Technology, 38(7), 2190-2197.

Sakata, M. and Marumoto, K. (2005): Wet and dry deposition fluxes of mercury in Japan. Atmospheric Environment, 39(17), 3139-3146.

Scholtz, M., Van Heyst, B. and Schroeder, W. (2003): Modelling of mercury emissions from background soils. Science of the Total Environment, 304(1-3), 185-207.

Schroeder, W., Beauchamp, S., Edwards, G., Poissant, L., Rasmussen, P., Tordon, R., Dias, G., Kemp, J., Van Heyst, B. and Banic, C. (2005): Gaseous mercury emissions from natural sources in Canadian landscapes. Journal of Geophysical Research-Atmospheres, 110(D18).

Schroeder, W. and Munthe, J. (1998): Atmospheric mercury -An overview. Atmospheric Environment, 32(5), 809-822.

Schroeder, W., Yarwood, G. and Niki, H. (1991): Transformation Processes Involving Mercury Species in the Atmosphere -Results from A Literature Survey. Water Air and Soil Pollution, 56, 653-666.

Schwesig, D. and Krebs, O. (2003): The role of ground vegetation in the uptake of mercury and methylmercury in a forest ecosystem. Plant and Soil, 253(2), 445-455.

Seigneur, C., Behrens, G. and Roberson, R. (2000): Assessment of Mercury Emissions, Transport, Fate and Cycling for the Continental Unites States: Model Structure and Evaluation. Report 1000522, EPRI, Palo Alto, CA.

Seigneur, C., Karamchandani, P., Lohman, K., Vijayaraghavan, K. and Shia, R. (2001): Multiscale modeling of the atmospheric fate and transport of mercury. Journal of Geophysical Research-Atmospheres, 106(D21), 27795-27809.

Seigneur, C., Lohman, K., Vijayaraghavan, K. and Shia, R. (2003): Contributions of global and regional sources to mercury deposition in New York State. Environmental Pollution, 123(3), 365-373.

Seigneur, C., Vijayaraghavan, K., Lohman, K., Karamchandani, P. and Scott, C. (2004): Global source attribution for mercury deposition in the United States. Environmental Science & Technology, 38(2), 555-569.

Sellers, P., Mintz, Y., Sud, Y. and Dalcher, A. (1986): The design of a Simple Biosphere model (SiB) for use within general circulation models. Journal of The Atmospheric Sciences, 43, 505-531.

Shannon, J. and Voldner, E. (1995): Modeling Atmospheric Concentrations of Mercury and Deposition to the Great-Lakes. Atmospheric Environment, 29(14), 1649-1661.

Shia, R., Seigneur, C., Pai, P., Ko, M. and Sze, N. (1999): Global simulation of atmospheric mercury concentrations and deposition fluxes. Journal of Geophysical Research-Atmospheres, 104(D19), 23, 747-23, 760.

Siegel, S., Siegel, B., Barghigiani, C., Aratani, K., Penny, P. and Penny, D. (1987): A Contribution to the Environmental Biology of Mercury Accumulation in Plants. Water Air and Soil Pollution, 33(1-2), 65-72.

Slemr, F., Junkermann, W., Schmidt, R. and Sladkovic, R. (1995): Indication of Change in Global and Regional Trends of Atmospheric Mercury Concentrations. Geophysical Research Letters, 22(16), 2143-2146.

Slemr, F., Schuster, G. and Seiler, W. (1985): Distribution, Speciation, and Budget of Atmospheric Mercury. Journal of Atmospheric Chemistry, 3(4), 407-434.

Slinn, S. and Slinn, W. (1980): Predictions for Particle Deposition on Natural-Waters. Atmospheric Environment, 14(9), 1013-1016.

Sommar, J., Gardfeldt, K., Stromberg, D. and Feng, X. (2001): A kinetic study of the gas-phase reaction between the hydroxyl radical and atomic mercury. Atmospheric Environment, 35(17), 3049-3054.

Sommar, J., Hallquist, M. and Ljungstrom, E. (1996): Rate of reaction between the nitrate radical and dimethyl mercury in the gas phase. Chemical Physics Letters, 257(5-6), 434-438.

Storelli, M., Ceci, E. and Marcotrigiano, G. (1998): Comparison of total mercury, methylmercury, and selenium in muscle tissues and in the liver of Stenella coeruleoalba (Meyen) and Caretta caretta (Linnaeus). Bulletin of Environmental Contamination and Toxicology, 61(4), 541-547.

Thompson, N., Barrie, I.A. and Ayles, M. (1981): The Meteorological Office Rainfall and Evaporation Calculation System: MORECS. Hydrological Memorandum No.45. The Meteorological Office, Brackwell, 1981

Thomsen, E.L. and Egsgaard, H. (1986): Rate of Reaction of Dimethylmercury with Oxygen-Atoms in the Gas-Phase. Chemical Physics Letters, 125, 378-382.

Travnikov, O. and Ryaboshapko, A. (2002): Modeling of mercury hemispheric transport and deposition, meteorological Synthesizing Centre East Report, June.

United Nations Environment Programme Chemicals. (2002): UNEP Chemicals Mercury Programme. Global Mercury Assessment. http://www.chem.unep.ch/mercury/Report/Chapter5.htm.

U.S. ATSDR (1999): Agency for Toxic Substances and Disease Registry (ATSDR). Toxicological Profile for Mercury. Public Health Service, U.S. Department of Health and Human Services, Atlanta, GA.

U.S. EPA (1994): U.S. Environmental Protection Agency. Summary Review of Health Effects Associated with Mercuric Chloride: Health Issue Assessment. EPA/600/R-92/199. Office of Health and Environmental Assessment, Washington.

U.S. EPA (1997): Environmental Protection Agency. Mercury study report to congress, Volume II: An inventory of anthropogenic mercury emissions in the united states. EPA-452/R-97-004.

U.S. EPA (1999): U.S. Environmental Protection Agency. Integrated Risk Information System (IRIS) on Elemental Mercury. National Center for Environmental Assessment, Office of Research and Development, Washington, DC.

U.S. EPA (2004): 1999 National Emissions Inventory (NEI) version 3 IDA Files. ftp://ftp.epa.gov/EmisInventory/99neiv3_ida.

U.S. EPA (2004): Mercury (Hg) Emission Inventory for the Clean Air Mercury Rule (CAMR). http://www.epa.gov/ttn/chief/emch/invent/hg_smoke /2001camr_112204.zip.

U.S. EPA (2006): Controlling Power Plant Emissions: Emissions Progress. http://www.epa.gov/mercury/control emissions/emissions.htm.

Veiga, M., Meech, J. and Onate, N. (1994): Mercury Pollution from Deforestation. Nature, 368(6474), 816-817.

Verseghy, D., Mcfarlane, N. and Lazare, M. (1993): Class -A Canadian Land-Surface Scheme for GCMs. 2. Vegetation Model and Coupled Runs, International Journal of Climatology, 13(4), 347-370.

Vijayaraghavan, K. (2002): Modeling Deposition of Atmospheric Mercury in Wisconsin, AER Report CP136-02-1, WE Energies, Milwaukee, WI.

Walcek, C., Brost, R., Chang, J. and Wesely, M. (1986): SO_2, Sulfate and HNO_3 Deposition Velocities Computed Using Regional Land-Use and Meteorological Data. Atmospheric Environment, 20(5), 949-964.

Wesely, M. (1986): On the parameterization of dry deposition of acidifying substances for regional models. Interagency Agreement DW89930060-01 to the US Department of Energy. Internal Report Nov. 1986. U.S. EPA. Research Triangle Park, NC.

Wigfield, D. and Perkins, S. (1985): Oxidation of Elemental Mercury by Hydroperoxides in Aqueous-Solution. Canadian Journal of Chemistry-Revue Canadienne de Chimie, 63(2), 275-277.

Xiao, Z., Munthe, J. and Lindqvist, O. (1991): Sampling and Determination of Gaseous and Particulate Mercury in the Atmosphere Using Gold-Coated Denuders. Water Air and Soil Pollution, 56, 141-151.

Xu, X., Yang, X., Miller, D., Helble, J. and Carley, R. (1999): Formulation of bi-directional atmosphere-surface exchanges of elemental mercury. Atmospheric Environment, 33(27), 4345-4355.

Xu, X., Yang, X., Miller, D., Helble, J. and Carley, R. (2000a): A regional scale modeling study of atmospheric transport and transformation of mercury. I. Model development and evaluation. Atmospheric Environment, 34(28), 4933-4944.

Xu, X., Yang, X., Miller, D., Helble, J. and Carley, R. (2000b): A regional scale modeling study of atmospheric transport and transformation of mercury. II. Simulation results for the northeast United States. Atmospheric Environment, 34(28), 4945-4955.

Zhang, H. and Lindberg, S. (1999): Processes influencing the emission of mercury from soils: A conceptual model. Journal of Geophysical Research-Atmospheres, 104(D17), 21,889-21,896.

Zhang, H. and Lindberg, S. (2001): Sunlight and iron(III)-induced photochemical production of dissolved gaseous mercury in freshwater. Environmental Science & Technology, 35(5), 928-935.